Effects of mutations in the junction between helices 5 and 6 of the 16S rRNA upon 30S biogenesis

by
Mollie Charlotte Kay Rappé

A dissertation submitted to The Johns Hopkins University in conformity with the requirements for the degree of Doctor of Philosophy

Baltimore, Maryland
August, 2015

Abstract

The ribosome is a large, compact RNA machine stabilized by conserved sequence motifs. The junction between helices 5 and 6 of the 16S 5' domain undergoes transient structural rearrangements during in vitro assembly and the sequence of Right Angle motif consensus sequence but not the structure. In this work I will show that *in vitro* rRNA folding, r-protein binding, and RNP chemical footprinting reveal mild defects such as a greater dependence on Mg^{2+} when folding in low K^{+}, approximately two-fold weaker r-protein association, and local structural perturbations. *In vivo*, the 30S ribosomes carrying mutations in this junction cannot support life, as they fail to mature. Neither an increase in growth temperature nor overexpression of ribosome assembly factors improves mutant pre-rRNA processing or polysomal localization. *In vivo* hydroxyl radical footprinting of wild type and mutant 16S rRNA revealed solvent exposures at helices 35-37 of the 3' head domain and cleavages at helix 2. This suggests that late r-protein S2 and the native tertiary interactions with other domains of the 30S ribosome are not present in the J5/6 Triple mutant. These data are consistent with a hypothesis that the J5/6 mutants perturb central pseudoknot formation and proper docking of the 3' head domain, perhaps communicated from the junction to helix 3 through helix 15 packing.

Advisor and primary reader: Dr. Sarah A. Woodson

Secondary reader: Dr. Gregory D. Bowman

Committee Members: Dr. Rachel Green, Dr. Christian M. Kaiser, and Dr. Elijah Roberts

Acknowledgements

Most importantly, I would like to thank my family. You have always been there for me and I know I wouldn't have made it without you.

I also need to thank my many mentors and teachers past, present, and future, with special thanks to Jack Lundt, Ron Estler, and Les Sommerville. I wouldn't be here without you.

I would like to thank my committee Rachel Green, Greg Bowman, Christian Kaiser, and Elijah Roberts as well as Scott Bailey and David Draper. Your advice over the years has been very helpful.

I must thank my labmates and friends. Megan Mayerle, Andrew Santiago-Frangos, Ryan Hulscher, Brittany Brown, Lauren Boucher, Carla Coltharp, Kat Jenkins, and Erin Macdonald all deserve special thanks. You are the highlights of my day.

I need to thank the Biophysics staff Ranice Crobsy, Nicole Goode, Jessica Appel, Alexias Ebert, Nancy Foltz, Chris Altizer, and Ken Rutledge. Without you the whole department would fall to pieces.

I must also thank Dr. Jodi Pendroy.

I would also like to thank BCI and ASBMB for my amazing science-writing internship, especially Arhonda Gogos, Angela Hopp and Rajendrani (Raj) Mukhopadhyay.

Table of Contents

List of Tables

List of Figures

Chapter 1: Introduction

1.1 Ribosomes are large RNA machines

Ribosomes are the vital and fundamental protein-producing machinery in all living cells. Ribosomes translate mRNA messages and, with the assistance of aminoacylated tRNAs, produce every protein in the cell (Littlefield 1955, historical review in Siekevitz 1981).

In bacteria, the 70S ribosome consists of 2 asymmetric subunits, the 30S and the 50S as defined by their characteristic sedimentation coefficients (Tissieres 1958). The small or 30S subunit is made up of the 16S rRNA and 20 ribosomal proteins (Craven 1969); it serves as the site of mRNA decoding (Wagner 1975, Figure 1.1A). The large or 50S subunit is made up of the 23S and 5S rRNA as well as 33 r-proteins (Mora 1971), and is the site of peptide bond formation (Sonenberg 1975, Figure 1.1B). The molecular weight of the 30S particle is 850 kDa and the mature 16S rRNA is 1542 nt long (Tissieres 1958, Fellner 1971, Brosius 1978). The 50S particle weighs 1.5 MDa and the mature 23S is 2904 nt long and the 5S is 120 nt long (Tissieres 1958, Brosius 1980). About 2/3^{rds} of the mass of the ribosome is made up of RNA (Roberts 1958), the rRNA is highly conserved (Woese 1975), and all of the functionally vital regions (e.g. decoding site, the peptidyl transferase center) are RNA-encoded (Figure 1.1 red nucleotides, Noller 1991).

These complex ribonucleoprotein particles can be further subdivided into structural domains. The 16S rRNA can be subdivided into 4 independently folding domains (Stern 1988c). The 5' domain is transcribed first and forms the body of the 30S

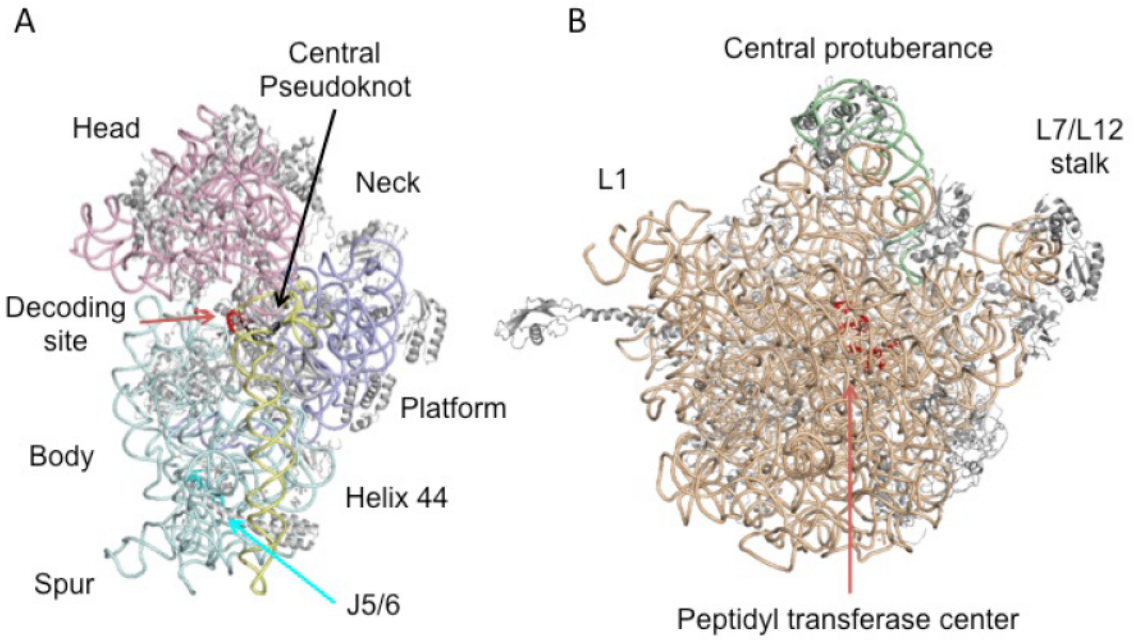

Figure 1.1: **Ribosomes are compact Ribonucleoprotein particles.** Interface views of the A) 30S and B) 50S *E. coli* ribosomes. r-proteins are grey while the 16S 5' domain is pale cyan, the 16S central domain is lilac, the 16S 3' major domain is rose, and the 16S 3' minor domain is light yellow. The 23S rRNA is wheat and the 5S rRNA is light green. Nucleotides important for mRNA decoding and peptide transfer are highlighted in red. Additionally, the central pseudoknot and the J5/6 residues are indicated in black and cyan. Other important structural features labeled. Figure adapted from Schuwirth 2005, PDB ID 2AVY and 2AWB.

subunit (Stern 1988c). The central domain makes up the platform of the 30S subunit. The 3' major domain makes up the head of the 30S subunit and the 3' minor domain contains the anti-Shine-Dalgarno sequence (Shine 1974) and the penultimate stem. The central pseudoknot connects three major domains, forms late during ribosome assembly, and is required for translational activity (Besancon 1999, Brink 1993).

The 23S can also be subdivided into domains, but full exploration of the 50S is not within the scope of this work (Noller 1981). One important structure is the central protuberance, which contains the 5S rRNA as well as several r-proteins.

1.2 Ribosome biogenesis is a multifaceted process

Producing ribosomes is a vital yet costly process. Bacterial growth rate is directly tied to the rate of ribosome synthesis (Kjeldgaard 1961). Bacterial growth is dependent on increased protein production but the rate of protein synthesis per average ribosome does not vary with growth rate (Brunschede 1977). Consider this: *E. coli* that are doubling every 20 minutes have on average 72,900 ribosomes per cell and 74% of the RNA polymerases are actively synthesizing more rRNA (calculated in Ehrenberg 2013, based off of data from Liang 2000). On the other hand, *E. coli* which are doubling every 40 minutes have only 25,900 ribosomes per cell and 48% of the RNA polymerases are actively synthesizing more rRNA. The rate of ribosome biogenesis is tightly controlled to ensure optimum growth in media with different carbon sources (Dennis 1973).

Despite the complexity and importance of ribosome biogenesis, under ideal conditions (in rich media at 37°C), this process takes less than 2 minutes *in vivo* (Lindahl 1975). The process of ribosome biogenesis is complex and involves: 1) transcription of rRNA; 2) nucleolytic processing of rRNA; 3) rRNA folding; 4) synthesis of r-proteins; 5) r-protein binding; 6) modification of the rRNA and r-proteins; and 7) quality control checkpoints. Many of these processes occur contemporaneously in a stochastic, parallel yet hierarchical manner. This introduction will primarily present the results isolated *in vitro* studies, as very few integrative or *in vivo* studies exist.

1.2.1 Ribosome biogenesis begins with rRNA transcription

E. coli has seven rRNA operons: *rrnA, rrnB, rrnC, rrnD, rrnE, rrnG*, and *rrnH* (Attardi 1965, Kenerley 1977). Each of these operons encode the 16S rRNA, a few tRNAs, the 23S rRNA, and the 5S rRNA (Doolittle 1971, Figure 1.2). The polycistronic transcript allows for equimolar production of the three rRNAs. Numerous mechanisms have evolved to produce large quantities of rRNA during rapid growth, and regulate rRNA transcription during lean times.

Every rRNA operon has two promoters: P1, a very efficient and strongly regulated promoter, and P2, a constitutive promoter (Glaser 1979, Glaser 1983). These promoters are both near the consensus sequence for the -10 and -35 sequences and are recognized by the 'housekeeping' σ^{70} subunit of the RNA polymerase (de Boer 1979). Upstream of the promoters are the strongly stimulating UP elements, which bind the α subunits of RNA polymerase (Ross 1993). The P1 promoter UP element contains consensus sequence binding sites for both the proximal and distal α subunits and they are positioned optimally in relation to the σ subunit binding site, which all contribute to the exceptional strength of the *rrn* P1 promoter (Meng 2001).

Yet another element involved in increasing rRNA transcription is the FIS transcription factor. Multiple FIS-binding sites are located even further upstream of the *rrn* promoters (Ross 1990). The closest site is required for RNA polymerase recruitment through σ subunit interactions and FIS unwinds the -10 region, stimulating rRNA transcription through stabilizing the formation of the open complex (Zhi 2003).

In addition to strongly stimulating transcription initiation, constitutive mechanisms have evolved to ensure efficient elongation even through the Rho-dependent

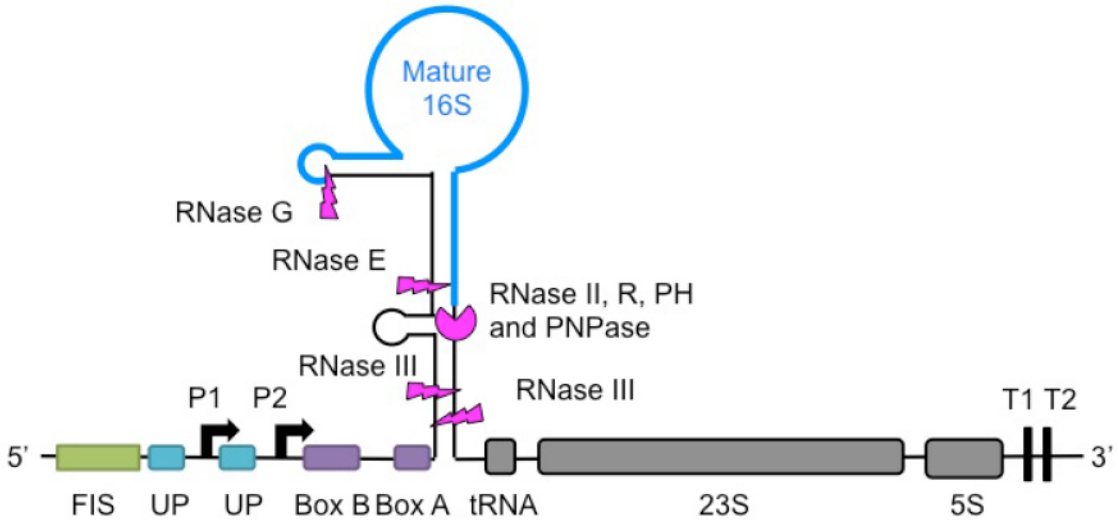

Figure 1.2: **Organization of an *rrn* operon and processing of the 16S rRNA.** A schematic drawing of an *E. coli* operon. Not to scale. Transcription is initiated at one of two promoters (P1 and P2) which is enhanced by UP and FIS-binding sites. The anti-termination *nut* site (Box B and Box A) promotes efficient transcription. Transcription is terminated at T1 or T2. The 17S precursor is cleaved off of the elongating transcript by RNase III. Further maturation of this precursor by RNases E, G, II, R, PH and PNPase removes 115 nt from the 5' end and 33 nt from the 3' end generating the mature 16S rRNA (adapted from Kaczanowka 2007).

terminators present within the *rrn* operons. The *rrn* operons contain two sequences homologous to the lambda anti-termination *nut* site (Li 1984). One of these is located downstream of P2 in the 16S leader region and the other is located in the spacer between the 16S and 23S genes (Morgan 1986). The *nut* site contains the conserved sequence elements BoxA and BoxB that are essential for antitermination (Olson 1982), but only the BoxA element was required in a test expression plasmid terminator read-through in vivo (Berg 1989).

The *rrn* anti-termination complex is homologous to the well-studied lambda anti-termination complex and includes the protein factors NusA, NusB, NusG, and S10 (also known as NusE, Condon 1995). The r-protein S4 was also shown to bind directly to RNA polymerase and exhibits strong Rho-dependent termination anti-termination (Torres 2001). The fact that at least 2 r-proteins, S10 and S4, are involved in enhancing rRNA transcription reveals interesting possibilities for feedback and fine-tuning translational control of ribosomal components, which will be explored more fully later (section 1.2.5)

Since the rRNA elongation complex has strong anti-termination activity, a similarly strong terminator is needed. The *rrn* operons each contain two tandem terminators, a Rho-independent stem-loop followed by a string of thymidine residues and then a Rho-dependent terminator (Albrechtsen 1991). In an *in vivo* plasmid translation termination assay, the tandem terminator leads to 98.5% termination of transcription, even with the anti-termination complex (Albrechtsen 1991).

Transcription of an *rrn* operon takes about 60 seconds, but interestingly, the elongation rate is not uniform throughout (Dennis 2009). Transcription of the 5' leader occurs at a rate of 230 nt/second while transcription of the 16S and 23S genes occurs at a

rate of 65 nt/second as determined by EM RNA polymerase distribution. The spacer between the 16S and 23S is transcribed at a rate of 90 nt/second. The incredibly fast rate of transcription in the presence of Nus anti-termination complex raises a question: If RNA polymerase can transcribe at a rate of 230 nt/second, why doesn't it throughout (Dennis 2009)? There are two possible answers. This could be an evolved trait as the RNA needs the time to fold correctly, or this could be just a side-product of the RNA polymerase being slowed by strong RNA secondary structures (Dennis 2009). Work using the much faster T7 RNA polymerase revealed that 23S rRNA transcribed at a rate of ~230 nt/sec produced non-functional or degraded 50S ribosomes, while at 25°C T7 transcribes slower, and produced functional ribosomes (Lewicki 1993). This suggests that the rate of RNA transcription has been evolutionarily optimized to allow for rRNA folding during ribosome biogenesis. A question worthy of exploration is the location and functional significance of RNA polymerase pause sites throughout an *rrn* operon.

For bacterial survival, rRNA transcription is finely regulated to ensure rapid ribosome biogenesis during rapid growth in order to outcompete their neighbors but also to not waste nutrients during early stationary phase or starvation conditions, to outlast the lean times. The slowdown of anabolism due to amino acid starvation is called the stringent response (Pardee 1956). The major regulator of this response is (p)ppGpp, which is synthesized by the phosphorylation of GDP and GTP by ATP (Cashel 1970). Two synthetases, RelA and SpoT, produce (p)ppGpp. RelA binds to the ribosome and when the cognate A-site tRNA is deacylated, RelA produces (p)ppGpp (Haseltine 1972). SpoT both synthesizes and degrades (p)ppGpp (Hernandez 1991); the synthetase activity of SpoT is dependent upon continuous protein synthesis but the hydrolase activity of

SpoT is not dependent on protein synthesis (Murray 1996). The proposed mechanism of action of (p)ppGpp is through direct competition with NTPs in the RNA polymerase active site (Artsimovitch 2004).

Transcription factors that directly fine-tune rRNA transcription initiation are also sensitive to (p)ppGpp regulation. One transcription factor, DksA, reduces the lifetime of the rRNA promoter-RNA polymerase open complex and tunes the sensitivity of the polymerase to initiator NTP and (p)ppGpp levels (Paul 2004). Additionally, the *fis* gene promoter is (p)ppGpp repressed so FIS transcription activation (mentioned above) is decreased during the stringent response (Ninnemann 1992).

Bacteria have evolved many mechanisms to produce large quantities of rRNA during rapid growth, and regulate rRNA transcription during lean times. The rate of rRNA transcription has been optimized to allow for rRNA folding during ribosome biogenesis. Proper rRNA folding (section 1.2.3) is essential for ribosome structure and function, and r-proteins help guide the formation of the native conformation (section 1.2.5).

1.2.2 rRNA processing occurs both early and late during ribosomal biogenesis

As the elongating transcript is being transcribed, it is processed by a series of ribonucleases (reviewed in Deutscher 2009). More than forty years ago, it was discovered that RNase III-deficient strains accumulated one large precursor 30S pre-rRNA (Dunn 1973). This 35S precursor rRNA could be treated by RNase III *in vitro* to generate 17S

pre-RNA and the 23S precursor rRNA (Dunn 1973). Additional work on RNase III revealed that it was specific for double-stranded RNA and co-purifies with ribosomes under low-salt conditions (Robertson 1968). Sequencing the ends of the 16S and 23S genes revealed long complementary sequences, which can form double-stranded RNase III cleavage sites (Young 1978 and Bram 1980). Interestingly, kinetic isotope labeling revealed that RNase III cleaves the 16S precursor off of the elongating nascent transcript before it is completely transcribed (Gegenheimer 1975).

This initial cleavage of RNase III generates a 17S rRNA precursor with a 115 nt leader and a 33 nt trailer. Processing these extra nucleotides and generating the mature 16S rRNA is a multi-step process (Deutscher 2009). Endoribonuclease RNase E acts on the 5' leader to generate a 16.3S rRNA precursor 66 nucleotides longer than the mature 16S (Li 1999). Then, endoribonuclease RNase G produces the mature 5' end (Li 1999). In strains lacking RNase G, RNase E can generate an almost mature end with a few extra nucleotides, and in strains lacking both RNases E and G can generate the mature 5' end, albeit a bit slower (Li 1999). Interestingly, strains lacking both 5' end processing ribonucleases are viable and can form 70S particles, despite containing the full 5' leader sequence (Li 1999). This observation has not been fully explained by the dominant model that processing the leader is a key checkpoint in permitting the 30S ribosome to enter the pool of active, translating ribosomes.

Processing of the 3' trailer sequence is even more complex. The removal of the 33 nt trailer occurs efficiently, with no detectible processing intermediates, in strains containing any one of four enzymes, three 3'-5' processive exoribonucleases RNase II, RNase R, RNase PH, and polynucleotide phosphorylase (PNPase); it is only when all

four are deleted or deactivated does the 3' end processing halt (Sulthana 2013). Strains without 3' end processing also accumulate immature 5' ends (Sulthana 2013). In addition, strains lacking the endoribonuclease YbeY and either RNase R or PNPase almost completely lack 16S rRNA species with mature 3' ends, though they have some small fraction of 16S rRNA species with mature 5' ends (Davies 2010). Whether YbeY has canonical rRNA processing-activity is an open question but deletion of YbeY leads to poor processing of 16S, 23S, and 5S rRNA 5' and 3' ends (Davies 2010). The defect in 16S maturation was quite pronounced; however, depletion of many ribosome assembly factors with no ribonuclease-activity also leads to an accumulation of immature 17S rRNA.

Conversely, 3' end processing can occur in the absence of 5' end processing, but it is slowed in the absence of RNase E (Sulthana 2013, Li 1999). This suggests that 3' end processing by the 3'-5' exoribonucleases is not dependent upon RNase E removing the remainder of the RNase III stem (Sulthana 2013). Interestingly, strains without 3' end processing exhibit a far more abnormal polysome profile than strains lacking 5' end processing (comparison of Li 1999 and Sulthana 2013). See Deutscher 2009 for a review on the processing of the 23S pre-RNA and the 9S pre-5S rRNA.

Pre-16S rRNA maturation is concomitant with the assembly process and final maturation is likely part of an assembly checkpoint and perhaps even a functionality test (Deutscher 2009). Very early work determined that pre-30S particles – with immature rRNA – spend most of their assembly time at a stage where they co-sediment with mature 30S particles (Lindahl 1975). Recent work inserting MS2 hairpins between the RNase III cut site and the RNase E, between the RNase E cut site and the RNase G cut site, and in

the 3' trailer followed by affinity purification revealed the major species of all three constructs was a 17S assembly platform with RNase III 5' and 3' ends (Gupta 2014). Further work revealed subtle differences in leader conformation and r-protein occupancy, and minor species with mature 5' or 3' ends while still supporting the underlying idea that many stages of ribosome biogenesis occur on a 17S assembly 'platform' (Soper 2013, Gupta 2014).

Since RNase III processing is co-transcriptional, and 17S processing is likely an assembly checkpoint, the accumulation of 17S rRNA is a common hallmark of assembly defects. rRNA mutations (Dammel 1993), r-protein mutations (Roy-Chaudhuri 2008), and assembly factor deletions (section 1.2.7) all lead to an accumulation of 17S rRNA, bolstering the integrative nature of ribosome biogenesis.

1.2.3 rRNA folding and refolding is vital for ribosome assembly

RNA folding, like protein folding, is a complex problem. How do four nucleotides of limited chemical diversity encode a native RNA structure? Early work on ribozymes suggested that RNA folding is hierarchical with local secondary structure formation followed by Mg^{2+} induced collapse, followed by slow formation of long-range, native contacts (Zarrinkar 1994). Further work revealed that RNA folding is hindered by misfolding and kinetic traps (Pan 1997, Rook 1998). Interestingly, tertiary interactions can form in folding intermediates and help guide the formation of the native state (Behrouzi 2012). These fundamental principles are generally applicable to rRNA folding

as well, with some additions. rRNA folding *in vivo* occurs co-transcriptionally, with additional sequences not present in the mature 30S ribosome, and involves r-proteins (discussed in section 1.2.5) and assembly factors (discussed in section 1.2.7).

The Mg^{2+}-dependence of 16S 5' domain folding has been explored by our lab. Hydroxyl radical cleavage patterns of *in vitro* transcribed 5' domain RNA folded in 120 mM NH_4Cl with varying amounts of $MgCl_2$ showed all of the tertiary contacts of the native 30S – with a few exceptions – formed in 20 mM $MgCl_2$ (Adilakshmi 2005). Many of these tertiary interactions required 2.5-6 mM Mg^{2+} to fold, which though it is non-physiological, it is not quite as high as the Mg^{2+}-dependence of ribosome reconstitutions (Adilakshmi 2005). The least stable interactions with were those involving helix 15 wedging up against J5/6 and the minor groove of helix 17 packing against other face of helix 15 (Adilakshmi 2005); these helices are of particular interest for my thesis work.

The kinetics of Mg^{2+}-induced folding studied using hydroxyl radicals produced rapidly by a synchrotron-generated X-ray beam with an experimental dead time of 15-20 ms (Adilakshmi 2005). Within 20 ms of being mixed with buffered 10 mM Mg^{2+}, the rRNA helices had assembled and oriented properly (Adilakshmi 2005). It took 5-10 seconds for the center of the 5' domain to structure as well as the 5-helix junction that makes up the S4 binding site (Adilakshmi 2005). Interestingly, the H6, H8, H10, and H15 protections took 10-40 seconds to form, and many residues displayed biphasic kinetics – being partly protected within a second, but taking 10-40 seconds to reach the level of protection exhibited in the native 30S (Adilakshmi 2005). As with the Mg^{2+}-dependent stabilities, portions of helix 17 were protected the slowest, taking 30-60 seconds (Adilakshmi 2005). Unlike the RNA folding pathway of the *Tetrahymena* ribozyme

(reviewed in Woodson 2011), the 5' domain folding kinetics mostly increased with increased Mg^{2+}, indicating the rate of folding is limited by the stability of the tertiary interactions rather than reorganization of misfolded intermediates (Adilakshmi 2005). Excitingly, these results show that ribosome structure is an intrinsic property of the rRNA sequence, at least for the 5' domain, and the kinetics of helix orientation can dictate the order of r-protein binding (Adilakshmi 2005).

RNA tertiary interactions have been found throughout the rRNA. The A-minor motif, a single-stranded adenosine binding in the minor groove of a Watson-Crick pair, stabilizes contacts between helices, contacts between loops and helices, and junctions throughout the rRNA (Nissen 2001). The kink-turn is a motif that produces a sharp turn within an internal loop stabilized by an A-minor interaction (Klein 2001). The along-groove stacking motif nestles the backbone of two RNA helices in the minor groove of one another (Gagnon 2002). This motif is found between helices 3 and 12 of the 16S rRNA, among others, and is vital for normal ribosome function and RNA-protein interactions (Gagnon 2006, Gagnon 2010). The Right Angle motif is a composite motif made up of an along-groove stacking motif stabilized by two A-minor motifs (Chworos 2004, Grabow 2012). The Right Angle motif is found between helix 18 and helix 3 and between helix 5 and 6 in the 16S rRNA (Grabow 2012). The importance of the junction between helix 5 and 6 on ribosome biogenesis will be explored in my thesis.

One of the proposed functions of the 16S leader is to serve as an assembly scaffold and prevent the formation of incorrect yet stable RNA helices (Theissen 1993). Early work exploring the function of the 16S 5' leader revealed that many mutations in the region 19-45 nt upstream of the mature 16S end caused cold-sensitive growth

phenotypes, reduced 70S formation, produced slight 5' and 3' processing defects, and reduced *in vitro* translational activity (Theissen 1993). A combination of nuclease footprinting and chemical probing techniques were used to determine the structure of the isolated leader (Pardon 1995). UV-crosslinking studies showed strong localization between the leader and the mature 16S rRNA in *trans* at G126 in helix 7, G117 near helix 7a, G68 in the base of helix 6, as well as extensive cross-linking in helix 3 and 4 (Pardon 1995). This was later supported by oligonucleotide hybridization studies that showed strong leader-dependent protections of helix 3 as well as leader-dependent increased folding kinetics of helix 6, but other helices were unaffected (Besancon 1999).

In a similar vein, a C23U point mutation in helix 1 confers a severe, dominant, cold-sensitive phenotype, likely by stabilizing an alternative pre-rRNA helix at the expense of the mature helix 1 (Dammel 1993). In support of this hypothesis, many second-site suppressor mutations of this cold-sensitive phenotype map to the central pseudoknot and leader sequences and either re-stabilize helix 1 (G11A) or destabilize the presumed competing precursor helix (C-5U) (Dammel 1993). The inability to form helix 1 would destabilize the vital central pseudoknot and thus the domain architecture of the 30S subunit.

The importance of transient structures including nucleotides not present in the mature rRNA is not limited to the 16S rRNA. In fact, transient hairpins located at either end of the pre-23S rRNA are important both in post-transcriptional *in vitro* refolding and ribosome assembly *in vivo* (Liiv 2004).

Though the secondary structure of the 16S rRNA has been known for decades from phylogenetic sequence analysis (Stern 1988c), and the native 30S structure has been

known for almost 15 years (Wimberly 2001), how the transcribed rRNA folds, restructures, and reaches its native state is still a work in progress.

1.2.4 Synthesis of r-proteins is regulated for stoichiometric ribosome assembly

Regulation of r-protein synthesis is important to achieve stoichiometry between the r-protein levels and the rRNA levels (reviewed in Keener 1996). Many r-proteins are located in polycistronic operons with other r-proteins, genes for RNA polymerase subunits, tRNA modification enzymes (tRNA m^1G methyltransferase), elongation factors, rRNA maturation enzymes (PNPase and RNase P) and even ribosome assembly factors (RimM) (Table 1.1 reviewed in Bjoerk 1985). Regulation of the translation of these operons is quite complex and is frequently mediated through a primary r-protein binding to the mRNA in a manner similar to the r-protein's ribosome binding site, this allows for finely tuned negative feedback (Fallon 1979). Regulation of the *spc*, α, and *trmD* operons will be briefly explored below to offer some insight into the complexity and diversity of r-protein level regulation.

The *spc* operon encoding L14, L24, L5, S14, S8, L6, L18, S5, L30, L15, L36 and SecY is regulated by S8 – a primary central domain protein (Dean 1981). S8 binds to the *spc* mRNA between the second and third cistrons in a binding mode very similar to the S8-16S helix 21 complex (Cerretti 1988; diagrammed in Table 1.1). In fact, the structure of *E. coli* S8 bound to the mRNA stem loop and the structure of the *T. thermophilis* S8 in complex with helix 21 of the 16S rRNA only has an RMSD of 2.0 Å, mostly due to two

Table 1.1: **r-protein operons.** The cistrons and structural elements of r-protein operons. Indicated in bold is the regulatory r-protein. Dashes indicate the sites of regulation, which can include a r-protein binding site, attenuators, translation terminators, and SD-protecting RNA hairpins. Table adapted from Keener 1996.

Operon	Gene order and operon structure
spc operon	L14 L24 -- L5 S14 **S8** L6 L18 L5 L30 L15 *secY* L36
α operon	-- S13 S11 **S4** α L17
S6	-- **S6** *priB* **S18** L9
trmD operon	S16 *rimM* -- *trmD* L19
S10 operon	-- S10 L3 **L4** L23 L2 S19 L22 S3 L16 L29 S17
str operon	S12 -- **S7** EF-G EF-Tu
L11 operon	-- L11 **L1**
β operon	-- **L10** L7/L12 -- β β'
S15 operon	-- **S15** -- *pnp*
L35 operon	IF3 -- L35 **L20**
S20 operon	**S20**
S1 operon	**S1**
S2	S2 EF-Ts
σ	S21 *dnaG* σ
L13	L13 S9
L25	L25
L28	L28 L33
L32	*yceD* L32
L34	L34 *rnpA*

bulged nucleotides in the mRNA, which reduce the binding affinity slightly (Merianos 2004). The S8 binding site is directly 3' of the Shine-Dalgarno sequence of L5, so the method of repression of that r-protein is clear. How S8 represses expression of the cistrons 5' of its binding site is unclear, and has been vaguely attributed to mRNA stabilization (Merianos 2004). Furthermore, the method of repressing cistrons 3' of L5 via translational coupling is also not satisfactory as the downstream cistrons mostly possess their own Shine-Dalgarno sequences, and translation of the 5' cistrons is not required for translation of 3' cistrons (Merianos 2004).

The *α* operon containing genes for S4, S13, S11, L17 and the α subunit of RNA polymerase is regulated by S4 (Olsson 1979). S4 is a primary 5' domain binding protein, and one of the earliest to associate with the assembling small subunit (Nowotny 1988). Free molecules of S4 in excess of what is required for ribosome synthesis bind to a nested pseudoknot structure in the 5' UTR of its mRNA (Spedding 1993). This binding stabilizes the inactive conformation of the mRNA and forms a ternary complex with a 30S subunit, trapping it and repressing translation (Schlax 2001). Similarly, the S6:S18 complex binds to a structural motif in the S6 mRNA 5' UTR that is quite similar to the three-way junction of helix 22 and helix 23 in the 16S rRNA (Matelska 2013).

On the other hand, the *trmD* operon, which includes S16, L19, RimM, and the tRNA m^1G methyltransferase is not under autogenous control (Wikstroem 1988). Overexpression of this operon from a high-copy number plasmid led to a three-fold increase in the level of *trmD* mRNA and a 10- to 25-fold increase in the translation of the four proteins (Wikstroem 1988). The excess r-proteins were degraded to two- or three-fold the level of plasmid-free cells, and the other two proteins were stable (Wikstroem

1988). In addition, expression of lac-Z fusions from two different cistrons in the chromosomal operon showed no alteration upon transformation with plasmids containing all or part of the operon, indicating no transcriptional or translational feedback of this operon (Wikstroem 1988). It was proposed that this operon could be regulated via transcriptional read-though and/or r-protein degradation (Wikstroem 1988). It was discovered that translation of RimM and the tRNA m^1G methyltransferase are independently regulated by a stem-loop structure that blocks the SD sequence (Wikstroem 1992).

Regulation of the levels of r-proteins is important as excess r-proteins would be wasteful and sub-stoichiometric concentrations could produce aberrant pre-ribosomes possibly unable to assemble or function. How the r-proteins help guide the folding of the rRNA to the native state during ribosome assembly is explored below (section 1.2.5).

1.2.5 r-protein binding is critical for guiding ribosome assembly

The aspect of ribosome biogenesis that is perhaps the most thoroughly studied is r-protein association with the rRNA. Seminal work in the late 60's and early 70's showed that functional 30S subunits can be reconstituted *in vitro* with the mature 16S and the 21 r-proteins, and determined the biochemical dependency of r-protein binding (Held 1973a, 1973b, 1974). This fundamental work has stood the test of decades of further work *in vitro* and *in vivo*. One of the most important discoveries is that r-protein binding is both cooperative and hierarchical (Figure 1.3). Six primary r-proteins: S4, S17, S20, S8, S15,

and S7 can bind stably to the 16S rRNA independent of any other r-proteins (Held 1974). Nine secondary r-proteins: S16, S6:S18, S12, S5, S11, S9, S19, and S13 require one or more r-protein to bind to the 16S rRNA before they can stably associate (Held 1974). The final five tertiary r-proteins: S10, S14, S21, S3, and S2 require many if not all of the previous proteins as well as a temperature-dependent conformational change before they can stably associate (Held 1974).

The observed cooperativity of r-protein binding is not due to direct protein-protein interactions; instead it is mediated through rRNA conformational changes where primary binding proteins reform the rRNA structure to allow secondary proteins to bind stably (Stern 1989). Since these reconstitution experiments clearly demonstrated that all of the information needed for assembly is present in the rRNA and r-proteins themselves, the 30S ribosome has served as an excellent model system for the principles of RNA folding (section 1.2.3), RNA-protein recognition, and protein-guided RNA conformational selection.

1.2.5.1 Kinetics of r-protein association

More recent work on r-protein association with rRNA has probed the kinetics of *in vitro* ribosome assembly using pulse-chase quantitative mass spectrometry (Talkington 2005). The binding kinetics generally supported the Nomura map as well as the proposed 5' to 3' directionality of assembly. Primary binding proteins S4, S17, S20, S8 as well as the secondary 5' domain protein S16 bound the fastest with rates of >30 to 20 min^{-1} at 40° C (Talkington 2005); these r-proteins are of particular interest for my thesis work. The central domain primary protein S15 and the secondary protein heterodimer S6:S18

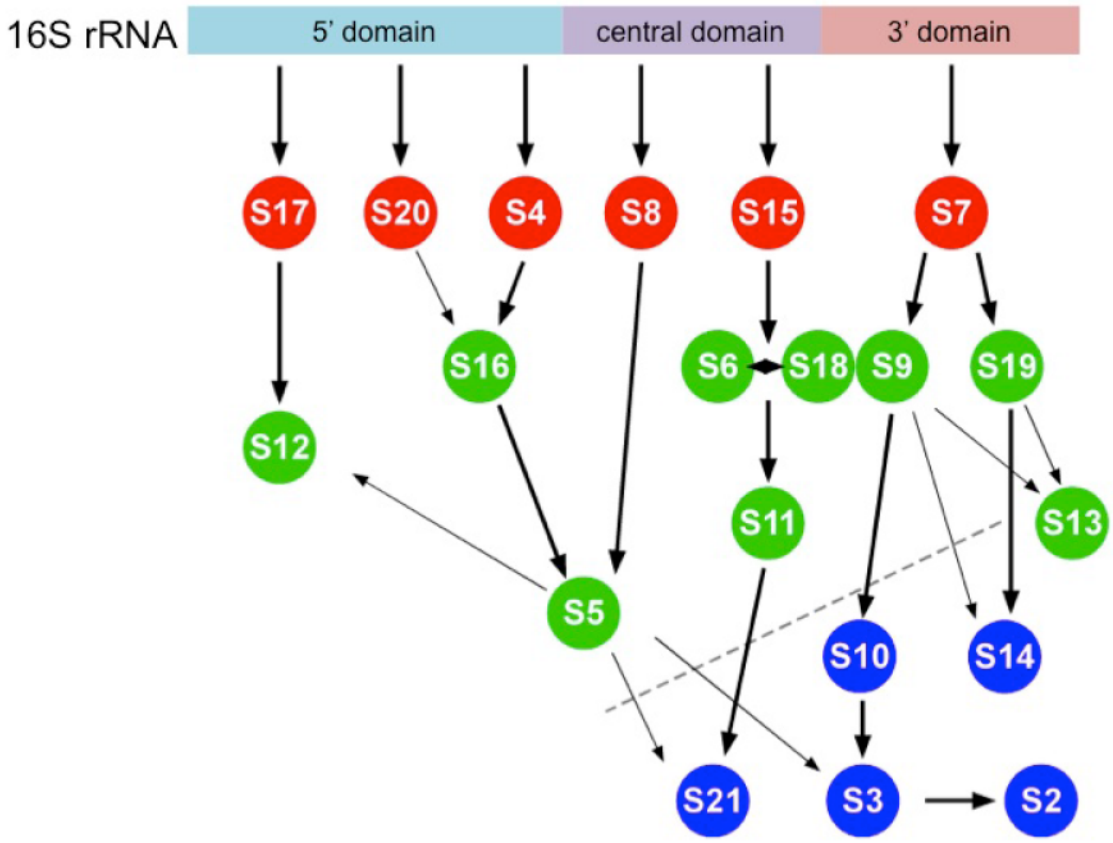

Figure 1.3: **The Nomura assembly map.** A diagram depicting the stability of r-protein binding with the 16S rRNA during 30S reconstitutions and single component omission experiments. The 16S domain structures are colored as in Figure 1.1. The primary assembly proteins, which bind stably and independently to the rRNA are indicated in red. The secondary assembly proteins, which require the presence of one or more of the primary proteins are green. The tertiary assembly proteins, which only bind stably after a temperature-dependent conformational change are in blue. Figure adapted from Held 1974.

bound next with rates of 15-8.1 min^{-1} (Talkington 2005). The secondary proteins S5, S11, S9, S19 and the tertiary protein S10 bound at rates of 2.2-1.2 min^{-1} (Talkington 2005). The other secondary tertiary proteins bound slower; S12 and S3 of the neck region were among the slowest proteins (Talkington 2005). Additionally, Talkington and coworkers performed these experiments at multiple temperatures and analysis of the Arrhenius plot indicates no global rate-limiting step, unlike what was inferred from the temperature-dependence of the RI to RI* conformational change seen in reconstitutions (Held 1973b). Instead ribosome assembly can take multiple parallel pathways with no universal bottleneck (Talkington 2005).

A method looking at the kinetics of *in vitro* ribosome assembly using time-resolved hydroxyl radical footprinting revealed a complementary yet contrasting picture. Instead of a 5' to 3' directionality, the protein-induced protections of the RNA backbone from hydroxyl radicals showed rapid protections (>20 sec^{-1}) throughout the 16S rRNA (Adilakshmi 2008). Many of the primary binding proteins protected a segment of their binding site during the first 50 ms (S4, S7, S8, S15), however it took much longer for the whole binding site to become protected, indicative of an encounter complex that needed to restructure the rest of the RNA binding site, or wait for the correct rRNA conformation to form and then stabilize it (Adilakshmi 2008). For example, nucleotides at the base of helix 16 are fully protected by S4 at a rate of ~100 sec^{-1} where as the nucleotides at the base of helix 17 exhibit a biphasic protection patter with rates of 70 sec^{-1} and 0.5 sec^{-1} (Adilakshmi 2008). The protection of the rest of helix 16, the formation of the helix 18 pseudoknot, and helix 3 also occurred slowly with rates of 2-0.2 sec^{-1} (Adilakshmi 2008). Part of the complexity of the S4 binding rates could be due to co-folding of the N-

terminal domain, however these multi-stage binding site protection kinetics seems to be more universal (Adilakshmi 2008), and the slowest protection rates for each r-protein are comparable to the rate measured by Talkington and coworkers above. *In vitro* r-protein binding seems to involve encounter complexes of early r-proteins that induce or stabilize rRNA structural changes before binding stably to their whole binding site, and these rRNA rearrangements allow later r-proteins to bind added stochasticity and heterogeneity to the complex parallel pathways.

Yet another complementary method provides larger-scale structural details of the ribosome assembly paths. Negative-stain EM of ribosome assembly intermediates at different time points followed by high-throughput data collection and reference-free alignment and classification revealed four assembly intermediate groups (Mulder 2010). Group I particles (most populated at early time points) are isolated 'body' or 'body with platform' particles containing primary proteins S4, S17, S20, S8, and secondary protein S16 (Mulder 2010). Group II particles contain a complete 'body and platform' with a missing, incomplete, or unanchored head domain (Mulder 2010). These particles have the central domain proteins S15, S6:S18 and sometimes S11and the 3' domain proteins S7, S9, S13, and S19 (Mulder 2010). Many of the Group III particles have missing platform density and rotated heads, possibly indicative of misassembled particles (Mulder 2010). The Group IV particles are mostly assembled with the head domain in the final orientation and contain all or most of the r-proteins (Mulder 2010). The tertiary proteins S10, S14, S2, S3, and S21 appear to bind in a parallel manner, which accounts for the subtle differences in the densities of Group IV particles (Mulder 2010). The easy

misassembly of the head domain is likely why so many of the ribosome assembly factors bind to the neck region of the 30S subunit (section 1.2.7).

These powerful *in vitro* studies revealed fascinating details of the cooperative, hierarchical, parallel, and yet stochastic process of ribosome assembly. More mechanistic details underlying the cooperative and hierarchical nature of r-protein binding will be explored further below (section 1.2.5.2).

1.2.5.2 Spotlight on individual r-proteins

By diving into the interactions of specific r-proteins with their binding sites, the origin of the complexity of the binding kinetics can be revealed. Tethered Fe(II) probing from the central domain primary protein S15 with and without the other central domain primary protein S8 shows increased cleavages of helices 22, 24, and 26, indicating a more compact and stable platform in the presence of both primary proteins (Jagannathan 2003). Tethered Fe(II) probing from S20 revealed interesting S17 and S16 dependent intermediate cleavages at the junction of helices 5 and 6 indicative of concerted 16S rearrangements, which is discussed in more detail in Chapter 2 (Dutca 2008). Time-dependent DMS probing of S17 binding to 16S rRNA showed four regions with different protection kinetics. This suggests a helix 11 encounter complex followed by a protein-dependent kink-turn formation to permit stable docking of helix 7 (Woolstenhulme 2009).

Hydroxyl radical footprinting of the 5' domain with and without each of the 5' domain primary proteins illustrated stabilization at lower Mg^{2+} globally by S4 and S17, but S20 produced only localized stabilization (Ramaswamy 2009a). Partial saturation of

protections and transient exposures of various helices indicates multistage folding and different intermediates, providing further support for the dynamics and synergy of ribosome assembly (Ramaswamy 2009a). The binding of the secondary r-protein S16 suppresses the formation of a non-native S4-S17-S20 assembly intermediate (Ramaswamy 2009b). More specifically, S16 eliminated the multistage folding of helices 12, 15, and 18, indicative of helix 3 being in a non-native 'flipped' conformation that perturbed packing of the 5' domain core (Ramaswamy 2009b). These data are of particular relevance to my thesis work.

Time-resolved SHAPE chemical probing of S4-rRNA complexes show slow formation of stable complexes, with most of the RNA conformational changes (such as helix 18 pseudoknot formation) occurring after 1 minute of co-incubation, but other vital conformational changes such as correct helix 3, 4 and 18 orientation require longer co-incubation (Mayerle 2011). Specific S4-rRNA interactions as probed by S4 mutational analysis and SHAPE chemical probing reveals the importance of S4 *ram* mutants in helix 18 pseudoknot formation; mutations Y47A and L51A destabilize pseudoknot formation while R200A over-stabilizes the pseudoknot, leading to temperature-sensitive growth (Mayerle 2013).

Single-molecule FRET between helix 3 of the 16S rRNA and a solvent-exposed site of S4 unveiled intriguing S4-helix 3 dynamics (Kim 2014). The S4-rRNA interconverts between a high-FRET (native) and low-FRET (flipped) state with dwell times around 1-10 seconds in 20 mM Mg^{2+} (Kim 2014). Single-molecule traces synchronized to the time of initial S4 contact showed a short-lived mid-FRET encounter complex, which was longer-lived at higher Mg^{2+} (Kim 2014). These S4-rRNA encounter

complexes went through the obligatory low-FRET state within 0.2 s (at 4 mM Mg^{2+}) before eventually reaching the high-FRET native state after several seconds (Kim 2014). Three-color FRET between helix 3, helix 16, and S4, shows that S4 binding suppresses helix 16 motions, which suggests that S4 binding actually guides the selection of accessible RNA conformations by influencing RNA dynamics (Kim 2014). Furthermore, S16 binding suppresses helix 3 motions (personal communications with S. Abeysirigunawardena), which would allow the central pseudoknot to fold and the 5' domain to orient correctly with the rest of the assembling ribosome.

Though r-protein binding to the rRNA is a well-studied component of ribosome biogenesis, each new technique reveals fascinating details of the complexity of the association of each r-protein with its binding site.

1.2.6 Modification of rRNA and r-proteins is important for assembly, but is not essential for ribosome function

The 16S rRNA contains 10 base methylations and 1 pseudouridylation (Table 1.2, reviewed in Kaczanowka 2007). These modifications are conserved and clustered around the functionally important decoding site (Figure 1.4) and yet functional – if somewhat less efficient – 30S subunits can be assembled with 16S rRNA devoid of these modifications (Kryzosiak 1987). Recently, crystal structures have been solved at a sufficiently high resolution with sufficiently optimized modeling to reveal the nucleotide modifications of native ribosomes and yet their functional importance is still unclear

Table 1.2: **Modified nucleosides in 30S rRNA.** The modification of m^5C is added half early during assembly and half late during assembly, but it is only proposed that RsmB (m^5C967) is the early enzyme and RsmF (m^5C1407) is the late enzyme. Table modified from Siiback 2010.

Modification	Enzyme	Known substrate	Stage of nucleoside accumulation
Ψ516	RsuA (YejD)	Some proteins	Early-intermediate
m^7G527	RsmG (GldB)	30S	Intermediate
m^2G966	RsmD (YhhF)	Requires S7, S19	Late
m^5C967	RsmB (RrmB)	Blocked by S7, S19	? Early
m^2G1207	RsmC (YjjT)	30S	Late
m^4C1402	RsmH	30S	Stochastic
Cm1402	RsmI	30S	Stochastic
m^5C1407	RsmF (YebU)	30S	? Late
m^3U1498	RsmE (YggJ)	30S	Late
m^GG1516	RsmJ (YhiQ)	30S	Late
$m^6{}_2A1518$	RsmA/KsgA	30S	Late
$m^6{}_2A1519$	RsmA/KsgA	30S	Late

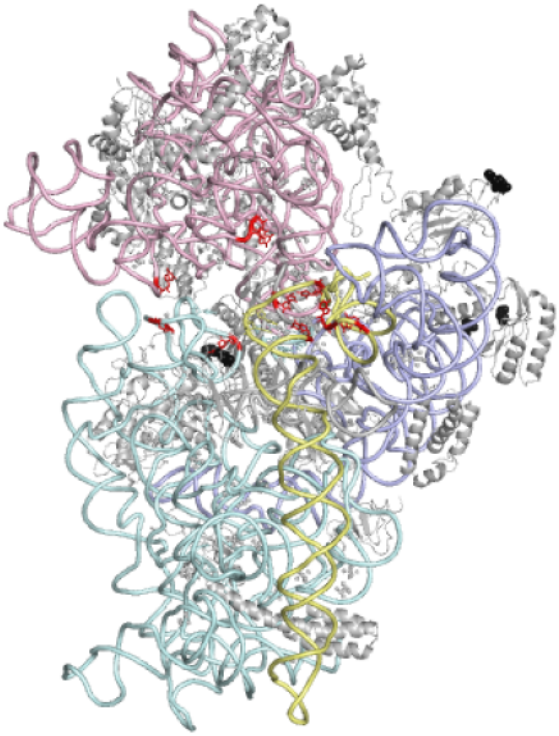

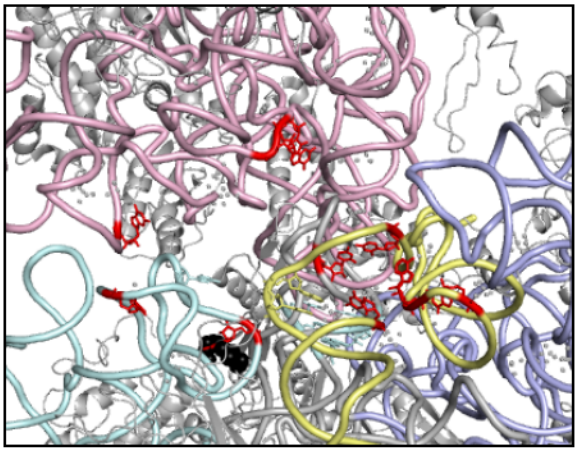

Figure 1.4: **rRNA and r-protein modifications cluster around decoding site.** Interface views of the A) 30S ribosome B) zoom-in of decoding site with modified nucleotides indicated in red and sites of r-protein modifications indicated in black spheres. Figure adapted from Wilson 2007. PDB ID 2AVY.

(Noeske 2015). This information suggests that the modifications could serve as an assembly checkpoint (Kaczanowka 2007).

Analysis of the nucleoside composition of chloramphenicol or erythromycin-stalled pre-ribosomes revealed the stages at which the rRNA nucleotides were modified (Table 1.2, Siiback 2010). In agreement with earlier work (Tscherne 1999, Andersen 2006, Basturea 2006, Okamoto 2007, Kimura 2010, Basturea 2012), most of the 16S modifications were detected late during assembly (Siiback 2010). The two dimethylations performed by KsgA were the last as determined by the ratio of modified nucleosides in the free 30S pool compared to mature 30S split from 70S (Siiback 2010). The role of KsgA in ribosome biogenesis has been explored biochemically, and will be discussed in more depth below. In addition, the 23S rRNA also contains 25 modifications: 14 methylations, 9 pseudouridylations, a methylated pseudouridine and one as of yet unidentified modification (Kaczanowka 2007).

Some of the r-proteins are also modified as a regulated part of ribosome biogenesis, but there are many gaps in our knowledge (Table 1.3 reviewed in Nesterchuk 2011). The most common posttranslational modification is the removal of the N-terminal methionine; this occurs in more than half of the r-proteins (Arnold 1999). Ribosomal proteins S2, S3, S4, S5, S7, S8, S9, S11, S12, S13, S14, S15, S17, S18, S19, S20, and S21 all do not have their N-terminal methionine (Arnold 1999).

The r-protein S5 is acetylated on the α-amino group of the N-terminal alanine by RimJ (Wittmann-Liebold 1978, Janda 1985). The N-terminal residues of S5 are solvent-exposed and unstructured in 30S crystal structures, observations that lead to questions as to its functional role (Nesterchuk 2011). Evidence suggests that S5 is modified in the

Table 1.3 **Modifications of ribosomal proteins.** The enzymes responsible for both S11 modifications have not yet been identified. The location of the isoaspartate residue, its function, and the regulation of the modification is unknown. Table modified from Nesterchuk 2011.

r-protein	Modification	Enzyme
S5	N-terminal acetylation	RimJ
S6	Addition of C-terminal glutamic acid residues	RimK
S11	N-terminal monomethylation and isopeptide bond formation	?
	Non-stoichiometric formation of isoaspartate residue	?
S12	Asp 88 methylthiolation	RimO
S18	N-terminal acetylation	RimI

context of the assembling ribosome, as 30S ribosomes with a central pseudoknot mutation have undermodified S5 (Poot 1997). S5 acetylation levels are low in pre-ribosomal particles, 88% in Δ*rimM* and 66% in Δ*rbfA* compared to 100% in K12 cells and 4% in overexpressed S5 (Soper 2013). Additionally, overexpression of RimJ – even catalytically inactive RimJ – can ameliorate growth and ribosome biogenesis defects from a cold-sensitive S5 mutation (Kelley 2008). This suggests a possible non-acetyltransferase role of RimJ in ribosome biogenesis (discussed more fully below).

The C-terminus of r-protein S6 is poly-glutamylated by RimK (Hitz 1975, Kang 1989). The function of these additional glutamic acid residues is unknown (Nesterchuk 2011).

The N-terminus of r-protein S11 is methylated and the methylated alanine is isomerized to form an isopeptide linkage (Chen 1977). In addition, during log phase growth about half of the r-protein S11 contains isoaspartate, but it is absent in stationary phase cells (David 1999). The location of the isoaspartate and the mode of this regulation are unknown. Neither the functions nor the enzymes involved in these modifications have been identified yet (Nesterchuk 2011).

S12 is methylthiolated at Aspartate 88 by RimO, and the function of this unique modification is unknown and the Δ*rimO* cells have only a very slight slow-growth phenotype (Anton 2008). The recent high-resolution crystal structures of *E. coli* ribosomes revealed the location and conformation of the methylthio group (Noeske 2015). The β-methylthioaspartate is in a 3R conformation. The methylthio is 3.8 Å from the nitrogen of m^7G527 (Noeske 2015). This proximity to the decoding loop suggests a role in mRNA decoding, perhaps during stress, but the evidence for this is weak.

The N-terminus of S18 is acetylated by RimI, and Δ*rimI* cells exhibit no growth phenotype (Isono 1980). Interestingly, S18 acetylation level is quite low in Δ*rimM* pre-ribosomal particles, but almost normal in Δ*rbfA* pre-ribosomal particles (Soper 2013). The low S18 acetylation level in Δ*rimM* cells is hard to explain as RimM acts on the head near S19, and S18 is a central domain protein.

As previously mentioned, the 30S rRNA and r-protein modifications cluster around the decoding site, and yet are not strictly required for ribosome function. They do improve the fidelity of mRNA decoding (Kryzosiak 1987), likely by altering the chemical properties of the bases such as base-stacking preferences, preferred sugar puckers, and hydration (Noeske 2015). The process of modifying the nucleotides and proteins does aid in the process of ribosome biogenesis and some modification enzymes have a role in biogenesis separate from their catalytic activity (KsgA, RimJ, maybe RsmC; section 1.2.7).

1.2.7 Protein co-factors aid ribosome biogenesis

Since ribosome assembly is such a complex process, it's no wonder that bacteria have evolved protein co-factors to make the expensive and vital process more efficient. These co-factors include GTPases, helicases, RNA-binding proteins without enzymatic activity, and proteins involved in other parts of ribosome assembly with an extracurricular biogenesis role (Table 1.4 and Figure 1.5). Much of what we know about *in vivo* ribosome assembly comes from assembly factor deletions.

The non-enzymatic chaperones involved in 30S biogenesis include RimM, RbfA, and RimP. The GTPases involved in 30S biogenesis are Era and RsgA. KsgA has

Table 1.4 **Ribosome assembly factors and their phenotypes.** Table of biochemical data on ribosome assembly factors including deletion and overexpression phenotypes and known binding partners and structural information.

	Particle Partner	Deletion/Depletion Phenotypes	Overexpression Suppresses	Structure
RimM	30S	Slow growth 17S accumulation More free 30S and 50S, fewer 70S and polysomes		NMR structure of independent protein Suzuki 2007
RbfA	30S	Cold sensitive 17S accumulation More free 30S and 50S, fewer 70S and polysomes	Cold-sensitive C23U mutation *ΔrimM*	Cryo-EM structure of factor-ribosome-complex Datta 2007
RimP	30S	Heat sensitive 17S accumulation More free 30S and 50S, fewer 70S and polysomes		NMR structure of independent protein Yu 2001
Era	16S and 30S	17S accumulation More free 30S and 50S, fewer polysomes	*ΔrbfA* *ΔrsgA*	Cryo-EM structure of factor-ribosome-complex Sharma 2005
RsgA/ YjeQ	30S	Slow growth 17S accumulation More free 30S and 50S, fewer 70S and polysomes		Cryo-EM structure of factor-ribosome-complex Guo 2011
KsgA	30S	Cold sensitive 17S accumulation More free 30S and 50S, fewer 70S	Cold-sensitive Era mutant	Cryo-EM structure of factor-ribosome-complex Boehringer 2012
RsmC	30S			Crystal structure of holoenzyme Demirci 2008
RimJ	pre-30S	'slightly altered ribosome profiles'	Cold-sensitive S5 mutant	Crystal structure of homologous holoenzyme Vetting 2005

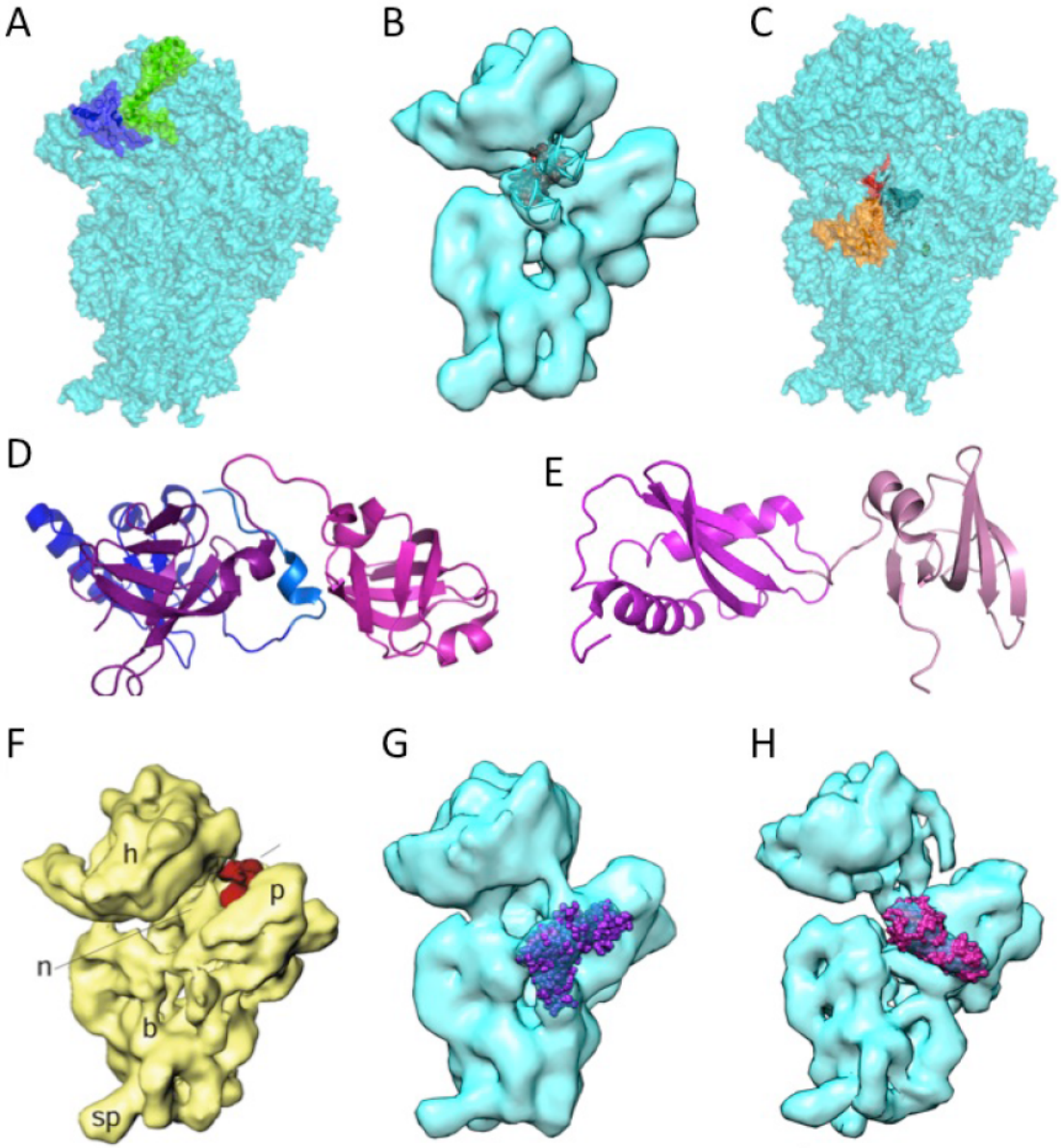

Figure 1.5: **The structure and site of activity for ribosome assembly factors.** Interface views of A) 30S crystal structure with RimM primary interaction partners S19 (blue) and S13 (green) PDB ID 2AVY B) Cryo-EM map of RbfA (brick red, underneath helices 44 and 45) bound to 30S ribosome EMD 1413 C) 30S crystal structure with RimP primary interaction partners S5 (red), S12 (orange) and central pseudoknot (black spheres). Crystal structures of D) RimM (purple and hot pink) with S19 (blue) in same orientation as in A, S19 C-terminus that is unstructured in ribosome structure is highlighted in light blue PDB 3A1P E) RimP N-terminal domain in magenta, C-terminal domain in pink PDB 1IB8. Interface views of Cryo-EM maps of F) Era (red) in complex with S1 depleted 30S subunit, figure from Sharma 2005 G) RsgA (purple) with GMPPNP bound to 30S subunit EMD1895 H) KsgA (red-purple) bound to 30S subunit EMD 2017. All cryo-EM map contour levels as recommended by authors.

evolved a ribosome assembly function distinct from that of methylation. Another rRNA methyltransferase, RsmC, has also been proposed to act as an assembly factor, but this has less experimental support. RimJ, the S5 acetylase, also seems to have a biogenesis role independent of its catalytic activity as an acetylase.

1.2.7.1 RimM

RimM is a 30S assembly factor that associates specifically with 30S subunits but not 70S particles (Bylund 1997). *ΔrimM* cells have a slow-growth phenotype (Bylund 1997), which can be ameliorated by overexpression of plasmid-encoded RimM (Loevgren 2001). *ΔrimM* cells accumulate immature 17S rRNA (Bylund 1998), and have an abundance of free 30S and 50S subunits and a depletion of 70S and polysome particles (Loevgren 2004).

Unfortunately, a cryo-EM structure of RimM in complex with 30S ribosomes has not yet been solved. However, the structure of free RimM from *T. thermophilus* solved by nuclear magnetic resonance spectroscopy revealed two domains: an N-terminal β-barrel fold and a C-terminal PRC-barrel (Suzuki 2007). The C-terminal domain showed pronounced chemical shifts upon binding with S19 of the head domain (Suzuki 2007). The structure corroborates the fact that S19 and helix 31or 33b mutations can ameliorate the *ΔrimM* slow-growth phenotype (Loevgren 2004). This structural information is substantiated by PC/QMS data showing that RimM accelerates the binding of S19 and S9 as well as modest effects on S10 and S3 (Bunner 2010). Interestingly, excess RimM may inhibit or occlude S12 and S13 binding, as shown in the reduced binding extent or those two r-proteins in the assay (Bunner 2010).

In addition, hydroxyl radical footprinting of *ΔrimM* immature particles reveals a perturbed structure. Helices 1, 2 and 44, as well as portions of the 3' major domain, are strongly solvent accessible in comparison to a WT 30S (Soper 2013). *ΔrimM* ribosomes lack all tertiary-binding proteins, and are low in S7, S5, S12, and S9 (Soper 2013). Interestingly, S18 is mostly unacetylated in *ΔrimM* ribosomes (Soper 2013). Cryo-EM maps of *ΔrimM* ribosomes lack electron density for helices 44 and 45 (Ortega 2013). Difference maps show low density for S2, S3, S7, S9, S11, S19, S14, S19 and S21 compared to the mature 30S (Ortega 2013).

1.2.7.2 RbfA

RbfA was originally discovered as a high copy number suppressor of a cold-sensitive mutation in helix 1 (Dammel 1993, 1995). RbfA interacts stably with helix 1 in free 30S subunits but not 70S ribosomes (Dammel 1995). *ΔrbfA* cells accumulate 17S rRNA, especially during cold shock, which can be suppressed by overexpression of plasmid-encoded RbfA (Xia 2003). *ΔrbfA* cells have an abundance of free 30S and 50S subunits and a depletion of 70S and polysome particles (Dammel 1995). Several mutations located throughout S5 can partially suppress the slow-growth and 70S depletion phenotypes of *ΔrbfA* but do not improve 17S processing (Nord 2015).

A cryo-EM structure of RbfA complexed to 30S ribosomes shows that RbfA binds to the important neck region of the 30S and displaces helix 44 and 45 (Datta 2007). RbfA is close to helices 1, 27, and 28 as well as r-proteins S12, S13, and S9 (Datta 2007). The fact that RbfA disrupts the A and P sites as well as inter-subunit bridges elucidates its role in preventing immature 30S particles from entering the translation pool (Datta

2007). This is supported by evidence that in *ΔrbfA* cells 17S pre-rRNA makes it into the polysome fractions (Soper 2013). In addition, the *ΔrbfA* immature particles have a perturbed structure. Helices 1, 2 and 44 are strongly solvent accessible in comparison to a WT 30S (Soper 2013). Furthermore, *ΔrbfA* ribosomes are missing S21, S2 and contain undermodified S5, that last of which is performed by the acetylase/assembly factor RimJ (Soper 2013).

1.2.7.3 RimP

RimP binds specifically to 30S subunits (Nord 2009). *ΔrimP* strains display an interesting heat-sensitive accumulation of 17S rRNA, which can be suppressed by overexpression of plasmid-encoded RimP (Nord 2009). *ΔrimP* cells have an abundance of free 30S and 50S subunits and fewer 70S and polysome particles (Nord 2009).

A cryo-EM structure of RimP in complex with 30S ribosomes has not yet been solved. However, the structure of a RimP orthologue from *Streptococcus pneumoniae* was solved by nuclear magnetic resonance spectroscopy, revealing two α/β domains (Yu 2001). The N-terminal domain is similar to the RNA-binding KH-domain structure of RbfA (Nord 2009). The functional interactions of RimP are unclear, but RimP does accelerate the binding of 5' domain/central pseudoknot proteins S5 and S12 and has modest effects on the 3' domain proteins S7, S9, S13, S3, S10, and S14 (Bunner 2010). Recent work shows that the central pseudoknot is not formed in more than 40% of *ΔrimP* ribosomes (Sashital 2014). *ΔrimP* ribosomes are missing S12, S2, S3, and S21 (Sashital 2014). Negative-stain EM density of *ΔrimP* ribosomes show an abundance of "floppy

head" particles in addition to more mature particles that only lack S21, S2, or S3 density (Sashital 2014).

1.2.7.4 Era

Era is an essential protein composed of an N-terminal GTPase domain and a C-terminal RNA-binding KH domain (Takiff 1989, Chen 1999). Era binds to deproteinized 16S rRNA and 30S subunits but not 50S or 70S subunits; co-sedimentation with 30S is inhibited by GTP, GDP, and GTPγS but not GMP (Sayed 1999). Depletion of Era leads to the accumulation of 17S rRNA (Inoue 2003). Depletion of Era also leads to an increase in free 30S and 50S subunits and a depletion of 70S and polysome particles, which can be ameliorated by overexpression of plasmid-encoded Era but not a cold-sensitive mutant of Era (Inoue 2003).

A cryo-EM structure of Era with S1-depleted 30S subunits, shows that Era binds to the neck of the 30S and induces a rotation of the head domain (Sharma 2005). The KH domain contacts helix 45 near the anti-Shine-Dalgarno sequence and other domains are near helices 23, 26, 28, and 37 and r-proteins S7, S18, S11 and S2 (Sharma 2005). In agreement with the cryo-EM structure, a crystal structure of Era bound to a helix 45 mimic showed strong, sequence specific interactions with the conserved 3' end of the 16S rRNA directly before the anti-SD sequence (Tu 2009). Recognition of the whole 3' end (including helix 45) stimulates GTP hydrolysis (Tu 2011). This structure hints at the role Era could have on aiding, regulating, or recognizing 3' end processing (Tu 2009). Interestingly, PC/QMS data shows that preincubation of 16S rRNA with Era accelerates

the binding of secondary proteins S5, S12, S11, and S9 as well as a subtle effect on S7, S13, S10 and S14 binding (Bunner 2010).

1.2.7.5 RsgA

RsgA/YjeQ is a non-essential yet conserved GTPase that binds stably to 30S ribosomes in the presence of the nonhydrolyzable analog GMP-PNP (Daigle 2004). The presence of 30S subunits greatly stimulates the rate of GTP hydrolysis (Daigle 2004). *ΔrsgA* cells accumulate 17S rRNA (Goto 2011). *ΔrsgA* cells exhibit a slow growth phenotype and a perturbed polysome profile with lots of free 30S and 50S subunits, and a reduction in 70S ribosomes, which can be overcome by overexpression of plasmid-encoded RsgA (Campbell 2008).

Mass spectrometry showed that *ΔrsgA* ribosomes have sub-stoichiometric amounts of r-proteins S7, S11, S5, S2, S3, S21, and S1 (Jomaa 2011). Cryo-EM structures of the RsgA 30S complex revealed a distorted electron density for helices 44 and 45 (Jomaa 2011). One cryo-EM structure of the RsgA 30S complex placed RsgA in the additional density with the oligonucleotide binding (OB) domain binding near S12 and helices 18 and 44 positioning the GTPase domain over helices 44 and 24 (Guo 2011). The C-terminal zinc-finger touches the head, specifically helix 29 and S13 (Guo 2011). The other structure flipped RsgA approximately 180 degrees such that the OB domain interacts with the platform, specifically helices 23 and 24, and the zinc-finger domain interacts with helix 44 (Jomaa 2011).

In order to resolve this conflict, the Ortega group began further biochemical studies, namely mutating residues predicted to be key for one structural model or the

other (Jeganathan 2015). Mutation of Lys 298 and Arg 300, predicted to be important by the Guo structure, had only a very mild decrease in RsgA binding (Jeganathan 2015). Deletion of the C-terminal alpha helix improved RsgA binding, but was unable to displace RbfA from mature 30S particles, and was toxic *in vivo* (Jeganathan 2015). The Jomaa structure places the C-terminal alpha helix along helix 44 where theoretically it could detect a mature conformation of helix 44, where as in the Guo structure the C-terminal alpha helix does not directly contact the 30S particle, making it difficult to explain its importance (Jeganathan 2015).

1.2.7.6 KsgA

In addition to KsgA's role as a methyltransferase, it also has a role as an assembly factor. KsgA associates specifically with 30S subunits but not 50S or 70S particles (Connolly 2008). Like other assembly factors, *ΔksgA* cells have a cold-sensitive phenotype and an accumulation of 17S pre-rRNA (Connolly 2008). *ΔksgA* cells have perturbed polysome profiles with lots of free 30S and 50S subunits, and a reduction in 70S ribosomes (Connolly 2008). Interestingly, overexpression of KsgA in the *ΔksgA* (or parental) strain has a deleterious effect; it increases the abundance of free 30S subunits and depletion of 70S ribosomes of the *ΔksgA* cells, likely due to dosage issues (Connolly 2008). Overexpression of the catalytically inactive mutant of KsgA exacerbates this depletion of 70S ribosomes, especially in the absence of any WT KsgA (Connolly 2008). One explanation for the fact that expressing inactive KsgA produces a more severe phenotype than completely lacking KsgA is that methylation is vital for KsgA release and

overexpressed inactive KsgA traps 30S particles in a translationally-inaccessible state (Connolly 2008).

A cryo-EM structure shows that KsgA binds to the platform of an unmethylated 30S subunit – helices 45, 27, and 24 specifically – and displaces helix 44 (Boehringer 2012). This indicates the importance of KsgA release for subunit joining and translation.

1.2.7.7 RsmC

RsmC is a methyltransferase that specifically methylates G1207 (Tscherne 1999). It has been suggested that it may play a role in ribosome biogenesis as RsmC is most active on reconstituted ribosomes at 0.9 mM Mg^{2+}, both higher Mg^{2+} and EDTA reduced activity, indicting it may act on pre-30S particles (Tscherne 1999). This substrate-specificity is also supported by the crystal structure of the ternary complex of *Thermus thermophilus* RsmC with AdoMet and guanosine is incompatible with the structure of the final 30S head (Demirci 2008). Mass spectrometric analysis of proteins associated with ribosomes in polysome profiles from exponentially growing wild-type *E. coli* detected RsmC in the lighter fractions of the 30S subunit (Chen 2013). Mass spectrometric analysis reveals methylation of G1207 occurs late during assembly (Siiback 2010). Neither the deletion nor the overexpression of RsmC had any effect on the cold-sensitive phenotype of an IF1 mutant that is suppressed by an adjacent nucleotide G1206A (Belotserkovsky 2011). But, to my knowledge no other studies on the effects of RsmC deletion or overexpression have been published.

1.2.7.8 RimJ

RimJ's role as an assembly factor was discovered when RimJ was identified as a high-copy suppressor of the cold-sensitive phenotype and ribosome biogenesis defects of an S5 mutant (Roy-Chaudhuri 2008), Even a catalytically inactive mutant of RimJ was able to ameliorate the assembly defect (Roy-Chaudhuri 2008). RimJ associates with light pre-30S subunits (Roy-Chaudhuri 2008). This, along with evidence that it does not acetylate free (overexpressed) S5, suggests it both acetylates and performs its ribosome assembly factor functions in the context of the pre-30S particle (Soper 2013). Additionally, non-acetylated S5 binds to the assembling ribosome at a faster rate than acetylated S5; this suggests a sequential S5 binding-modification path (Talkington 2005). The deletion of RimJ slows growth slightly and mildly perturbs polysome profiles (Roy-Chaudhuri 2008). A crystal structure of the homologous RimL from *Salmonella typhimurium* has been solved (Vetting 2005); however, the dimerization and r-protein-recognition surface is located in the divergent N-terminal domains (Nesterchuk 2011).

1.2.7.9 Ribosome assembly factor compensation network

Interestingly, many ribosome assembly factors can partially compensate for depletion of another assembly factor suggesting a complex web of partially overlapping functions (Figure 1.6). For example, RbfA overexpression can partially compensate for the deletion of RimM, but the converse is not true (Bylund 1998). Era overexpression can partially compensate for the deletion of RbfA, but the converse is not true (Inoue 2003). Also, Era overexpression can fully compensate for RsgA/YjeQ deletion, while deletion of KsgA and RimM exacerbates the slow growth phenotype of *ΔrsgA* (Campbell 2008).

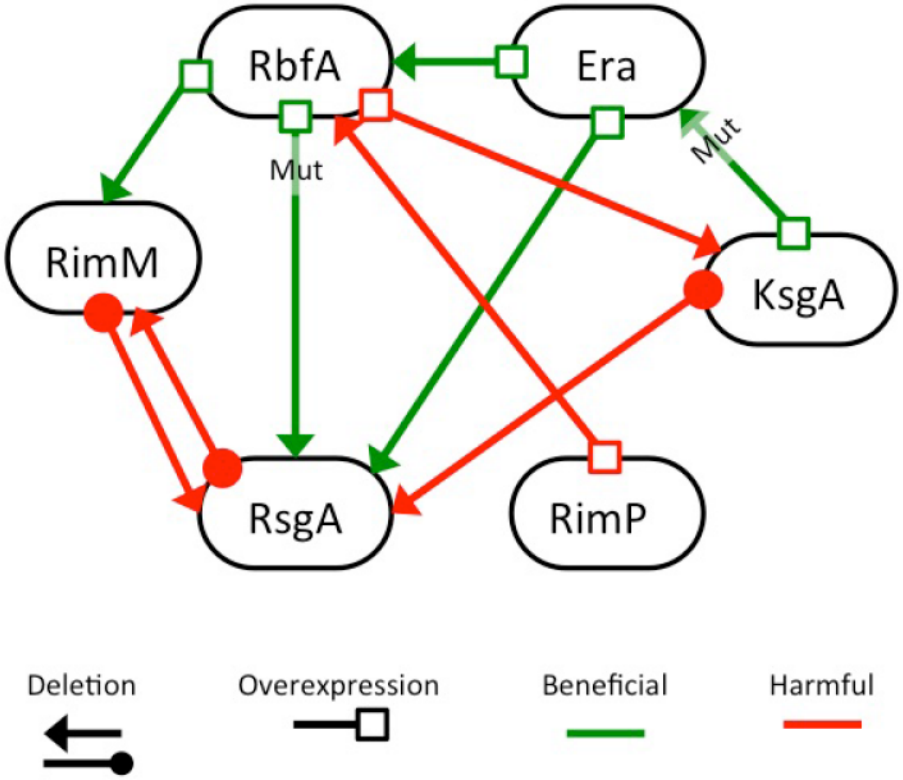

Figure 1.6: **Ribosome assembly factor compensation network.** Diagram of beneficial and harmful interactions of ribosome assembly factors. Overexpression or deletion of one assembly factor can ameliorate (green) or exacerbate (red) the phenotype of another assembly factor. Assembly factor deletions are indicated by a shaded arrow or circle. Assembly factor overexpression are indicated by an open square. Mutant specific effects are labeled "Mut". Figure adapted from Shajani 2011.

Conversely, overexpression of RbfA exacerbates the *ΔksgA* phenotype (Connolly 2013). Overexpression of RimM, RbfA, Era, KsgA, and RsgA fail to suppress the slow growth phenotype of the *ΔrimP* strain (Nord 2009). Interestingly, overexpression of RimP is lethal to a *ΔrbfA* strain (Nord 2015). RsgA/YjeQ is involved in the release of RbfA from 30S subunits and overexpression of RbfA mutants that bind less tightly to 30S particles can partially compensate for *ΔrsgA* (Goto 2011). To add even more complexity to this web of ribosome assembly factor interactions, overexpression of KsgA can suppress a cold-sensitive mutant of Era (Lu 1998). This independence and partial complementarity of ribosome assembly factors is just another indication that ribosome biogenesis is complex with multiple parallel pathways and many small troublesome spots instead of one main bottleneck.

1.2.8 Quality control is a critical part of ribosome biogenesis

Since transcription of the 5.5 kbp *rrn* operon and synthesis of the ~55 r-proteins is so costly, ribosome biogenesis must be efficient despite the vast complexity outlined above. Incorrectly assembled ribosomes are, at the minimum, a huge waste of resources and can possibly lead to error-prone translation. Increasing translation errors to produce toxic 'junk' proteins is mechanism of several aminoglycoside antibiotics (Davies 1965). However, not much is known about the process of recognizing and degrading incorrectly assembled ribosomes.

The most thoroughly understood aspect of ribosome turnover is the process of degrading functional ribosomes during starvation or stress conditions (reviewed in Deutscher 2009 and Maiväli 2013). During normal laboratory conditions ribosome turnover is most prevalent during the slow-down immediately preceding stationary phase; during log growth and stationary phase ribosome degradation is less common (Piir 2011). During stressful conditions, the cell membrane can be affected, leading to the introduction of the periplasmic nonspecific endoribonuclease RNase I, which is quite effective at recycling ribosomes *in vitro* (Deutscher 2009).

During glucose starvation the exoribonucleases RNase PH, RNase II, and RNase R are vital for complete degradation of rRNA fragments (Basturea 2011). Endonucleolytic cleavage near the central pseudoknot between A919 and U920 could be detected in cells lacking RNase II, RNase R and greatly reduced PNPase during both starvation and normal conditions (Basturea 2011). The identity of this endonuclease is a mystery. In fact, initiation of ribosome degradation by endonucleases during stress conditions is one big open question.

Recent work on YbeY, a heat shock protein with single-strand specific endoribonuclease activity, revealed a new ribosome quality control pathway (Jacob 2013). YbeY, when combined stoichiometrically with the exoribonuclease RNase R, selectively degrades 70S ribosomes with defective 30S subunits, even those found in polyribosomes (Jacob 2013). 70S ribosomes with defective 50S subunits and individual 30S and 50S subunits are not YbeY/RNase R targets (Jacob 2013). Deletion of YbeY leads to poor processing of 16S, 23S, and 5S rRNAs (Davies 2010), but even ribosomes with mature rRNA purified from *Δybey* strains are targets for YbeY degradation (Jacob

2013). How YbeY/RNaseR recognizes the *Δybey* 30S ribosomes is an open question, as is how YbeY/RNaseR can physically degrade 70S ribosomes. Interestingly, YbeY also recognizes and degrades 70S ribosomes isolated from kasugamycin-treated *E. coli* (Jacob 2013). Treatment with kasugamycin produces aberrant 30S subunits lacking S12, S6, S18, S2, and S21 as well as having a malformed central pseudoknot (not protected from DMS modification, Kaberdina 2009). These aberrant 30S subunits are still found in 70S-like 61S particles that can somehow effectively translate leaderless mRNAs (Kaberdina 2009).

Even less is known about a quality control pathway that recognizes incorrectly assembled 50S subunits. Recent work on several different 23S rRNA mutants revealed half were stable and half led to the degradation of both 16S and 23S rRNA plasmid-derived rRNA (Paier 2015). Four mutations were selected to destabilize intersubunit bridges. Three mutations destabilized B2a; A1919G led to degradation while the deletion of helix 69 and A1912G were stable. A1960G, which destabilized B3, led to degradation (Paier 2015). Why A1919G led to ribosome degradation while A1912G was stable is still an open question (Paier 2015). Interestingly, the mutant 23S rRNAs also led to an increased degradation of WT 50S subunits in addition to WT 30S subunits (Paier 2015). This degradation of 50S (or 30S) ribosomes did not occur when protein synthesis was halted, indicating a 70S or polysome-dependent pathway for the removal of defective 50S ribosomes, in a similar manner as with YbeY-dependent 30S degradation (Paier 2015). The mechanism for faulty 50S degradation is as of yet unknown, but the authors propose the expression of a quality-control endoribonuclease to explain the degradation of the WT 50S subunits as well (Paier 2015).

Since the YbeY/RNase R quality control pathway, and possibly the 50S quality-control pathway, work at the 70S ribosome stage, there must be another, earlier quality-control pathway that works on ribosomal precursors stuck at some earlier stage of assembly that are physically unable to form 70S particles.

It has been proposed that ribosomal precursors can be eliminated in fast-growing *E. coli* by degradosomes. Analysis of the RNA components of FLAG-tagged RNase E affinity-purified degradosomes showed a preponderance of 16S and 23S rRNA fragments (Bessarab 1998) likely due to their relative abundance, thus degradosomes degrade both "stable" rRNA and mRNA. The degradosome consists of RNase E (an endonuclease), polynucleotide phosphorylase (PNPase), and a DEAD-box helicase RhlB. Even without inorganic phosphate and ATP to permit PNPase and helicase activity, RNase E-containing degradosomes were effective at degrading rRNA but not tRNA *in vitro* (Bessarab 1998). The precise mechanism and regulation of pre-ribosome degradation is unknown, but it could require polyadenylation and degradation of endonuclease-cut anomalous particles in a manner homologous to the degradation of yeast pre-ribosomes by the TRAMP complex and the exosome (Maiväli 2013).

Degradation of aberrant or stalled ribosomes is still an area of ongoing research with many open questions, but what is not in question is how important this process is to understanding ribosome biogenesis. Many approaches to studying ribosome biogenesis *in vivo* involve enriching the pool of ribosomal assembly intermediates by perturbing assembly (Chapter 3), and determining if these particles are on-path or destined for degradation is a critical step to understanding how the fundamental protein-producing machinery gets made.

1.3 Specific Aims

The general goal of my work is to better understand ribosome assembly, especially the early stages of ribosome assembly. The specific goal of my thesis is to understand the role of the helix 5/6 junction upon 30S ribosome assembly. The bacterial 16S rRNA encodes a highly conserved Right Angle motif between helices 5 and 6; however, those helices do not form a Right Angle in 30S crystal structures, as helix 6 interacts with helix 15. This raises the question as to whether or not some RNA sequence motifs are conserved because they form metastable structures during ribosome assembly.

I studied a selection of J5/6 mutants predicted to destabilize this predicted Right Angle Motif intermediate state without interfering with the final assembled state. Along the way I have pursued several sub-aims: can the J5/6 mutants fold and assemble correctly *in vitro*, do the J5/6 mutants affect ribosome biogenesis, and what is the structure of the mutant ribosomes *in vivo?*

I have found some modest *in vitro* assembly abnormalities, which are unable to fully explain the severe ribosome biogenesis defects of the J5/6 mutants. Additionally, the mutants cannot be rescued by growth conditions or the overexpression of ribosome assembly factors. I have made significant progress in troubleshooting a method for affinity purifying mutant ribosomes out of a heterogeneous mixture after *in vivo* hydroxyl radical footprinting. I have also determined the solvent accessible surface area of the 3' head domain of the J5/6 Triple mutant via allele-specific primer extension from *in vivo* hydroxyl radical footprinted samples.

Chapter 2: *In vitro* assembly of *E. coli* 5' domain with J5/6 mutations

2.1 Introduction

RNA structural motifs are found throughout the rRNA and help to fold it into a compact, native state (Noller 2005). For example, the A-minor motif is a simple RNA structural element found throughout the 16S and 23S rRNA (Nissen 2001). The A-minor motif consists of a single-stranded adenosine bound in the minor groove of a neighboring Watson-Crick pair (Cate 1996). Typically both the base and the ribose of the adenosine are involved in making tight van der Waals contacts and several hydrogen bonds with at least one of the Watson-Crick 2' OH.

A more complex RNA motif, the Right Angle motif, was identified by Luc Jaeger (Chworos 2004, Grabow 2012). The Right Angle motif is made up of an along-groove stacking interaction between neighboring helices, and is held together and stabilized by two A-minor motifs. The along-groove stacking motif packs the backbone of two RNA helices in the minor groove of the other and is found in four locations in the 16S rRNA; helix 6 with helix 15; helix 3 with helix 12; helix 3 with helix 18; and helix 20 with helix 25 (Gagnon 2002). The Right Angle motif is found between helix 18 and helix 3 and between helix 5 and 6 in the 16S rRNA, among others (Figure 2.1). Interestingly, though the H5/H6 junction consists of the consensus sequence of the Right Angle motif, it does not form a Right Angle motif in fully assembled ribosomes (Figure 2.1). Instead the tip of

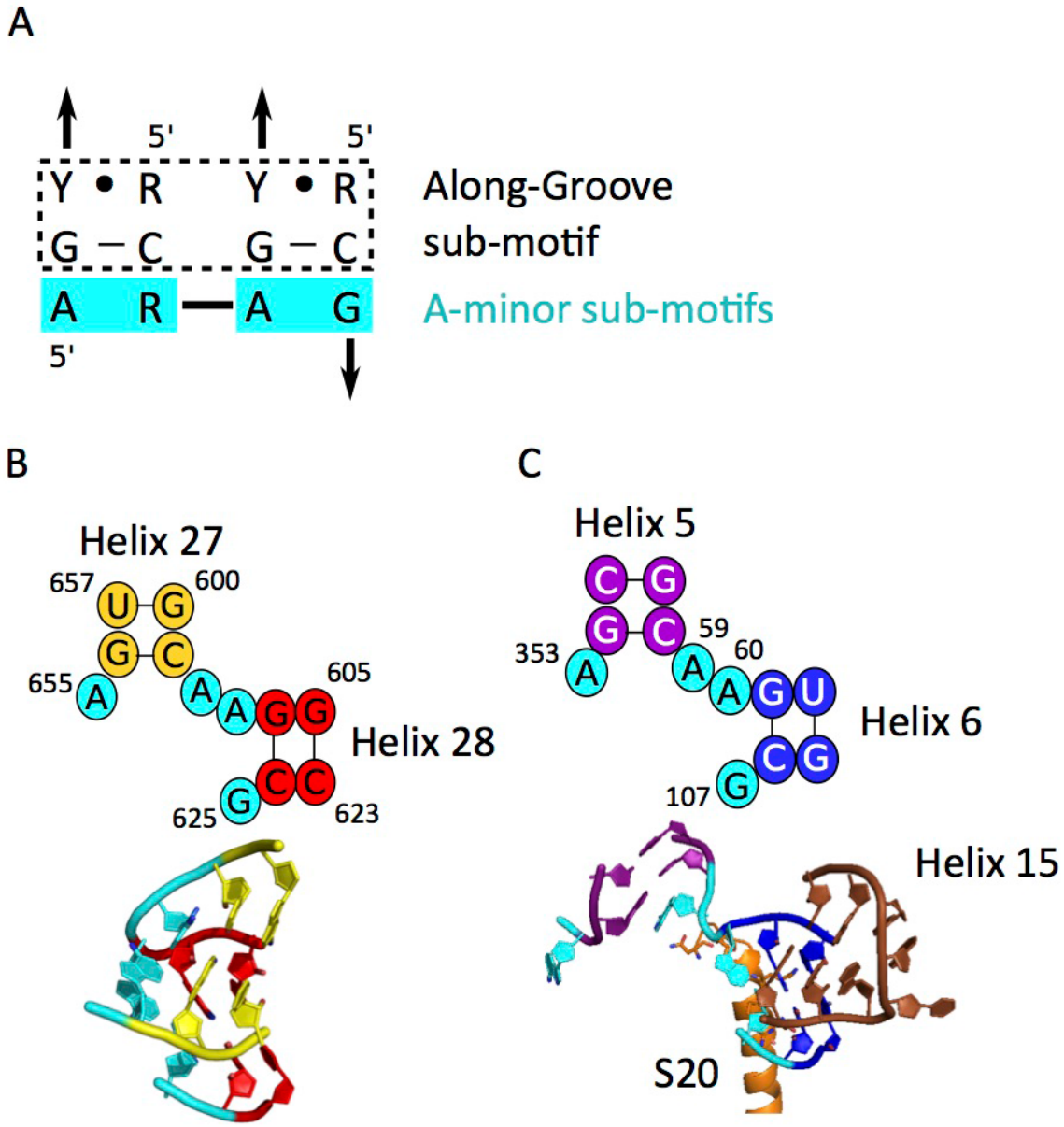

Figure 2.1: **The sequence and structure of the junction of helices 5 and 6.** A) Consensus sequence for the Right Angle motif (from Grabow 2012). Dashed box highlights the Along-Groove stacking portion of the Right Angle motif. Cyan boxes indicate the two A-minor sub-motifs of the Right Angle motif. B) Secondary and tertiary structures of a canonical right angle motif located between helix 27 (yellow) and helix 28 (red) in the 23S rRNA. Junction/A-minor motif resides are in cyan. C) Secondary and tertiary structures of the helix 5-6 junction. Secondary structure of the helix 5/6 junction with sequence information for helix 5 (purple), helix 6 (blue) and the junction residues (cyan). Helix 5 interacts with the tip of helix 15 (brown) via the Along-Groove stacking motif. The N-terminus of S20 (orange) wedges up against the major grove of helix 5. (PDB 2AVY).

helix 15 interacts with the along-groove stacking surface of helix 6. The J5/6 region Right Angle motif consensus sequence is completely conserved throughout Bacteria and Archaea (Grabow 2012) and the isolated *E. coli* J5/6 region sequence forms a Right Angle motif in a model *in vitro* system (Grabow 2012). Additionally, the helix 6-helix 15 along-groove stacking interaction is conserved in all known ribosome structures, including the mitochondrial ribosome which has a short, almost vestigial helix 6 (Schuwirth 2005, Ben-Shem 2010, Armache 2012, Weisser 2013, Voorhees 2014, Greber 2015). In the higher eukaryotes an adenine from helix 15 base pairs with a uracil in helix 6, further stabilizing this interaction. However, our initial hypothesis is that at some stage in ribosome biogenesis helices 5 and 6 form a right angle, which later undergoes a conformational switch to the structure observed in the mature ribosome.

Earlier data suggest that J5/6 of the 16S 5' domain is an important region during 30S assembly. It is one of the slowest regions of the 5' domain to fold in 20 mM Mg^{2+}, indicating the possible role of S17, S20, and S16 binding in correcting or guiding these non-native intermediates (Figure 2.2, Adilakshmi 2005). Also, tethered Fe(II) hydroxyl radical probing of regions near the N-terminal alpha helix of S20 revealed intriguing cleavages in the region unique to assembly intermediates (Dutca 2008). Interestingly, cleavages in the J5/6 region (nt 56-63 and 354-357) not present in the minimal 16S•S20 RNP or the full 30S appear in 16S•S20+S17 RNPs, and the addition of S16 was sufficient to eliminate these intermediate cleavages to produce the cleavage pattern of the complete 30S. Dutca and Culver postulate that the r-protein S16 binding packs helix 15 against helix 5, (also seen in Stern 1988a). Additionally, they propose that the N-terminal helix of S20 may structure at some point during assembly.

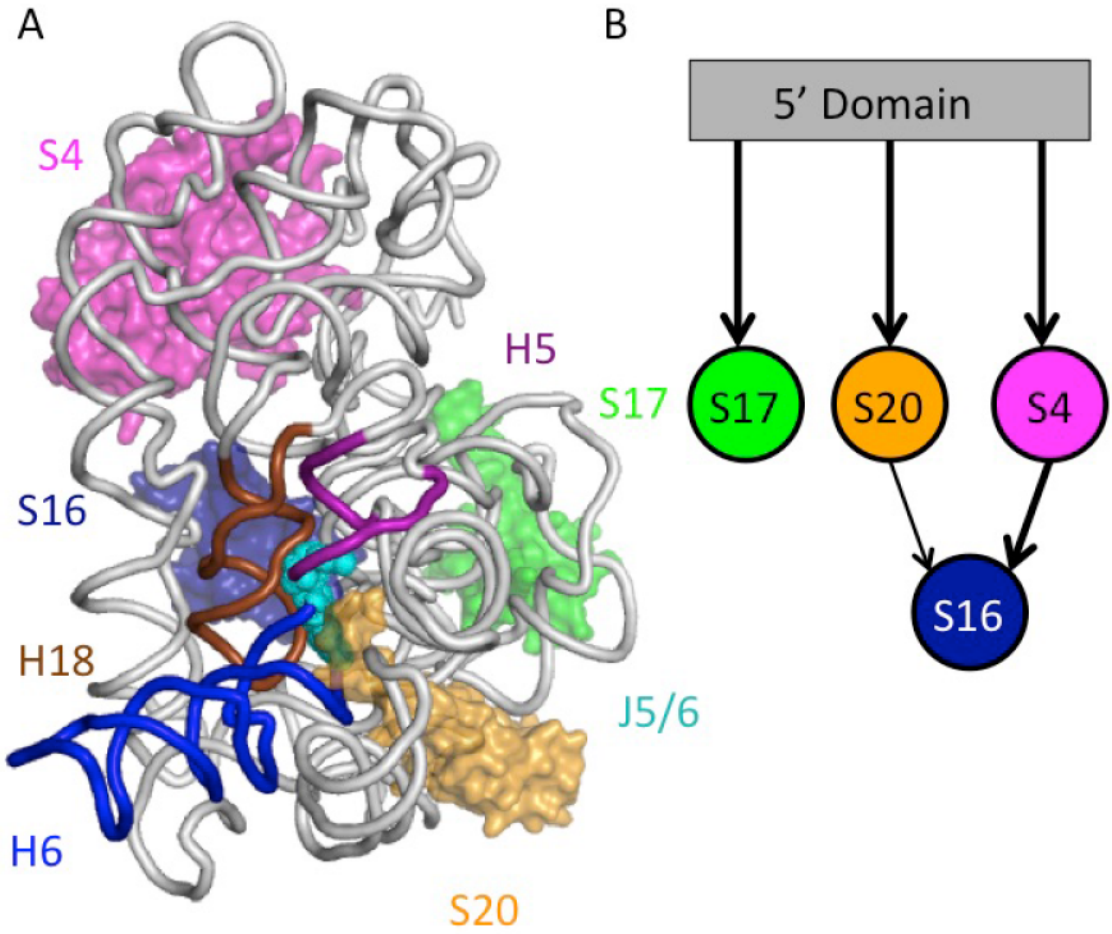

Figure 2.2: **The structure of the 16S rRNA 5' domain.** A) Ribbon of the 5' domain with helices and J5/6 residues colored as in Fig. 2.1, from PDB 2AVY. Primary r-proteins S4 (pink), S17 (green), and S20 (orange) and secondary r-protein S16 (dark blue) are shown as semi-transparent surfaces. B) *In vitro* assembly map of the 5' domain (Held 1974). The primary assembly proteins bind stably and independently to the rRNA, and are colored as in A. S16 requires the presence of one or more of the primary proteins to bind stably.

These data suggest that the junction between helices 5 and 6 can adopt multiple conformations during assembly, and it needs the secondary r-protein S16 to achieve its native conformation. S16 is also required to stabilize the native conformation of helix 3, which is critical for allowing the central pseudoknot and proper domain-domain interactions to form during 30S assembly (Ramaswamy 2009b). This provided further motivation for exploring if the J5/6 Right Angle motif was required during an early stage of ribosome assembly and if perturbing this region would cause assembly defects.

Earlier work by Grabow et al. identified mutations that destabilize the Right Angle motif (2012). We selected some of these mutations that were not predicted to affect the final structure of the J5/6 region in the 30S ribosome. J. Morrell incorporated three of these mutations – G107U, A59,60C, and a A59,60C, G107U Triple mutant – into the 16S rRNA 5' domain. Then I assayed their affect on 5' domain folding, r-protein association, and the structure of assembled 5' Domain RNPs. I discovered mild defects such as a greater dependence on Mg^{2+} when folding in low K^{+}, local structural perturbations, and interestingly a stabilization of a non-native conformation of helix, but these mild defects do not explain the pronounced phenotypes seen *in vivo* (Chapter 3).

2.2 Materials and Methods

2.2.1 Generation of J5/6 mutants

J. Morrell introduced G107U, A59,60C, and A50,60C G107U J5/6 mutations into the transcription vector pRNA1 (which contains the *E. coli* 16S 5' domain sequence, Adilakshmi 2005) using Quikchange (Stratagene) and primers **G107U Fwd, G107U Rev, A59,60C Fwd A59,60C Rev** (Table 2.1). The Triple mutant was generated by two rounds of Quikchange.

2.2.2 rRNA preparation

The 16S rRNA 5' domain (nucleotides 21-562, plus an additional G on the 5' end), with or without the J5/6 mutants, was transcribed from an EcoRI (NEB) linearized pRNA1 plasmid DNA (Adilakshmi 2005) linearized with *Eco*RI (NEB), or from a PCR template generated using standard methods {primers?}. Briefly, 10 µg linearized plasmid DNA or 5 µg PCR template was combined with 1 mM each NTP and 5 µl T7 RNA polymerase in T7 Buffer (40 mM Tris-HCl pH 7.5, 15 mM $MgCl_2$, 2 mM spermidine, 5 mM DTT) for 2 mL reaction at 37°C for 2 hours. The transcribed RNA was ethanol precipitated and purified on a 4% polyacrylamide gel containing 1X TBE (89 mM Tris, 89 mM boric acid, 3 mM EDTA) and 8 M urea. If the eluted RNA was needed for SHAPE experiments, it was subsequently extracted with phenol and chloroform once and purified through a ChromaSpin TE-100 size exclusion column (Clontech).

For EMSA assays that needed uniformly radiolabeled rRNA; the transcription

Table 2.1: **Quikchange primers and primers used for fluorescence.** The sequences of the primers used in cloning the J5/6 mutants are shown. Capital text shows the location of the mutations/insertions. Underlined text illustrates site of primer annealing. The Triple mutant A59,60C G107U was made by two rounds of Quikchange with the primers.

Mutation	Primer	Sequence
G107U	Fwd	ttgctgacgagtggcTgacgggtgagtaatg
G107U	Rev	cattactcacccgtcAgccactcgtcagcaa
A59,60C	Fwd	gcaggcctaacacatgcCCgtcgaacggtaacagga
A59,60C	Rev	tcctgttaccgttcgacGGgcatgtgttaggcctgc
Helix 6 extension	Fwd	cggtaacaggaagaaGCGCGTCGCCAGACCAGACGC TCCGCGcttctttgctgacg
Helix 6 extension	Rev	cgtcagcaaagaagCGCGGAGCGTCTGGTCTGGCAC GCGcttcttcctgttaccg
Helix 10 extension	Fwd	caaagagggggaccCGCGGTAAGCGACGGTAGCAC GACGcgggcctcttgcc
Helix 10 extension	Rev	ggcaagaggcccgCGTCGTGCTACCGTCGCTTACCG CGGgtccccctctttg
SA5		cctgtgtcctgtgtgtcctgtccaaa-Fluorophore
Helix 6 RNA primer		cggagcgucuggucug
Helix 10 RNA primer		ucgugcuuaccgucg

reaction was scaled down to 40 µL with 5 µL (10 µCi/µL) α- ^{32}P-ATP (3000 Ci/mmol, Perkin Elmer). 1 µg linearized plasmid and 1 µl T7 RNA polymerase was used, and the reaction was transcribed at 37°C for 30 minutes. The transcript was purified through a ChromaSpin TE-100 column. Total counts were obtained using scintillation counting.

2.2.3 Nondenaturing electromobility shift assays

For equilibrium studies with Mg^{2+}, 150,000 cpm uniformly radiolabeled 5' domain was incubated 30 minutes in 4 µL HKE Buffer (8 mM K-Hepes pH 7.5, 33 mM KCl, 0.1 mM EDTA) with varying concentrations of $MgCl_2$ (0-200 mM). Immediately prior to loading, 2 µL Loading Dye (50% glycerol, 0.25% xylene cyanol dye) was added and 2 µL mixture was loaded onto a native 8% polyacrylamide gel in THEM10 (34 mM Tris pH 7.5, 66 mM Hepes pH 7.5, 0.1 mM EDTA, 10 mM $MgCl_2$). Gels were run at 15 W/gel for 5-6 hours at 4°C. Gels were dried, imaged and quantitated using a phosphorimager (Molecular Dynamics). Data were fit to a 2- or 3-state Hill equation using Kaleidgraph (Synergy):

$$f(x) = y_0 + y_1[([Mg^{2+}]/C_{m1})^{n1}/(1+([Mg^{2+}]/C_{m1})^{n1})] +$$

$$y_2[([Mg^{2+}]/C_{m2})^{n2}/(1+([Mg^{2+}]/C_{m2})^{n2})]$$

in which y_0, y_1, and y_2 represent the amplitudes of each transition, C_{m1} and C_{m2} are the magnesium concentrations at which one half of the RNA has folded to this stage, and n_1 and n_2 represent the cooperativity of each folding transition.

For kinetics studies, 75,000 cpm/µL uniformly radiolabeled 5' domain RNA in 28 µL HKE Buffer was incubated at 25-47°C. 2 µL $MgCl_2$ was added to bring the master mix to a final concentration of 10 mM $MgCl_2$. 2 µL aliquots were removed at specific

intervals (15 seconds to 120 minutes) mixed with 2 µL Loading Dye, and loaded onto a THEM10 8% polyacrylamide gel. Gels were run at 15 W/gel for 5-6 hours after the last time point. Data were fit using a one or two exponential rate equation:

$$f(x)=y_0 + y_1(1 - e^{(-k1\ t)}) + y_2*(1 - e^{(-k2\ t)})$$

in which y_0, y_1, and y_2 represent the amplitudes of each transition, and k1 and k2 are the rates of each folding transition.

2.2.4 SHAPE chemical probing

4 pmol 5' dom-1199 rRNA (5' domain with a 3' 1199 extension, Mayerle 2011) with and without the J5/6 mutants was pre-folded for 15 minutes at 37°C in HKM20 Buffer (80 mM K-Hepes pH 7.5, 330 mM KCl, 20 mM $MgCl_2$). After pre-folding, 8 µl Binding Buffer (80 mM K-Hepes pH 7.5, 330 mM KCl, 20 mM $MgCl_2$, 0.01% Nikkol, 6 mM β mercaptoethanol); or Binding Buffer containing 16 pmol S4; 16 pmol S4, 40 pmol S17, and 20 pmol S20; or with 16 pmol S4, 40 pmol S17, 20 pmol S20, and 20 pmol S16 was added and incubated for 45 minutes at 37°C. These 1:4:10:5:5 ratios were empirically determined by test SHAPE titrations (data not shown).

After protein incubation, 2 µl extra dry dimethylsulfoxide (DMSO; Acros Organics 326881000) or 30 mM N-methylisatoic anhydride (NMIA) in extra dry DMSO was added and incubated for 5 half-lives (45 minutes) at 37°C (Wilkinson 2006). The r-proteins were removed from modified rRNA by three phenol extractions, two chloroform extractions, and ethanol precipitation with 0.3 M sodium acetate and 1 µl 20 mg/ml glycogen carrier.

Primer extension reactions using fluorescently labeled primers **323** and **1199** (Table A.3) were set up as previously specified (Vasa 2008). Briefly, 1 pmol modified rRNA was combined with 1.2 pmol D4-labeled primer and 1 pmol mock-treated 5' dom-1199 rRNA was combined with 1.2 pmol D3-labeled primer. The reactions were heated to 65°C for 5 min and then incubated on ice for more than 1 minute. First Strand Buffer (for SuperScript III Reverse Transcriptase from Invitrogen), 1.5 mM dNTPs (final), 5 mM DTT (final) and 50 U SuperScript III Reverse Transcriptase (Invitrogen) were added to each reaction. Reactions were incubated at 55°C for 45 min. In parallel, a large reaction of an IR800-labeled ddCTP sequencing ladder and a D2-labeled ddGTP sequencing ladder were prepared as above, 24 pmol unmodified 5' dom-1199 rRNA was combined with 29 pmol primer, 15 µl 5 mM indicated ddNTP, 1 mM dNTPs (final), First Strand Buffer, 5 mM DTT (final), and 50 U SuperScript III Reverse Transcriptase.

For each RNP condition, I combined 15 µl each the four reactions above in a well of 96-well tray (D4-labeled cDNA library prepared from the NMIA modified 5' dom-1199 rRNA, D3-labeled negative control cDNA library, IR800-labeled ddCTP sequencing ladder, and a D2-labeled ddGTP sequencing ladder). 180 µl 100% ethanol and 6 µl 3M sodium acetate were added to each well to precipitate the cDNA overnight at -20°C. The 96-well tray was centrifuged for 1 hour at 6,100 x *g* in a swinging bucket JS-5.3 rotor (Beckman-Coulter). The supernatant was carefully decanted, then 100 µl ice-cold 75% ethanol was added to further wash the cDNA pellets. After 15 min incubation on ice, The 96-well tray was centrifuged for 15 minute at 6,100 x *g*. The salty-ethanol supernatant was carefully decanted and the 96-well tray was dried under vacuum for 10 minutes (SpeedVac, Savant). The dry fluorescent pellets were protected from light and

resuspended in Sample Loading Solution (Beckman Coulter) prior to being run on a CEQ800 (Beckman Coulter).

2.2.5 Analysis of SHAPE data

The raw CEQ traces were processed with ShapeFinder to determine peak areas for each 5' domain nucleotide (Vasa 2008). The peak area for the negative control was subtracted from the peak area for the NMIA-treated rRNA to determine the SHAPE reactivity of each nucleotide. Occasionally the peak areas from the negative control needed to be rescaled to adjust for user error in the ShapeFinder scaling process and to minimize the number of nucleotides with negative reactivities in each trace after background subtraction. This scaling factor was adjusted so the average of the bottom 10% peak areas equaled approximately 0. The values were further normalized such that the average of the 92-97 percentile peak areas equaled 100. Due to the limited range of linearity for the CEQ800 CCD camera, the peak areas of the top 3% were irreproducible from run to run and well to well and were discarded. Nucleotide reactivity values from the region of overlapping primers **323** and **1199** were scaled slightly to minimize the difference between the two traces. Further processing of this data is outlined in the results section.

2.2.6 S20 EMSA assays

EMSA co-localization assays were performed by S. Abeysirigunawardena using Cy3-labeled SA5 oligonucleotide (Table 2.1) annealed to the 5' domain rRNA with a 3'

helix 3 extension (5'dom-h3, Kim 2014), with and without J5/6 mutations by incubating at 70°C for 5 min in HK Buffer (80 mM K-Hepes pH 7.5, 330 mM KCl) followed by 25°C for 5 min. $MgCl_2$ was added to bring the solution up to 20 mM $MgCl_2$ before varying concentrations of S20 labeled at position 23 (S23C) with Cy5 (0-100 nM) were added and incubated at 37°C for 15 min. S20-RNA complexes were resolved on a 8% native TBE polyacrylamide gel. The gels were imaged using a Typhoon scanner with multiple excitation channels (Amersham Biosciences). The fraction of RNA complexed with S20 was estimated from co-migration of Cy3 and Cy5 signals in the gel.

2.2.7 Ensemble FRET

Ensemble FRET experiments were performed as described in (Abeysirigunawardena, paper in press). Briefly, Cy5-labeled SA5 primer was annealed to 5'dom-h3 rRNA (J5/6 mutant or WT) by incubating at 70°C for 5 min in HK Buffer (80 mM K-Hepes pH 7.5, 330 mM KCl) followed by 25°C for 5 min. The volume was brought up to 500 µL in Binding Buffer and the labeled RNA was pre-folded at 37°C for 15 minutes before titration with Cy3-labeled S4 (C32S, S189C). The data were fit to a complex quadratic equation due to the high affinity of S4 for the 5' domain (0.2 nM; S. Abeysirigunawardena, paper in press) and the four state model of S4 binding and helix 3 flipping as derived by S. Abeysirigunawardena (paper in press):

$$E_{FRET} = \left(E_N + E_F K_2\right)\frac{\left\{\left(R_T + S_T\right)\left(1+K_2\right)+\beta\right\} - \sqrt{\left\{\left(R_T + S_T\right)\left(1+K_2\right)+\beta\right\}^2 - 4\left(1+K_2\right)^2 R_T S_T}}{2R_T\left(1+K_2\right)^2}$$

where E_N was set to 0.18 and E_F was set to 0.02. R_T is the total concentration of RNA, and S_T is the total concentration of S4, the titrant. K_2 is the equilibrium constant between

the two S4•rRNA complexes (helix 3 flipped out and helix 3 in the native state). β is a fitting parameter that takes into account both the equilibrium constant of S4 binding to the native state of helix 3 and the equilibrium constant of conformational equilibrium in the unbound state.

2.2.8 H6-H10 FRET primer design and testing

Unstructured extensions to 16S helix 6 and helix 10 were designed by S. Abeysirigunawardena based on previous work (Dorywalska 2005). Using inverse PCR S. Abeysirigunawardena added the helix 10 extensions to pRNA1 (Table 2.1 for primers). Subsequently, I added the helix 6 extensions to pRNA1-H10B using inverse PCR. Once the clone with both helix extensions was generated and sequenced, I added the G107U and A59,60C mutations to pRNA1-H6A+H10B using standard Quikchange. The Triple mutant was generated by two rounds of Quikchange.

For determining optimal primer binding conditions, varying concentrations (0.1 to 100 nM) unlabeled 5'dom-h6,h10 rRNA was mixed with 0.5 nM ^{32}P-labeled Helix 6 or Helix 10 RNA primers (Table 2.1 for sequences) in HK Buffer. Three different denaturing temperature were tested: 65°C for 10 min, 55°C for 10 min, and 37°C for 10 min followed by annealing at 25°C for 5 min. 65°C was marginally better. After annealing, $MgCl_2$ was added to bring each sample to a final concentration of 4-40 mM $MgCl_2$, and the 5' domain was pre-folded for 20 minutes at 37°C. The proportion of annealed primer was assessed by native EMSA on 6% THEM10 gels run 90 minutes at 15W/gel. Data were fit to a Langmuir binding equation

$$F_B = ([RNA]/K_d)/(1+[RNA]/K_d).$$

To test for anti-cooperativity, the opposite unlabeled primer was added in the same concentration as the 5'dom-h6,h10 rRNA. To measure the rate of dissociation, I combined 5 nM 5'dom-h6,h10 rRNA with 100 nM ^{32}P-labeled Helix 6 or Helix 10 primers. I annealed the primer at 65°C for 10 min in HK Buffer and 25°C for 5 min. I ran the mixture through a HKM20 equilibrated TE-100 size exclusion column and then incubated the mixture at 37°C. Aliquots were removed at specific intervals (1 to 60 min) and loaded onto a THEM10 6% polyacrylamide gel. Gels were run at 15 W/gel for 5-6 hours after the last time point. The appearance of free primer was fit to a double or single exponential

$$f(x)=(1- y_1)(1 - e^{(-k1\ t)}) + y_1(1 - e^{(-k2\ t)})$$

in which y_1 represents the amplitudes of second transition, and k1 and k2 are the rates of dissociation.

2.3 Results

2.3.1 rRNA folding of the J5/6 mutants

In order to determine how the J5/6 mutants changed the stability of 16S rRNA 5' domain, I performed equilibrium Mg^{2+} titrations and measured the fraction of folded RNA by native gel electrophoresis (Figure 2.3). In 33 mM KCl, the WT 5' domain folded with $C_{1/2}$ = 0.4 ± 0.1 mM Mg^{2+}The J5/6 Triple mutant folded with at least one intermediate species until it reached a state with the same electrophoretic mobility as the folded WT 5' domain (Figure 2.3 B). The U to I transition had a similar Mg^{2+} dependence as folding of the WT RNA, while the I to F transition required much more Mg^{2+} with $C_{1/2}$ =11.4 ± 0.4 mM Mg^{2+}. The G107U and A59,60C J5/6 mutants both folded like the WT RNA, with $C_{1/2}$ = 0.2 ± 0.2 mM Mg^{2+} and $C_{1/2}$ = 0.5 ± 0.04 mM Mg^{2+} respectively (Figure 2.3 C and D).

In order to determine how the J5/6 mutants changed the 16S rRNA 5' domain folding pathway, I measured the 5' domain folding kinetics (Figure 2.4). In 33 mM KCl, the WT 5' domain folds fast with k_{obs} = 1.5 ± 0.2 min^{-1}. The folding kinetics of the Triple mutant folding was complex with at least two kinetic intermediate species. The unfolded RNA disappeared at a rate of 2.7 ± 0.5 min^{-1} but the fully folded species appeared quite slowly, not reaching saturation after 2 hours at 47°C. Much of the Triple mutant 5' domain rRNA appeared to be kinetically trapped in I_2, the rate of disappearance of I_2 was 0.001 ± 0.0007 min^{-1}. The kinetics of folding of G107U and A59,60C were not assayed.

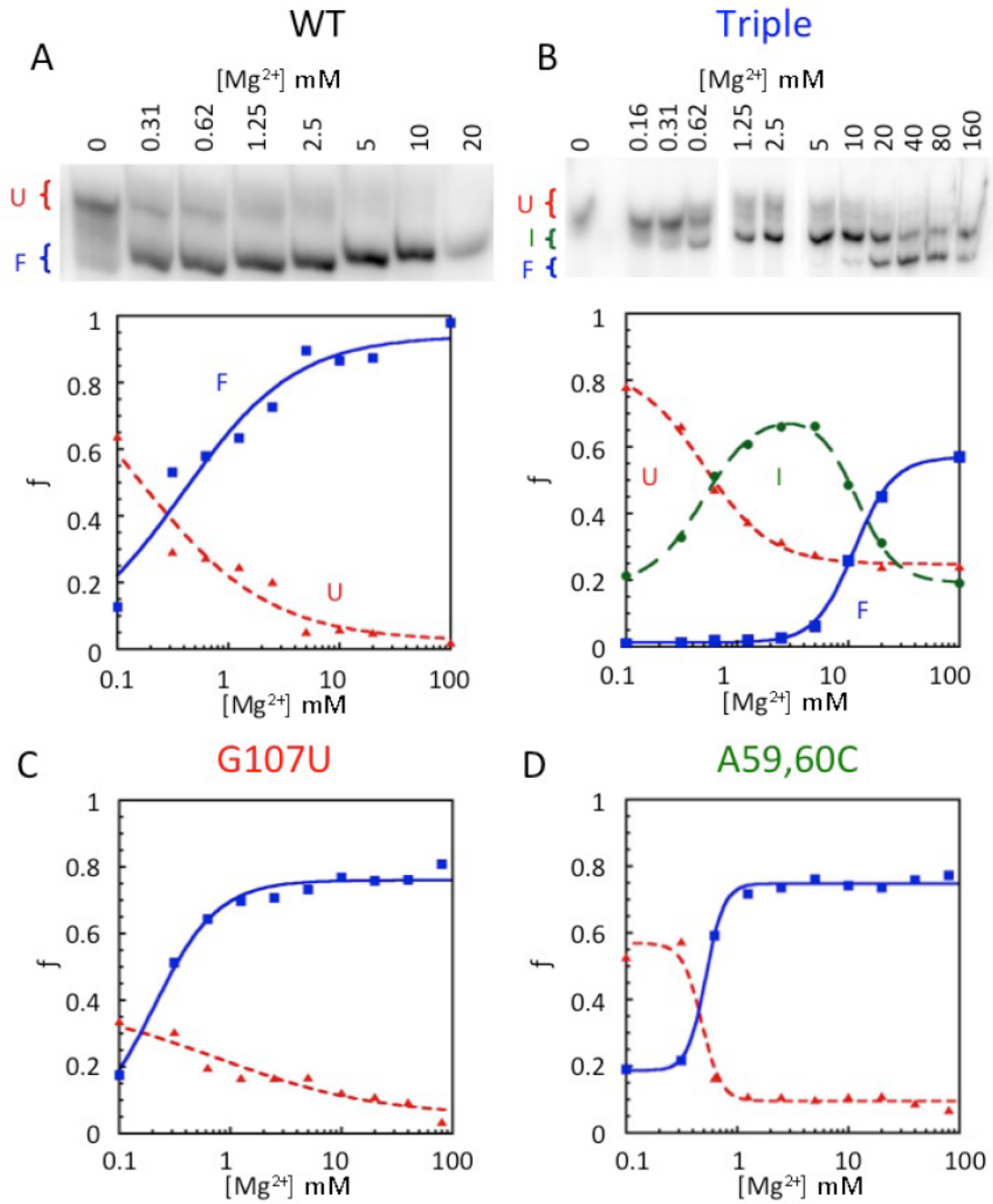

Figure 2.3: **The J5/6 Triple mutant is less stable than the WT 5' domain in low K^+.** Native EMSA assay of equilibrium Mg^{2+} titrations of uniformly ^{32}P-labeled 5' domain rRNA and fraction rRNA folded as a function of Mg^{2+} concentration for A) WT B) Triple C) G107U and D) A59,60C. The WT and Triple mutant U and F species both have the same electromobility. Data were fit to $F_f = y_0 + y_1[([Mg^{2+}]/C_{m1})^{n1}/ (1+([Mg^{2+}]/C_{m1})^{n1})] +y_2[([Mg^{2+}]/C_{m2})^{n2}/ (1+([Mg^{2+}]/C_{m2})^{n2})]$ or $F_f = y_0 + y_1[([Mg^{2+}]/C_{m1})^{n1}/ (1+([Mg^{2+}]/C_{m1})^{n1})]$. For the WT the $C_{1/2} = 0.4 \pm 0.1$ mM and $n_H = 0.7 \pm 0.1$. For G107U $C_{1/2} = 0.2 \pm 0.2$ mM Mg^{2+} and $n_H = 1.5 \pm 0.2$. For A59,60C $C_{1/2} = 0.5 \pm 0.04$ mM Mg^{2+} and $n_H = 5 \pm 1$. For the Triple mutant, the U to I transition $C_{1/2} = 0.50 \pm 0.07$ mM and $n_H = 1.5 \pm 0.2$ while the I to F transition $C_{1/2} = 11.4 \pm 0.4$ mM and $n_H = 2.5 \pm 0.2$. Experiments were performed in 33 mM KCl.

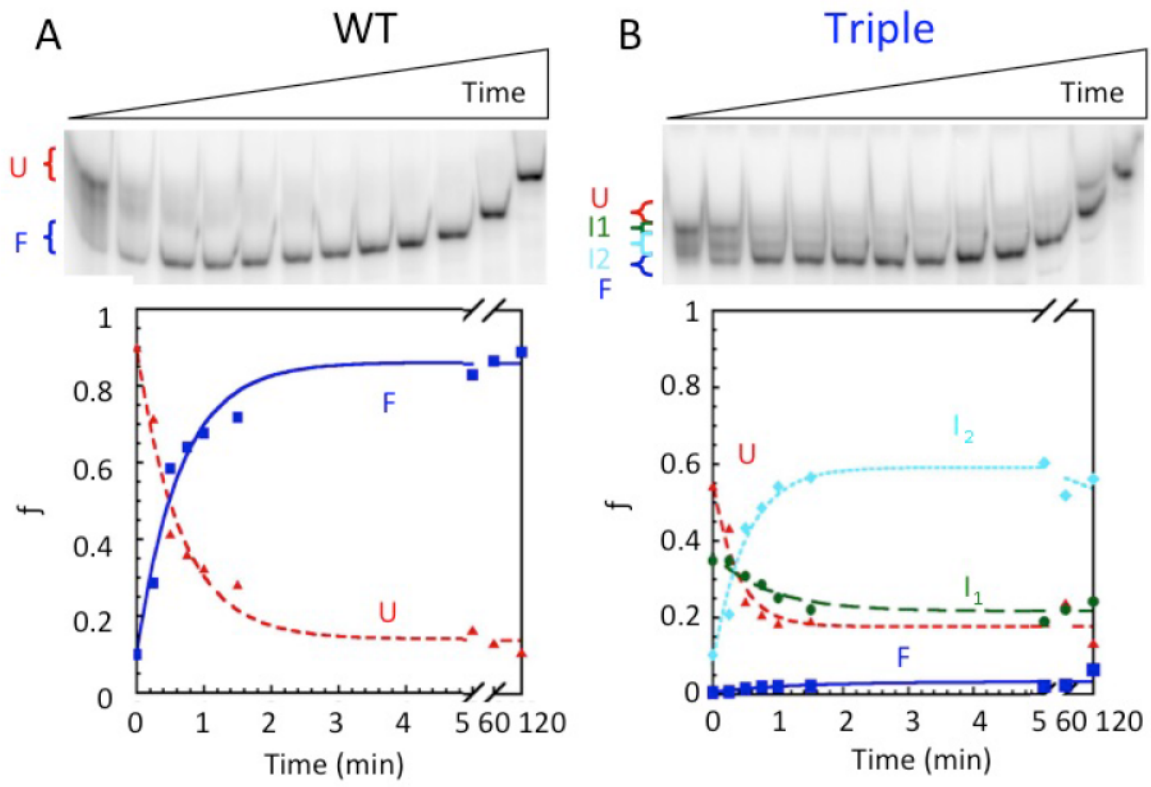

Figure 2.4: **The J5/6 Triple mutant becomes trapped in intermediates in low K^+.** A continually-running native EMSA assay of rRNA folding kinetics experiments of uniformly ^{32}P-labeled 5' domain rRNA and fraction rRNA folded as a function of time for A) WT and B) Triple mutant. Data were fit to $F_f = y_0 + y_1(1 - e^{(-k1\ t)}) + y_2(1 - e^{(-k2\ t)})$ or $F_f = y_0 + y_1(1 - e^{(-k1\ t)})$. The WT 5' domain folded with $k_{obs} = 1.5 \pm 0.2$ min^{-1}. The Triple mutant folded with at least two intermediate species, the rate of disappearance of U was 2.7 ± 0.5 min^{-1}, the rate of disappearance of I_1 was 1.2 ± 0.3 min^{-1}, the rate of appearance of I_2 is 2 ± 0.3 min^{-1} while the rate of disappearance of I_2 was $.0001 \pm 0.0007$ min^{-1}. The folded species appeared very slowly. Experiments were performed in 33 mM KCl and RNA was folded at 47°C.

2.3.2 The structure of J5/6 RNPs is locally disrupted

In order to gain insight into the structure of the J5/6 mutant 5' domain rRNA, I assayed the structure of the rRNA using SHAPE chemical footprinting at various stages along the *in vitro* assembly path. This assay provided residue-level information on the secondary structure and flexibility of the 5' domain rRNAs and RNPs. SHAPE chemical footprinting is sensitive to the flexibility or conformation of the 2' OH group (Steen 2012). To a first approximation, nuclotides that are more reactive are more flexible.

A histogram of the normalized reactivity for each nucleotide showed that 50% of nucleotides have a normalized reactivity close to zero (between -5 and 5; Figure 2.8 A). Nucleotides with high reactivity in each rRNA were mapped onto the 5' domain secondary structure (Figure 2.8 C and D). With some exceptions such as helix 12, which requires S16 to adopt the native secondary structure (Moazed 1986a, Stern 1988a), and the difficult-to-fold helix 8-10 four-way junction, the SHAPE data was consistent with the known 5' domain secondary structure.

To more clearly identify regions altered by the J5/6 mutants, I calculated the ratios of nucleotide reactivity of each mutant compared to the WT control. All nucleotides with a reactivity of less than 2.5 were considered "non-reactive" and set equal to a baseline value of 2.5. This was done to eliminate huge log ratio differences between nucleotides with, for example, a reactivity of 0.01 in G107U and 1.5 in WT. The log ratios of the exposure in J5/6 mutant over the WT for each nucleotide were plotted on a histogram and the protection and exposure bins were empirically determined (Figure 2.6 A). Nucleotides with strong changes between the WT and J5/6 mutants were mapped onto the 5' domain secondary and tertiary structures (Figures 2.6-2.8).

Figure 2.5: **SHAPE reactivity of WT and Triple mutant 5' domain rRNAs.** A) Histogram of WT nucleotide reactivity folded in HKM20 Buffer. Outliers (~8σ) were discarded, and reactivity clusters were empirically determined and colored. B) Sample hydroxyl radical footprinting data. Plot comparing WT (black), G107U (red), A59,60C (green) and Triple mutant (blue) SHAPE reactivities for the 16S 140-220 nucleotide (helix 8-10 region), lines represent the lower bound of that bin. Note the overall similarities between the four rRNAs. SHAPE chemical footprinting pattern of C) WT and D) Triple mutant 5' domain rRNAs folded in HKM20. Nucleotides with SHAPE reactivities greater than 25 are plotted in colors of increasing warmth, non-reactive nucleotides are grey. 16S helices and residues are labeled. With some exceptions such as helix 12, the SHAPE data is consistent with the known secondary structure.

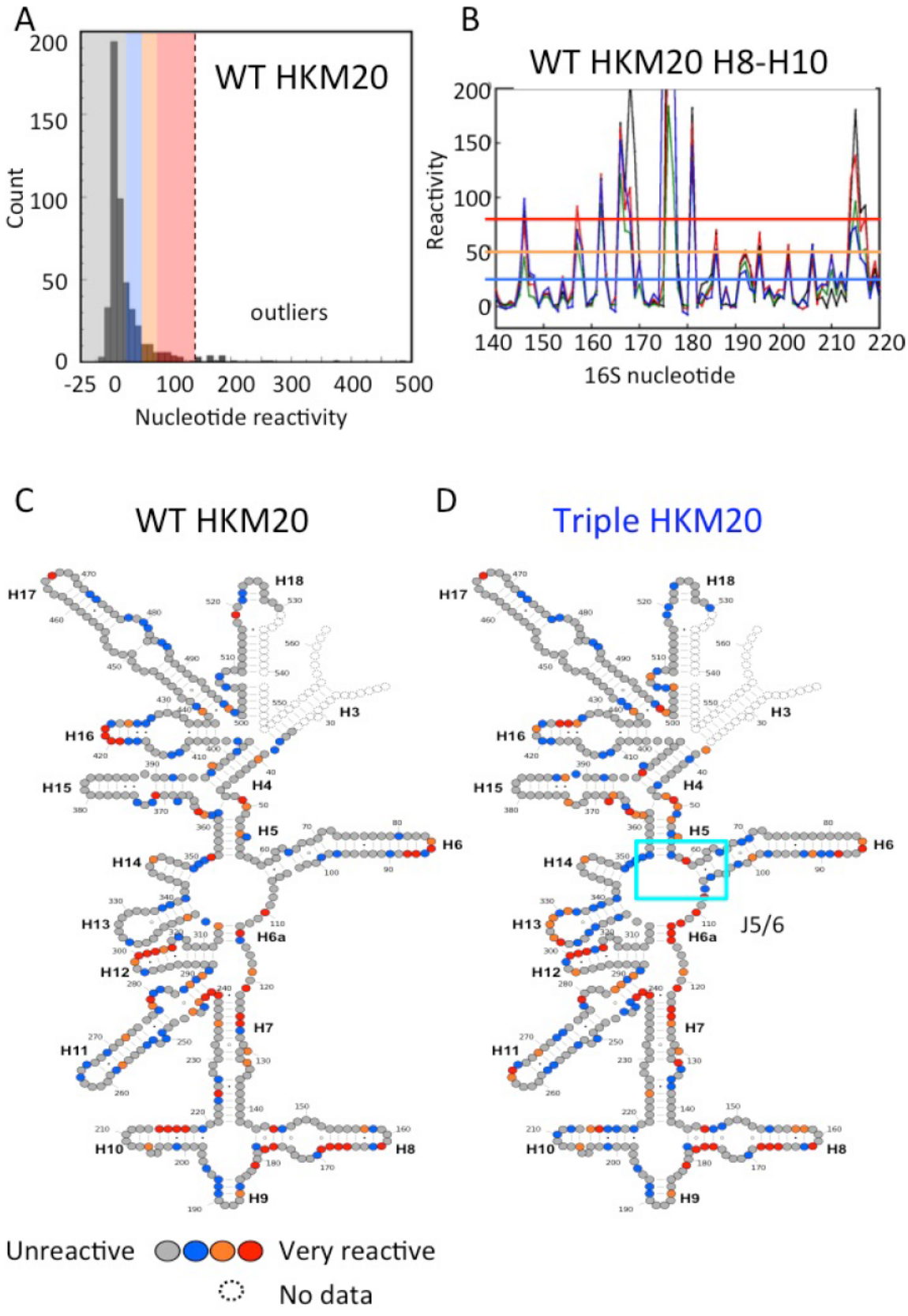
A
WT HKM20
Count
Nucleotide reactivity
outliers
B
WT HKM20 H8-H10
Reactivity
16S nucleotide
C
WT HKM20
D
Triple HKM20
J5/6
H1
H2
H3
H4
H5
H6
H6a
H7
H8
H9
H10
H11
H12
H13
H14
H15
H16
H17
H18
Unreactive
Very reactive
No data

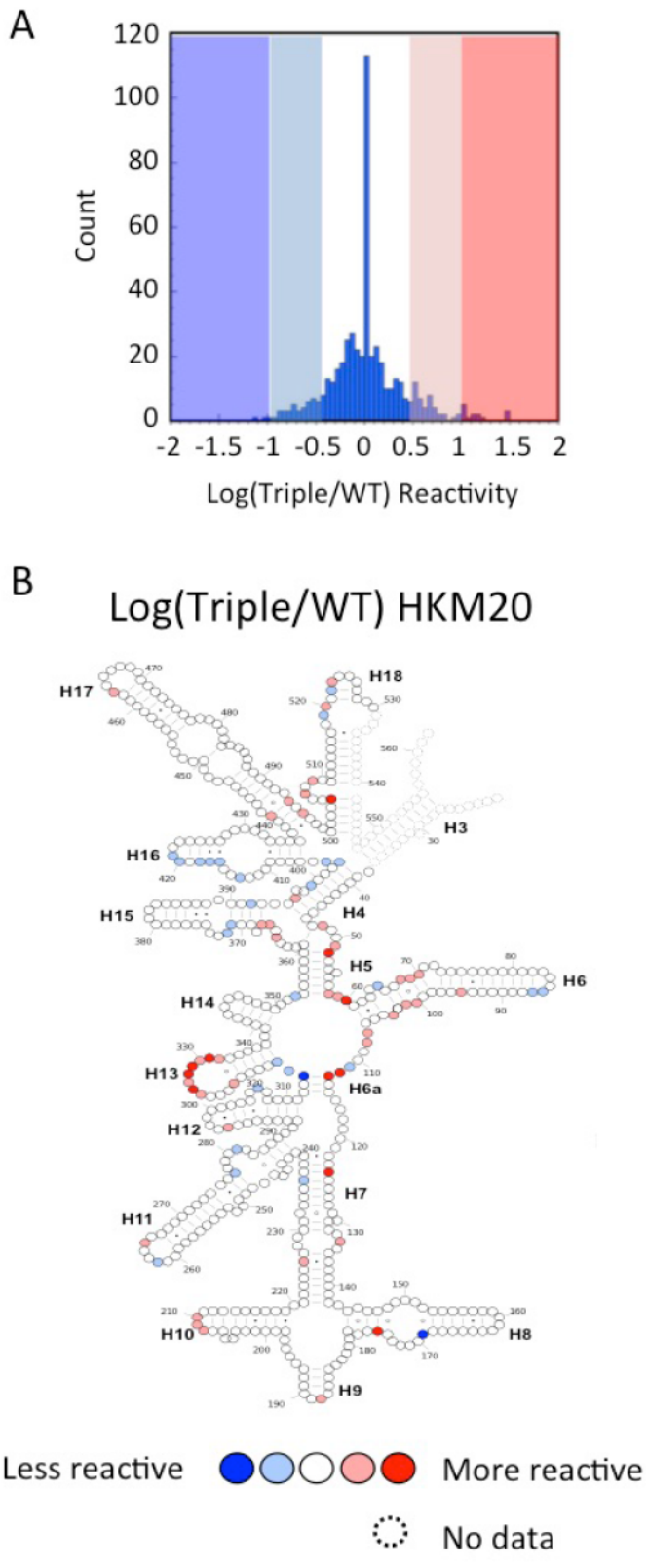

Figure 2.6: **Local increases in SHAPE chemical reactivity of J5/6 mutant.** A) A representative histogram, of the log ratio of the reactivity of each nucleotide in Triple mutant over the WT folded in HKM20 Buffer. Positive log ratios represent nucleotides more reactive in the mutant while negative log ratios represent nucleotides less reactive in the mutant. These log ratios were plotted on a histogram and empirical cut-off values were selected for each cluster. B) SHAPE chemical footprinting pattern of the J5/6 Triple mutant. Nucleotides with altered reactivity in the J5/6 Triple mutant folded in HKM20 are mapped onto the 16S 5' domain secondary structure. J5/6 and helix 13 (G331 base stacks with A59) are more reactive. Nucleotides with log ratios less than -1 are dark blue, nucleotides with log ratios between -1 and -0.5 are light blue, nucleotides with log ratios between 0.5 and 1 are light red, nucleotides with log ratios greater than 1 are red. Dotted-outline residues: data not available. 16S helices and residues are labeled.

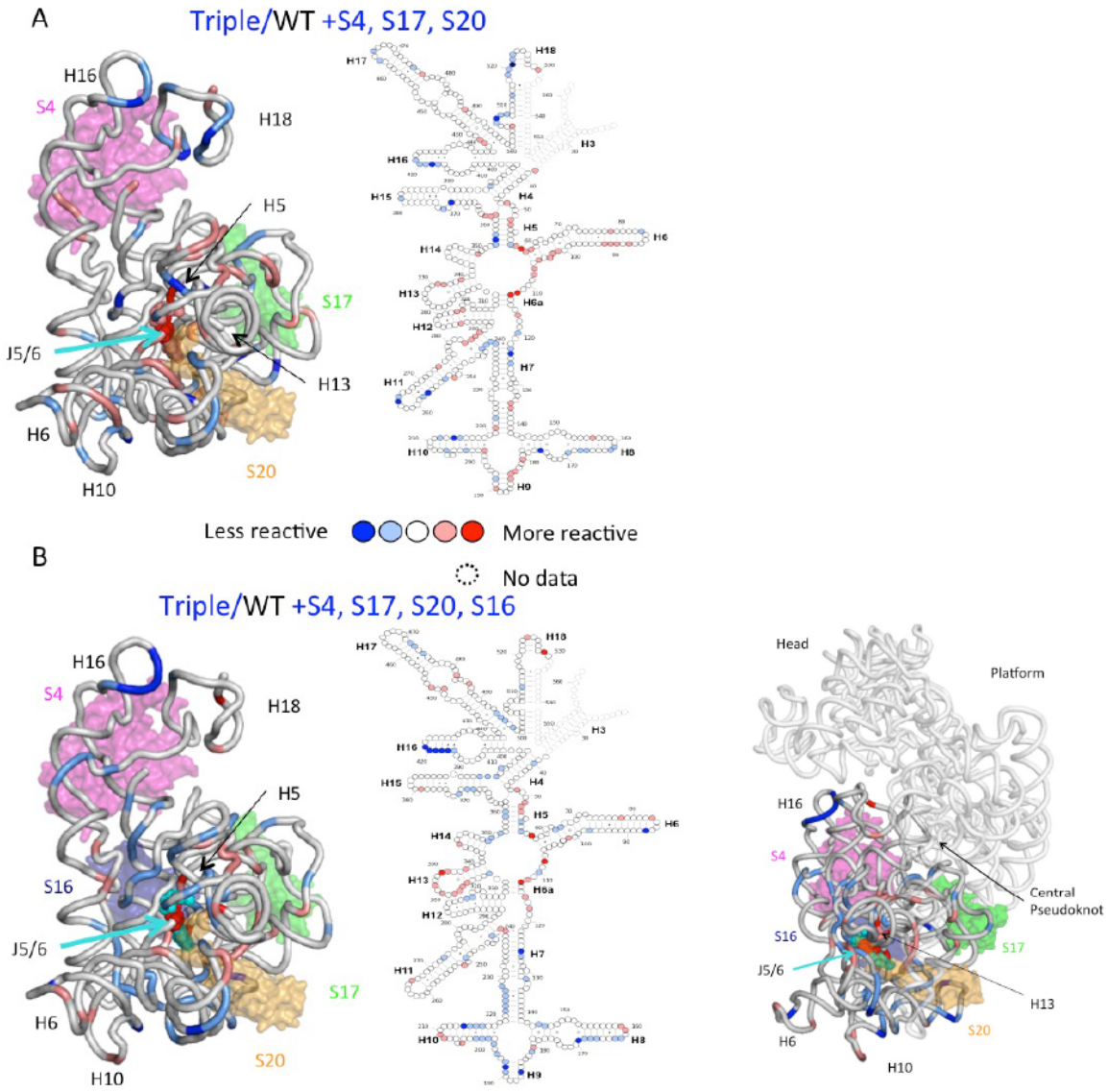

Figure 2.7: **SHAPE chemical footprinting of J5/6 Triple mutant RNPs.** SHAPE chemical footprinting pattern of the J5/6 Triple mutant. Nucleotides with altered reactivity in the J5/6 Triple mutant RNP compared to the WT RNP are mapped onto the 16S 5' domain secondary structure and tertiary structure. Structures of the triple mutant RNP with the A) primary r-Proteins S4, S17, and S20 and B) primary r-Proteins S4, S17, and S20 and secondary r-protein S16. Also shown is a ribbon diagram illustrating the orientation of the 5' domain within the 30S ribosome, the other domains are labeled. Nucleotides with log ratios less than -1 are dark blue, nucleotides with log ratios between -1 and -0.5 are light blue, nucleotides with log ratios between 0.5 and 1 are light red, nucleotides with log ratios greater than 1 are red. Dotted-outline residues: data not available. 16S helices and residues are labeled.

Figure 2.8: **SHAPE chemical footprinting changes during J5/6 mutant RNP assembly.** SHAPE chemical footprinting pattern of the J5/6 mutants compared to the WT during 5' domain RNP assembly. Nucleotides with altered reactivity in the J5/6 mutant RNP compared to the WT RNP are mapped onto the 16S 5' domain secondary structure and tertiary structure. The secondary structure depicts perturbations of the rRNA folded in HKM20. The middle tertiary structure depicts perturbations of the RNP with the primary r-Proteins S4, S17, and S20. The right-most tertiary structure depicts perturbations of the RNP with the primary r-Proteins S4, S17, and S20 and the secondary r-protein S16. Structures of the A) Triple mutant B) G107U and C) A59,60C 5' domain RNP assembly paths. Nucleotides with log ratios less than -1 are dark blue, nucleotides with log ratios between -1 and -0.5 are light blue, nucleotides with log ratios between 0.5 and 1 are light red, nucleotides with log ratios greater than 1 are red. Dotted-outline residues: data not available. 16S helices and residues are labeled.

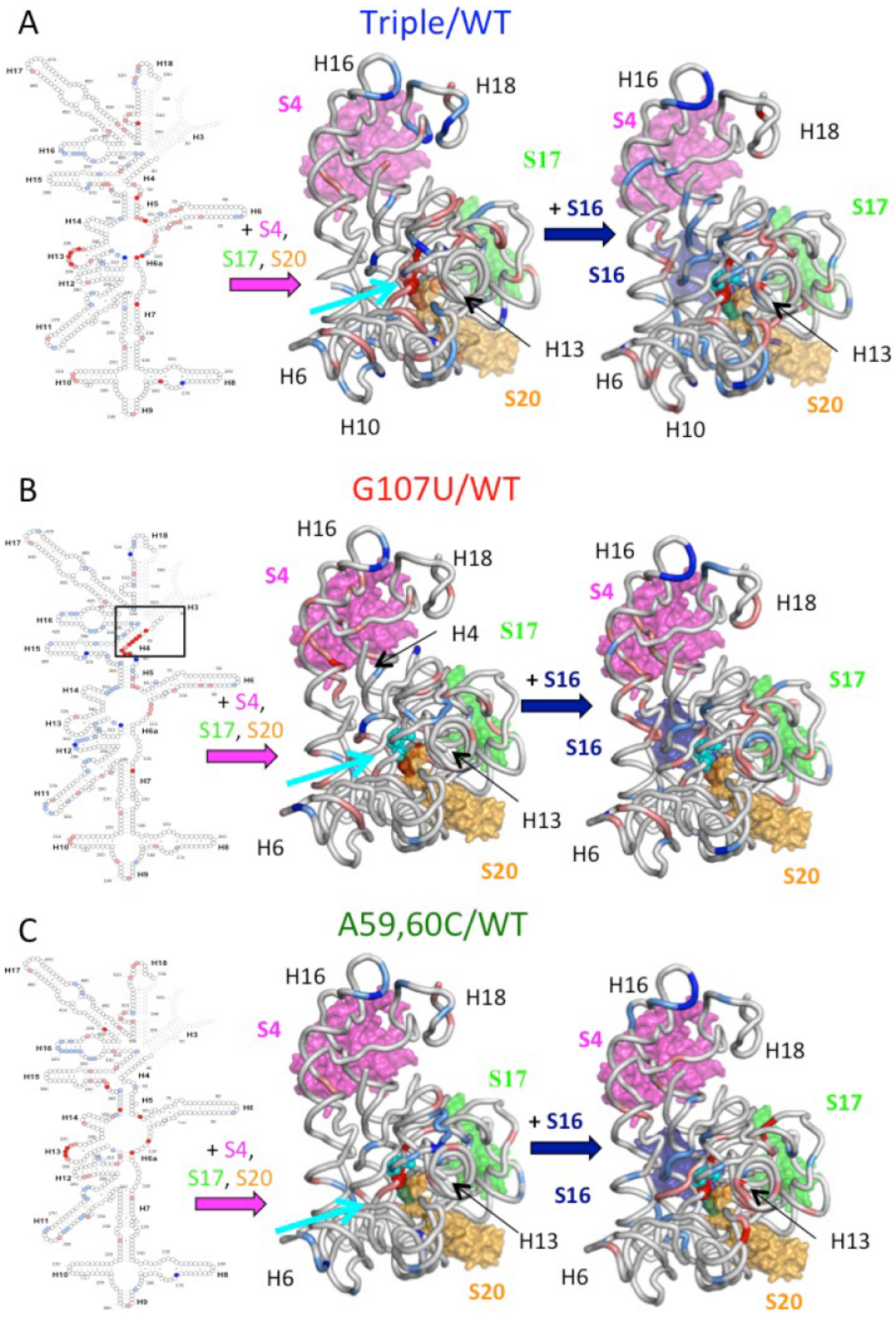
A
Triple/WT
H16
H18
S4
S17
+ S16
S17
S16
H13
H6
S20
H10
+ S4,
S17, S20
B
G107U/WT
H4
C
A59,60C/WT

The most perturbed regions of the J5/6 Triple mutant rRNA folded in HKM20 were the regions right around the mutations and helix 13 (Figure 2.6 B). The addition of the primary r-proteins S4, S17, and S20 restructured helix 13 to the native structure, but the J5/6 region was still more reactive to the SHAPE reagent. Interestingly, helix 18, including the G530 loop and pseudoknot, and one face of helix 16 was less reactive than WT (Figure 2.7 A). Upon the addition of S16 both the J5/6 region and helix 18 became native-like, but helix 16 was still less reactive (Figure 2.7 A).

Some perturbations appear to be universal for the J5/6 mutants, especially the increased reactivity of the region around the J5/6 mutations (without S16), and the decreased reactivity of helix 16 (with S4, S17, S20 with or without S16) (Figure 2.8). However, there are perturbations specific to each mutant.

The G107U mutant had a very reactive helix 4 in the folded rRNA without S4 (Figure 2.8 B). In addition, the G107U RNA in HKM20 was less reactive around helix 12, but had a native-like helix 13, unlike A59,60C or the Triple mutant. This is likely due to the unperturbed the A59-G331 base stacking interaction. Upon the addition of the primary r-proteins, the helix 4 reactivity of G107U becomes native-like. Unlike the Triple mutant and A59,60C, helix 18 is native-like in G107U.

The A59,60C mutant had an *in vitro* RNP assembly pattern very similar to that of the Triple mutant.

2.3.3 Binding of S20 to the J5/6 mutants

In order to determine if the J5/6 mutations disrupt binding of protein S20, which contacts the J5/6 region (Figure 2.1), S. Abeysirigunawardena measured co-migration of

Cy5-labeled S20 and Cy3-labeled 5'dom-h3 rRNA in native polyacrylamide gels (Figure 2.9 A). In this experiment, S20 only enters the gel and migrates toward the anode if it forms a stable complex with the RNA. Even small quantities of Cy5-labeled S20 co-migrated with WT 5'dom-h3 rRNA (Figure 2.9 B), corresponding to an approximate $K_D \leq 15$ nM. Cy5-labeled S20 only visibly co-migrated with the Triple mutant 5'dom-h3 rRNA above 30 nM S20. This interaction did not appear to be specific, due to the smeariness of the bands (Figure 2.9 C). The significance of Cy5-labeled S20 co-localization with a species with a slightly faster electromobility than Cy5-labeled SA5 annealed to Triple mutant 5'dom-h3 rRNA is unclear (faint red band underneath green band in Figure 2.9 C). Cy5-labeled S20 did not bind G107U 5'dom-h3 rRNA with WT affinity (Figure 2.9 D). Thus, the J5/6 mutations weaken interactions with protein S20. The mutant 5'dom-h3 may adopt an alternative conformation that cannot bind S20, or the mutations may inhibit restructuring of the N-terminal alpha helix of S20 during assembly (Dutca 2008). Further experiments showed that the addition of protein S4 could not rescue the Triple mutant 5'dom-h3 (I. Sharma).

2.3.4 Conformation of helix 3 in the J5/6 mutants

In order to explore the association of S4 with the J5/6 mutants, FRET assays between Cy5-labeled S4 and Cy3-labeled SA5 primer annealed to 5'dom-h3 rRNA with and without the addition of S20 and S16 were performed by S. Abeysirigunawardena. These FRET assays are sensitive to the conformation of helix 3 (helix 3 flipped out and helix 3 in the native state) and to the association of S4 to these states (Figure 2.10 A). The FRET data were fit to a quadratic due to the high affinity of S4 for the 5' domain (0.2 nM;

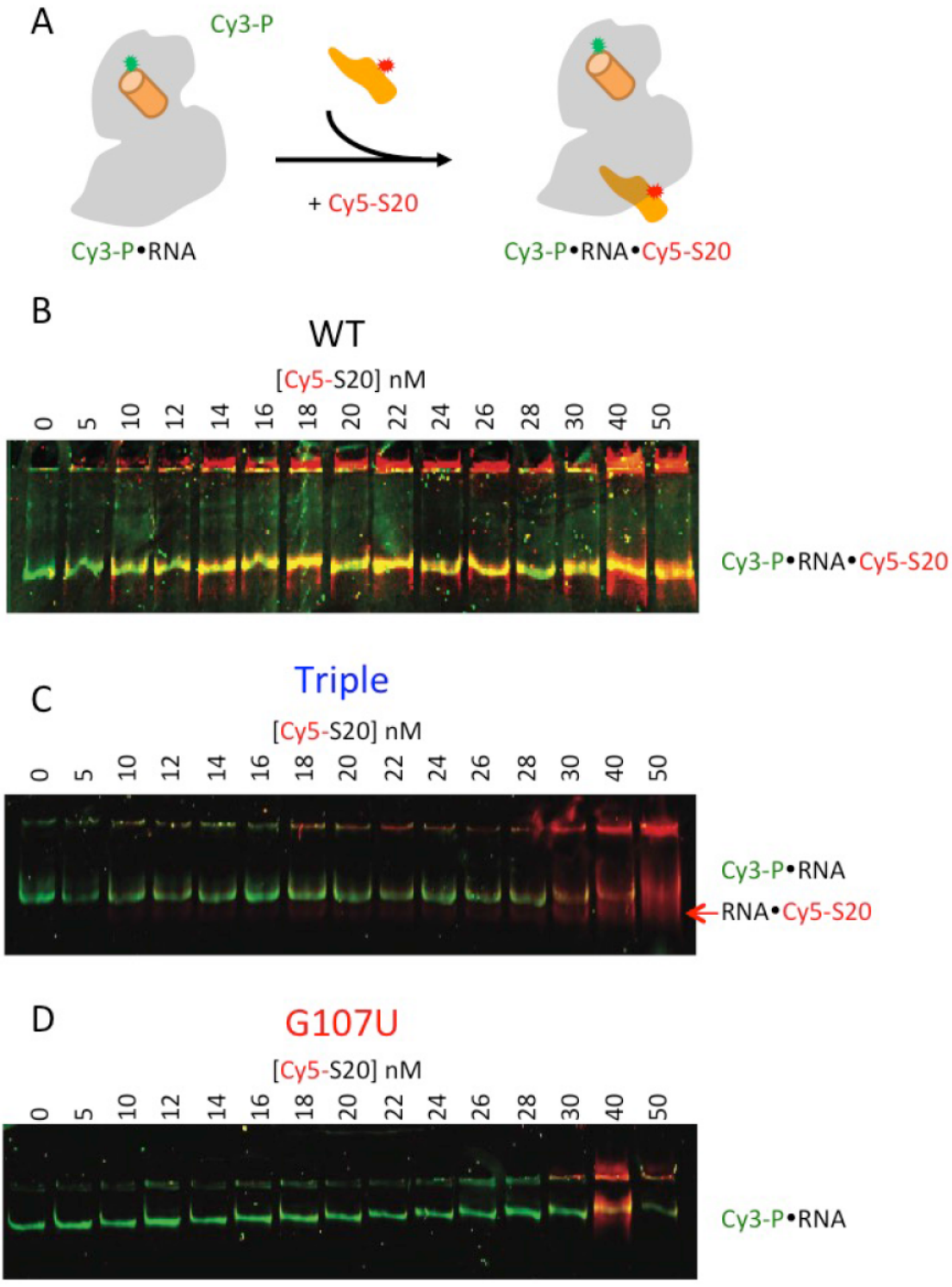

Figure 2.9: **Loss of high-affinity S20 binding in the J5/6 mutants.** EMSA co-localization A) scheme between Cy5-labeled S20 and a Cy3-labeled primer annealed to 5'dom-h3 rRNA and assay for B) WT C) Triple mutant and D) G107U mutant. Data and figure from S. Abeysirigunawardena.

S. Abeysirigunawardena, paper in press) the four state model of S4 binding and helix 3 dynamics as derived by S. Abeysirigunawardena (Figure 2.10 A). The four state model supposes S4 can bind to the 5' domain rRNA with helix 3 in both the flipped and native conformations (K_F and K_N) and helix 3 can access both the flipped and native conformations with or without S4 present (K_2 and K_1), which has significant support from footprinting and smFRET data (Ramaswamy 2009b, Mayerle 2013, Kim 2014). Calculation of the thermodynamic linkage parameter, α or K_N/K_F, between S4 binding and helix 3 being in the native conformation depends on the determination of the fraction of the free 5'dom-h3 RNA in the native conformation as determined by *in vitro* hydroxyl radical footprinting (S. Abeysirigunawardena, paper in press). It is hasty to assume that this is not affected by the J5/6 mutations given the differences in SHAPE reactivity between the mutants (below). For this reason, the less processed K_2 and fitting parameter β or $K_N*(1+K_1)$ were used instead of α and K_N.

The J5/6 mutants did not seem to affect the preferred S4 binding path as expressed by the fitting parameter $K_N*(1+K_1)$, which takes into account both the equilibrium constant of S4 binding to the native state of helix 3 and the equilibrium constant of conformational equilibrium in the unbound state (Figure 2.10; S. Abeysirigunawardena, paper in press). However, the mutants did affect K_2. Upon the addition S20 and S16, the WT 5' domain preferred the 'native' conformation of helix 3, but the J5/6 mutants still preferred the 'flipped' conformation of helix 3 (Figure 2.10). If we assume that these mutations do not directly alter S4 contacts with the rRNA and thus K_N is the same, then K_1 becomes larger, indicating the J5/6 mutations also favor the flipped state in the free RNA, but this is fairly mild compared to K_2.

A

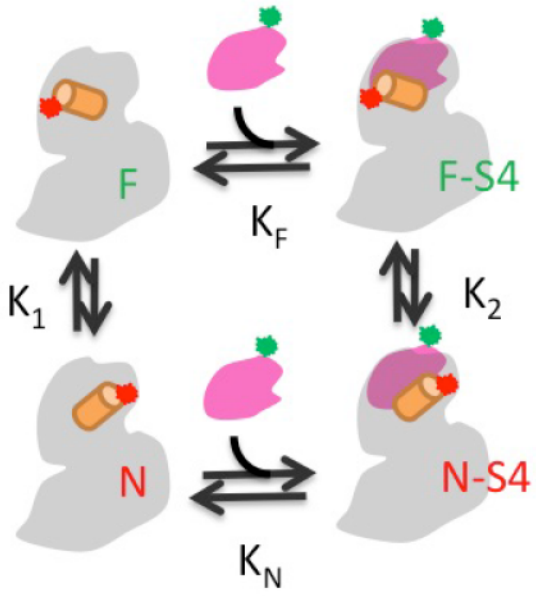

B

RNA	K_2	$\beta K_N(1+K_1)$
WT	1.8±0.1	1.0±0.3
G107U	5.8±0.9	1.6±0.6
Triple	11±1.6	2.4±0.7
WT + S20, S16	0.6±0.1	0.6±0.2
G107U + S20, S16	4.1±0.3	0.7±0.2
Triple + S20, S16	6.8±0.4	0.7±0.2

Figure 2.10: **J5/6 mutants stabilize the flipped conformation of helix 3.** FRET assays between Cy5-labeled S4 and Cy3-labeled primer annealed to 5'dom-h3 rRNA. A) Diagram illustrating the four state model of S4 binding and helix 3 conformational change. B) Table of equilibrium constants for the rRNA mutants. Diagram and data collected by S. Abeysirigunawardena.

2.3.5 Primer binding to extended 5' domain rRNA

In order to test the model derived from the SHAPE chemical footprinting results and whether or not the conformation of helix 6 changed during 5' domain assembly, I attempted H6-H10 FRET.

First, the binding affinity of the H6 and H10 RNA primers for 5'dom-h6,h10 rRNA was optimized. Even under the best primer annealing and rRNA folding conditions the binding affinity for the H10 primer to 5'dom-h6,h10 rRNA was 4.1 ± 0.7 nM. The binding affinity for the H6 primer to 5'dom-h6,h10 rRNA was 9 ± 2 nM. This was insufficient to insure complete or near-complete dual labeling, which is critical for analyzing the FRET data (Figure 2.11). To test for anti-cooperativity, the opposite unlabeled primer was added in the same concentration as the unlabeled rRNA. The K_D for the labeled primer did not vary in the presence of the other primer (data not shown).

Since the labeled oligonucleotides bound 5'dom-h6,h10 rRNA weakly, I tested the k_{off} to see if saturating the 5'dom-h6,h10 rRNA with oligonucleotide, and then using a size exclusion column to get rid of the unbound oligomer would achieve near-complete occupancy of both primers. Unfortunately, the helix 10 oligomer had a fast dissociation rate with $koff_{,1} = 0.90 \pm 0.01$ min^{-1} (data not shown). The helix 6 primer had a slow dissociation rate of 0.0012 ± 0.0001 min^{-1}.

I designed many new primers to bind to the H10 extension, without success. I did not test the dissociation kinetics of these new primers. At this point I gave up on using H6-H10 FRET to test the model derived from the SHAPE chemical footprinting results.

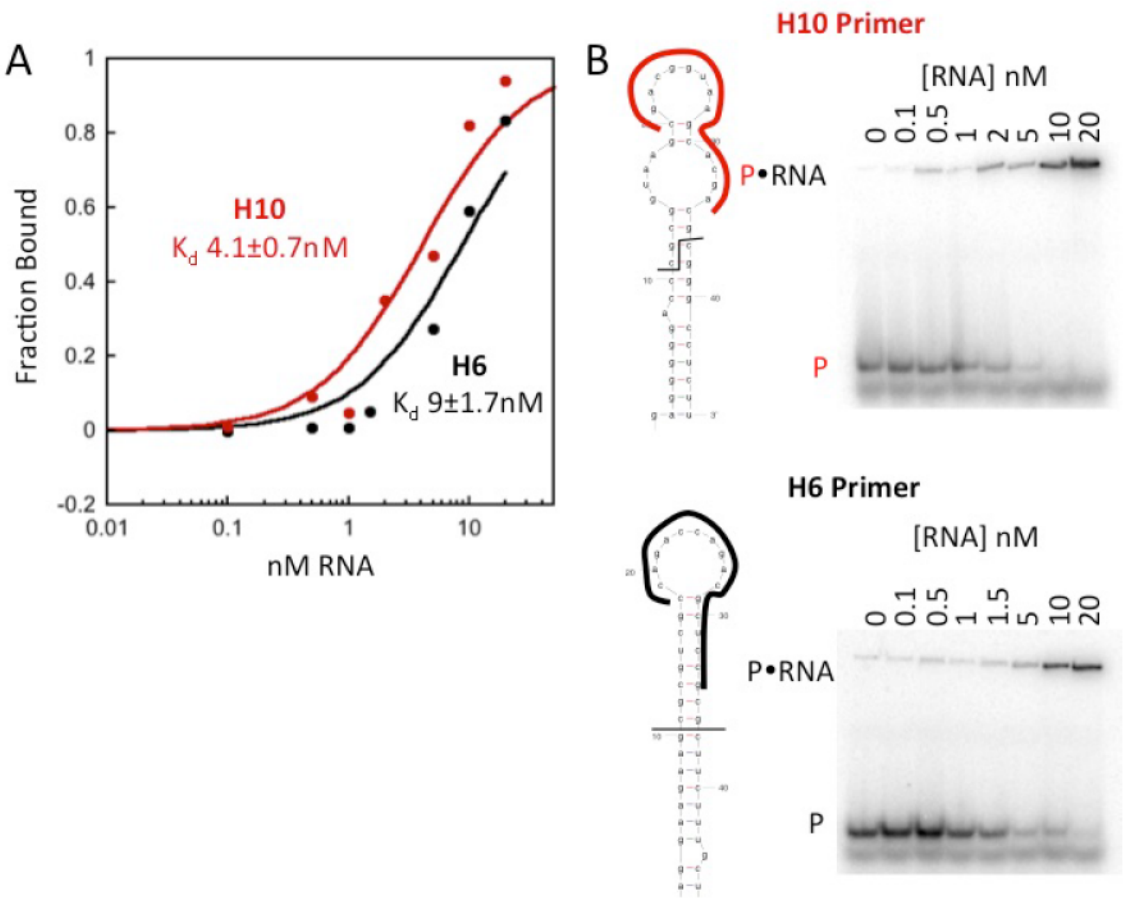

Figure 2.11: **Helix 6 and Helix 10 primers bind 5'dom-h6,h10 rRNA with moderate affinity.** A) Fraction primer bound to 5' domain as a function of 5' domain concentration. Data fit to $F_B = ([RNA]/K_d)/(1+[RNA]/K_d)$. B) Native EMSA assay of ^{32}P-labeled helix 6 and helix 10 primers. Binding to 5'dom-h6,h10 rRNA produces a decrease in mobility. Also shown is mfold predicted secondary structure of the helix extensions and the primer binding locations.

2.4 Discussion

2.4.1 Folding of J5/6 mutants is locally perturbed

The J5/6 Triple mutant is less stable than the WT 5' domain and becomes trapped in intermediates in low monovalent ions. In more physiological monovalent concentrations, such as buffer conditions commonly used for ribosome reconstitutions and *in vitro* assembly assays, the J5/6 mutants form a compact species indistinguishable from that of the WT 5' Domain rRNA.

The data are supported by the SHAPE chemical footprinting and indicated that the J5/6 mutations cause local differences in folding but not large perturbations. SHAPE chemical footprinting on the J5/6 Triple mutant rRNA alone (folded in 330 mM KCl, 20 mM $MgCl_2$) shows a folded structure very much like that of the WT with small local increases in SHAPE reactivity to the J5/6 region and helix 13 (G331 base stacks with A59, an interaction that is destabilized in A59C-containing mutants in the absence of r-proteins) (Figure 2.5). Some of the nucleotides that are less reactive in the Triple mutant could be lacking tertiary contacts that hold the nucleotides in a more reactive conformation.

It is interesting to note that G107U and A59,60C fold like WT by EMSA but have similar structural perturbations as the Triple mutant when assayed by SHAPE chemical probing. For example, G107U has drastic changes in reactivity for helix 4 (left panel of Figure 2.8) but folds like WT by EMSA. The kinetically trapped folding of the J5/6 Triple mutant in 33 mM K+ suggests that its folding pathway is perturbed; however, this was not detected at physiological monovalent conditions.

2.4.2 S20 binding to J5/6 mutants is weaker

The SHAPE chemical footprinting data of the J5/6 mutants does show some perturbations to the sites of S20 binding, namely the base of helix 6 (nt 100-108), the junction between helix 8 and 9 (nt 180-185), and helix 13 (nt 331-332). These regions are moderately more reactive in the Triple mutant S4, S17, S20 RNP than in the WT RNP with the primary r-proteins. The SHAPE chemical footprinting assays were performed with 4- to10-fold excess of each of the 5' domain r-proteins, concentrations empirically determined to saturate the changes to the r-protein binding sites. Taking this into account, the SHAPE patterns are illustrative of what the final state of r-protein binding is, and should be insensitive to small differences in r-protein affinity for the different J5/6 mutants. With these caveats in mind, the SHAPE footprinting can provide some structural information underlying the loss of S20 binding affinity in the J5/6 mutant.

The N-terminus of S20 has been suggested to fold during ribosome assembly (Dutca 2008). However, the S20-J5/6 interactions should not be directly inhibited by the mutations. In the 30S crystal structures, the N-terminus of S20 wedges up against the major grove of helix 5 (Schuwirth 2005). Lys 4 is within hydrogen bonding distance of the 2' hydroxyl of A60. This interaction is unaltered in A60C. Arg 9 can hydrogen bond with O6 of G107. This interaction is conserved in G107U. Asn 2 can hydrogen bond with the backbone of G331.

However, the J5/6 mutations could inhibit folding of the N-terminus of S20 and thus EMSA-stable binding. This could explain the differences in S20 binding affinity as assayed by fluorescence anisotropy and EMSA co-localization studies. Additional explanations for this difference include the fact that fluorescence anisotropy was

performed in the presence of unlabeled S4 and S17. These additional r-proteins were determined to be necessary to stabilize the interaction of S20 with WT rRNA in smFRET studies (personal communication S. Abeysirigunawardena).

The lack of high-affinity S20 binding to the G107U J5/6 mutant in the EMSA assay could be due the absence of S4. This is corroborated by the SHAPE chemical footprinting data, which detected structural perturbations to the helix 4 region in the absence of S4. Further work is needed to test this hypothesis.

2.4.3 Binding of S4 and S16 to J5/6 mutants

FRET assays between the extended helix 3 of the J5/6 mutants and S4 shows that the mutations destabilize the native conformation of helix 3, but S4 binding affinity as expressed by $K_N*(1+K_1)$ is less sensitive. The addition of S20 and S16, which have previously been shown to strongly stabilize the native conformation of helix 3 in the WT rRNA (Ramaswamy 2009b), only shifts the conformational equilibrium slightly for the J5/6 mutants. This suggests that the J5/6 mutants somehow interfere with the native conformation of helix 3, which may prevent proper structuring of the central pseudoknot and correct domain-domain orientations of the pre-30S ribosome (discussed more in chapter 4). This FRET data is somewhat corroborated by the SHAPE chemical footprinting data.

The SHAPE chemical footprinting data of the J5/6 mutants does show some perturbations to the S4 binding site – specifically decreases in SHAPE reactivity of helix 18 (nt 507-510 and 519-523) and helix 16 (nt 417-421) relative to WT. These are consistent with a S4 interaction, but not quite native-like binding, with the helix

pseudoknot conformational rearrangement and S4 N-terminal extension-helix 16 interactions (Mayerle 2011).

Additionally, there are some mild decreases in SHAPE reactivity of helix 7 (nt 123-126) and helix 11 (241-243, 257-258, 264-265) of the S17 binding site for the Triple mutant in comparison to the WT. However, the sites of S20 binding, namely the base of helix 6 (nt 100-108), the junction between helix 8 and 9 (nt 180-185), and helix 13 (nt 331-332) are moderately more reactive in the Triple mutant than in the WT S4, S17, S20 RNP. The SHAPE footprinting of the S4, S17, S20 5' domain RNP does suggest a slightly different from WT S4 binding mode and a perhaps not fully saturated S20 binding.

The addition of S16 repairs almost all of these differences in SHAPE reactivity of the r-protein binding sites, further supporting S16 role as a keystone in 5' domain structural dynamics (Ramaswamy 2009b; S. Abeysirigunawardena, paper in press). S16 does not stabilize the native conformation of helix 3 for the J5/6 mutants. Clearly, a perturbation of S16-binding does not explain the assembly defects observed.

2.4.4 A model of 5' Domain assembly

Combining all of the *in vitro* r-protein association data and SHAPE chemical footprinting data, I propose a model for 5' Domain assembly and how the J5/6 mutants perturb assembly (Figure 2.12). S4 binds early to the 16S rRNA (Nowotny 1988) nucleating the folding of the 5-way junction of the 5' domain (Bellur 2009). At this point, the lower sub-domain including (but not limited to) helices 5, 6, and 10 certainly would have secondary structure (Adilakshmi 2005), and helices 5 and 6 would form the

predicted Right Angle motif. This is corroborated by analysis of the protein and Mg^{2+} dependence of various tertiary contacts in the 5' domain of the 16S rRNA (Ramaswamy 2009a and 2009b).

When the N-terminus of S20 structures is unknown. As S16 binds, it packs helix 15 against helix 5, displacing helix 6, this allows helix 3 to adopt its native conformation. This model explains earlier data in which the along-groove stacking motif of helix 6 is always protected but the tip of helix 15 goes through an oscillatory semi-protected, exposed, protected pattern; and the addition of S16 de-protects the base of helix 6 (Ramaswamy 2009a and 2009b). In the absence of S16, the J5/6 mutants are more flexible in the J5/6 region, which could suggest a failure to form the proposed Right Angle motif, and possibly a lack of structuring of the S20 N-terminus. Upon S16 binding, somehow the J5/6 mutants disrupt helix 15 packing, which leads to disruptions of helix 3 via helix 4. This could lead to issues with long-range domain-domain interactions through the central pseudoknot (Ramaswamy 2009b).

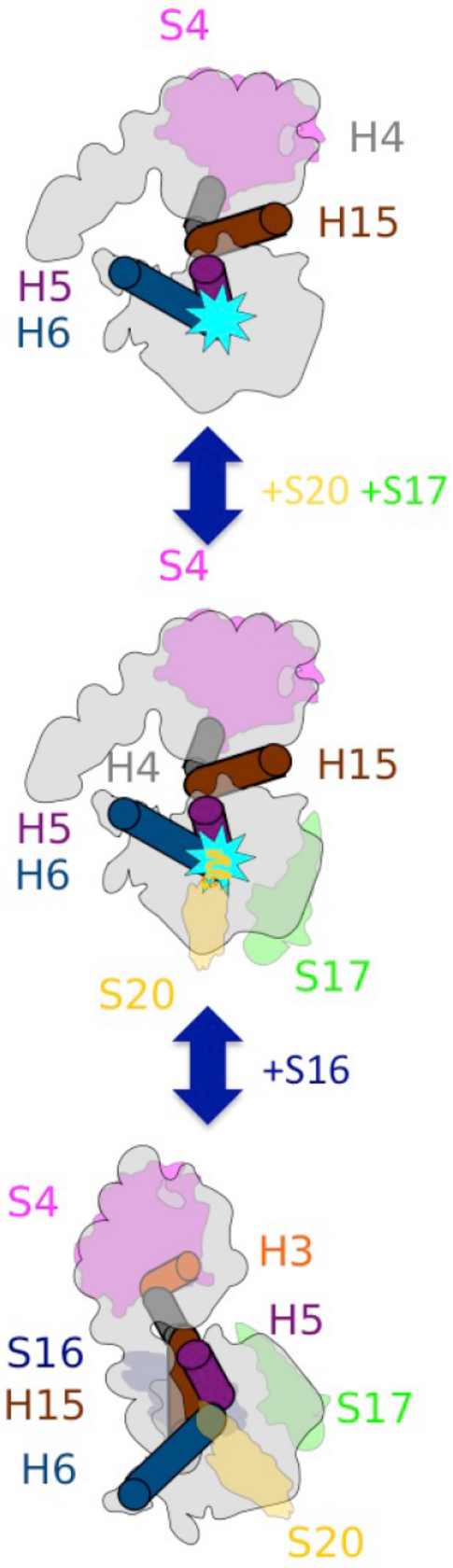

Figure 2.12: **Model for J5/6 mutant 5' domain RNP assembly.** A model for the assembly of the 5' domain 16S rRNA with r-proteins S4 (pink), S20 (yellow), S17 (green), S16 (blue). Key helices and their proposed structures are indicated in colored cylinders.

Chapter 3: *In vivo* biogenesis of J5/6 mutant ribosomes is stalled

3.1 Introduction

There have been numerous *in vitro* ribosome assembly studies, but they do not account for the complexities of *in vivo* biogenesis such as the presence of assembly factors and concurrent transcription and rRNA processing. Under normal conditions ribosome assembly intermediates are scarce, and heterogeneous, yet understanding how this critical macromolecular machine assembles could provide greater understanding of RNA-protein interactions, RNA folding, and novel insight into antibiotic manufacture.

Only recently, due to technical innovations, has studying ribosome biogenesis *in vivo* been feasible. Various approaches have handled those limitations by either enriching the pool of ribosomal assembly intermediates via chemical inhibitors (neomycin, Sykes 2010) or protein deletion (RimM or RbfA, Soper 2013); or purifying intermediate complexes via sucrose gradient sedimentation velocity (Sykes 2010, Chen 2013, Sashital 2014) or affinity tags (Gupta 2014). This enrichment was followed by sensitive analytical techniques such as quantitative mass spectrometry, electron microscopy, or hydroxyl radical footprinting, which are able to deal with heterogeneous populations.

The Williamson lab has spearheaded efforts to study r-protein association during ribosome biogenesis *in vivo* using quantitative mass spectrometry (Sykes 2010, Chen 2013, Sashital 2014). Using ^{15}N pulse labeling and high precision LC-MS they were able

to determine that the smaller, incomplete ribosomal particles found in lighter fractions of polysome profiles from exponentially growing wild-type *E. coli* were genuine assembly intermediates (Chen 2013). Combining their data with model-free clustering of each r-protein, they determined a new *in vivo* assembly map with a strong degree of correlation to the Nomura map (Chen 2013). This works suggests that the vast body of *in vitro* r-protein association work has *in vivo* validity.

In order to get an integrated understanding of the coupling of 16S rRNA processing to other ribosome biogenesis events such as r-protein binding and rRNA folding, the Culver lab affinity-purified ribosomes containing pre-rRNA (Gupta 2014). Regardless of the location of the affinity purification tag within the pre-rRNA, the vast majority of the purified particles contained 17S rRNA. Only by using modified 3'-5' RACE could they detect subsequent processing intermediates (Gupta 2014). This suggests that most stages of ribosome assembly occurs on a 17S-containing 'platform' and 3' and 5' processing is coordinated with the final steps of maturation, yet can proceed independently (Gupta 2014). Complexes purified by pulling down MS2 tagged species labeled in three different locations had slightly different r-protein complements and moderately different rRNA structures (as determined by kethoxal reactivity) suggesting they represent slightly different 'snapshots' of ribosome biogenesis (Gupta 2014). These data underline the importance of understanding the 17S pre-rRNA as the platform for ribosome assembly and the need to understand the timing of rRNA processing relative to other stages of biogenesis.

Recent work from our lab characterized pre-30S ribosomes in strains lacking RimM or RbfA grown at low temperature (Soper 2013). RbfA was originally discovered

as a high copy number suppressor of a cold-sensitive mutation in helix 1 (Dammel 1993, 1995). The primary method of characterization was *in vivo* hydroxyl radical footprinting – a method of directly probing the structure of assembly intermediates *in situ* that is capable of revealing residue-level structural details. This method revealed widespread structural differences between the mature and pre-30S particles suggesting global reorganization of the RNA during the maturation of the 30S particle (Soper 2013). The immature particles have pronounced perturbations to the central pseudoknot and helix 44, contain 17S rRNA, and lack the tertiary r-proteins (as suggested by solvent exposures and supported by quantitative mass spec of purified particles (Soper 2013). This work added another powerful and RNA-centric technique for determining the structure of assembly intermediates. One of the possible limitations of this work is the hydroxyl radical footprinting is less able to resolve differences between subspecies within heterogeneous populations – hence the use of assembly factor deletions to enrich the pool of ribosomal assembly intermediates – and the intermediates assayed may not be on path.

The Williamson lab has recently expanded their work on *in vivo* biogenesis to include a more structural level of analysis – negative stain electron microscopy with single-particle analysis of the polysome profile fractions (Sashital 2014). Random conical tilt analysis of the reference-free aligned EM particle classes revealed 3D maps of ribosome assembly intermediates isolated from exponentially growing wild-type *E. coli* (Sashital 2014). The earliest identifiable assembly intermediate has electron density for the body and platform of the 30S subunit but is lacking density for the head domain. Other assembly intermediates contain density for the head domain, in many different non-native conformations, or in its mature conformation. Electron density for late r-

proteins S21, S3, and S2 is lacking in density maps for the late assembly intermediates. Furthermore, chromosomal deletion of RimP, a ribosome assembly factor, led to an increase in the population of "floppy head" class II particles, decreased stability of the central pseudoknot, and depletion of S5 and S12 from the 30S particles purified from the *ΔrimP* strain. *In vitro* RimP accelerates the binding of 5' domain/central pseudoknot proteins S5 and S12 and has modest effects on the 3' domain proteins S7, S9, S13, S3, S10, and S14 (Bunner 2010). The structural information from this paper also supports the validity of earlier analyses of *in vitro* reconstituted ribosomes as well as providing provocative insight into the process of ribosome assembly *in vivo* and an explanation for the observation that so many ribosome assembly factors cluster around the neck. These assembly factors could aid in the formation of the central pseudoknot and help the "floppy head" particles properly assemble or prevent them from forming in the first place.

Given this recent explosion of *in vivo* biogenesis work corroborating five decades of work on *in vitro* ribosome assembly, determining how the J5/6 mutants affect *in vivo* biogenesis is of paramount interest. In Chapter 2, I showed that the J5/6 Triple mutant 5' domain rRNA is less stable and becomes trapped in folding intermediates in low monovalent ions. I also found that the mutant RNA is also more flexible in the J5/6 region and helix 13 and that this correlates with non-specific binding of protein S20 to J5/6 Triple mutant 5' domain rRNA. One of the most interesting *in vitro* findings was that J5/6 mutants destabilize the native conformation of helix 3. The addition of protein S16 is unable to overcome this destabilization even though the Triple mutant 5' domain RNP with S4, S17, S20, and S16 has a SHAPE reactivity close to that of the WT native

structure. This destabilization of helix 3 may interfere with proper structuring of the central pseudoknot and correct domain-domain orientations of the 30S ribosome *in vivo*.

To correlate these findings with *in vivo* 30S assembly, I incorporated the J5/6 mutations – G107U; A59,60C; and A59,60C, G107U (Triple) – into a plasmid (pLK45 or pSpur; Powers 1990, Green 2005) conditionally expressing the full *rrnB* operon. I discovered that the mutant ribosomes cannot support life independently because the mutant pre-rRNA is unable to be processed, and the mutant pre-30S ribosomes never mature. This was a stronger phenotype than originally expected based on the *in vitro* data in Chapter 2, but it highlights the complexity of ribosome biogenesis.

3.2 Materials and Methods

3.2.1 Generation of *in vivo* expression plasmids

Starting with the mutant pRNA1 plasmids (Chapter 2) the rRNA sequences between the *Bcl*I and *Bgl*II restriction sites were added using overlap extension PCR (Table 3.1) and the amplified mutant rDNA fragments were inserted into the pCR2.1-Topo vector (Invitrogen) to create pMCR-Topo X(Table 3.2). The pMCR-Topo plasmids were sequenced, digested with *Bcl*I and *Bgl*II (NEB), and the rDNA fragment (nucleotides 15-704) was subcloned into pRNA5. The *Bcl*I -- *PspOM*I fragments of the pRNA5 derivatives were subcloned into the same sites of pLK45 (Powers 1990) (Figure 3.1).

The J5/6 mutations were inserted into pSpur, a pLK45 derivative with an MS2-hairpin at the tip of helix 6, in a multi-step process based upon the method of Youngman and Green (2005). A *Spe*I recognition site was inserted into the pRNA5 derivatives using Quikchange and primers **Insert SpeI Fwd** and **Insert SpeI Rev**. These vectors (pRNA5-Spe-X) were then digested with *Spe*I and combined with an annealed and digested synthetic MS2 hairpin oligonucleotide (**MS2 hairpin Fwd** and **MS2 hairpin Rev**). Another round of Quikchange was then used to remove the tip of helix 6 and correct the hairpin sequence (**GCUU deletion Fwd** and **GCUU deletion Rev**). The correct J5/6 mutant-MS2 fragments (nucleotides 15-704 plus 36 nt insertion at nucleotide 82) were digested and subcloned from pRNA5 into pSpur using *Bcl*I and *PspOM*I. The pSpur-WT plasmid was a kind gift from the Green lab.

Table 3.1: **Quikchange primers.** The sequences of the primers used in cloning the J5/6 mutants are shown. Capital text shows the location of the mutations/insertions. The Triple mutant A59,60C G107U was made by two rounds of Quikchange with the above primers.

Mutation	Primer	Sequence
Insert SpeI	Fwd	acggtaacaggaagaagACTAGTcttgcttctttgctgac
Insert SpeI	Rev	gtcagcaaagaagcaaagACTAGTcttcttcctgttaccgt
MS2 hairpin	Fwd	ccaggaACTAGTTTTTGATGAGGATTACCCATCCTTT ACTAGTaggtcc
MS2 hairpin	Rev	ggacctACTAGTAAAGATGGGTAATCCTCATCAAAA ACTAGTtcctgg
GCUU deletion	Fwd	ccatctttactagtctt****ctttgctgacgagtggc
GCUU deletion	Rev	gccactcgtcagcaaag****aagactagtaaagatgg

Table 3.2: **Overlap extension PCR templates and primers.** The three individual PCR products were combined to generate the elongated template.

	Template	Forward Primer	Reverse Primer	Product
5' end BclI	pKK3535	Past BclI aagcggcactgctctttaac	BclI Rev gcgttcaatctgagccatga	189 nt
Site of mutation	pRNA1 derivatives	BclI addition agagtttgatcat- ggctcagattgaacgctg	Past ScaI gttagccggtgcttcttctg	504 nt
3' end BglII	pKK3535	BglII Fwd attgacgttacccgcagaag	Past BglII cctccaagtcgacatcgttt	124 nt
Full template	PCR fragments above	Past BclI aagcggcactgctctttaac	Past BglII cctccaagtcgacatcgttt	986 nt

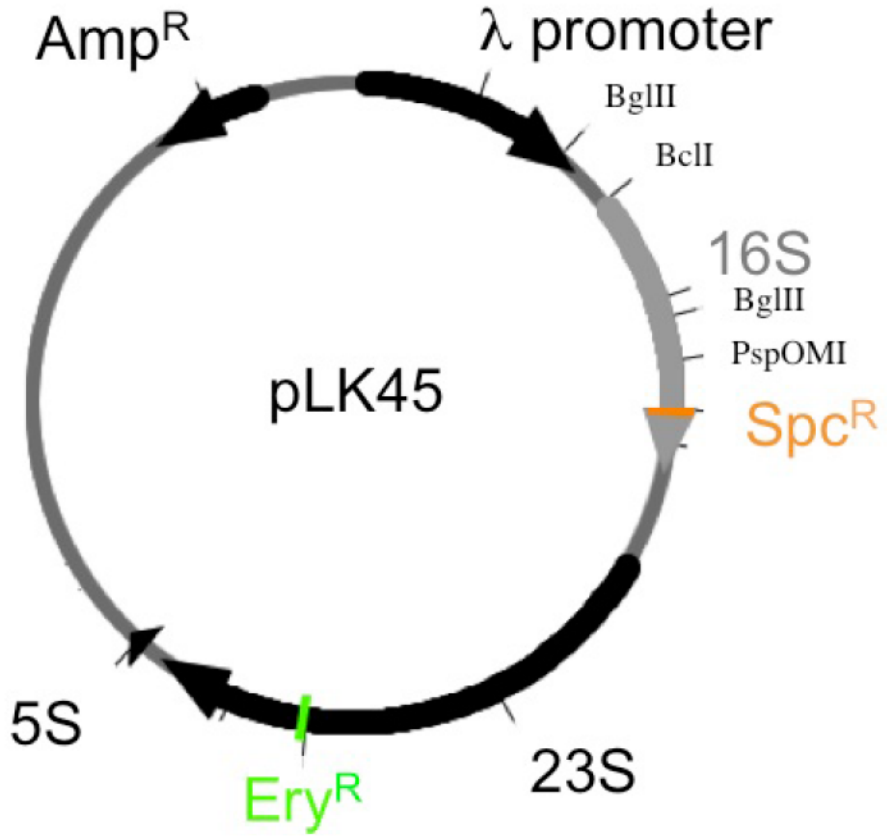

Figure 3.1: **pLK45 vector for the *in vivo* expression of mutant rRNA.** The plasmid pLK45 (Powers 1990) contains the *E. coli rrnB* operon under repressible control by the lambda promoter. Single point mutations in the 16S and 23S rRNA genes confer resistance to spectinomycin (orange) and erythromycin (green). The point mutations also allow for quantitation of plasmid-encoded rRNA. Restriction sites used for cloning 16S J5/6 mutations into this vector are indicated.

3.2.2 Bacterial strains

DH1 (F⁻ *glnV44 recA1 endA1 gyrA96 thi1 hsdR17 ((rK⁻ mK⁺) relA1)*/ pCI^{857} with plasmid pCI^{857} harboring the temperature-sensitive λ repressor was used for initial growth assays as the repression would allow for the study of the J5/6 mutants even if they were dominant lethal (Zhang 1995 and Powers 1990).

SQZ10 strain (F- *ara Δlac thi Δ(purDH-rrnE-metA) polA1 zih*::Tn*10 Δ(rrsB-gltT-rrlB)101 Δ(rrsH-ileV-alaV-rrlH)103 Δ(rrsG-gltW-rrlG)30::lacZ*$^+$ *polA* $^+$*Δ(rrsA-ileT-alaT-rrlA)34 Δ(rrsD-ileU-alaU-rrlD)25::cat*$^+$ *Δ(rrsC-gltU-rrlC)15::cat*$^+$ *ilv* $^+$/pTRNA67, pHK-rrnC$^+$ sacB) lacking chromosomal *rrn* operons (Δ7*rrn*) and covered by the pHK-rrnC$^+$sacB and pTRNA67 helper plasmids was used to study the J5/6 mutants without a background of chromosomal ribosomes (Asai 1999, Zaporojets 2003).

DH5α (F- *endA1 hsdR17 (rK⁻ mK⁺) glnV44 thi-1 recA1 gyrA relA1 Δ(lacIZYA-argF)U169 deoR (φ80dlacΔ(lacZ)M15)*) was used for growth rate and polysome profile determination without repression at multiple growth temperatures.

MRE600 (F- *rna*) – a strain lacking the periplasmic endonuclease RNase I – was used for growth rate and polysome profile determination assays, as well as for *in vivo* structural determination (Chapter 4).

BW25113 (*Δ(araD-araB)567 ΔlacZ4787*(::rrnB-3) *λ- rph*-1 *Δ(rhaD-rhaB)568 hsdR514*) was used as the WT|parental strain for the Keio collection single gene knockouts and also the parental strain in this study for the ribosome assembly factor overexpression, which was a kind gift from the Xiao lab.

JM3136 (BW25113 *ΔrbfA779*::kan) from the Keio collection of single gene knockouts was obtained from the National BioResource Project (NIG, Japan) (Baba

2006).

3.2.3 Growth of J5/6 mutants

DH1/ pCI^{857} cells transformed with pLK45 or derivatives containing J5/6 mutations were grown under permissive conditions (30° C) or non-permissive (42° C) conditions in LB with 25 mg/L carbenicillin and 25 mg/L kanamycin. For the plating assay, cells were grown at 30° C until they reached mid-log (0.45-0.6 OD_{600}). The cultures were diluted to a calculated OD_{600} = 0.05 and 5 µl of eight serial 10-fold dilutions were spotted onto LB agar plates with 25 mg/L carbenicillin, 25 mg/L kanamycin or 25 mg/L carbenicillin and 10 - 60 mg/L spectinomycin. Plates were grown 16-36 hours at 32° (permissive) or 42° C (non-permissive) as previously described (Powers 1990).

Δ7*rrn*/pTRNA67(Spc^{R}), pHK-rrnC^{+}sacB(Kan^{R}) cells transformed with pLK45 or derivatives were grown at 37° C in either 100 mg/L ampicillin and 50 mg/L kanamycin or just 100 mg/L ampicillin. After 120 minutes, 3% sucrose was added to the ampicillin cultures to select for loss of the *rrnC* plasmid (Asai 1999, Zaporojets 2003).

Saturated overnight cultures of BW25113 or JM3136 cells transformed with pSpur derivatives and plasmids overexpressing ribosome assembly factors as indicated in the figures were diluted to OD_{600} = 0.01 in pre-warmed LB with 50 mg/L ampicillin and sometimes 50 mg/L kanamycin when required. Bacteria were grown at 25º, 37º, and 42º C with shaking. Optical density measurements were taken every 30 minutes until past mid-log. Growth data from induction to OD_{600} = 0.5 were fit to

$$y = I_o + Ie^{\wedge}((t - t_L)/t_D)$$

in which I_0, the initial inoculum, was adjusted manually to minimize the error in the early time points. I, the active inoculum, t_L, the lag time, and t_D, the doubling time, were all fit via least squares regressions (KaleidaGraph).

3.2.4 Quantitation of plasmid-encoded rRNA

Primer extension reactions to quantitate the percentage plasmid-derived 16S rRNA were performed as previously described (Triman 1989). Briefly, 0.1 pmol ^{32}P-labeled primer (Table A.3 for sequence) was annealed to 500 ng Total RNA. Primers were extended by AMV reverse transcriptase (NEB) in the presence of dATP, dTTP, dCTP, and ddGTP. Reactions were incubated for 15 minutes at 42° C prior to being loaded onto a 15% acrylamide gel with 8M urea in TBE. The gel was run at 15 W for 2-4 hours and exposed to a Phosphorimager screen. Band volumes were quantified with ImageQuant (Molecular Dynamics).

Primer extension to quantitate the percentage plasmid-derived 23S was performed almost identically. The 23S primer was extended in the presence of dATP, dGTP, dCTP, and ddTTP, and reactions were incubated for 15 minutes at 48° C (Table A.3 for sequence).

3.2.5 Analytical sucrose gradients

Analytical sucrose gradients were performed as described (Spedding 1990) with several additions. Briefly, cells were grown to mid-log (OD_{600} = 0.45-0.6) and 5 mL aliquots of culture were chilled on ice immediately prior to centrifugation at 5,000 x *g* for

15 minutes and washed with cold buffer (10 mM Tris pH 7.5, 20 mM $MgCl_2$, 200 mM NH_4Cl, 3 mM β-mercaptoethanol). Pellets were stored at -80° C until needed. Cells were resuspended in 1 mg/mL egg white lysozyme (in 10 mM Tris pH 7.8, 15 mM $MgCl_2$), frozen in an ethanol-dry ice bath and slowly allowed to thaw on ice. Clarified lysates were loaded onto 10%-40% analytical sucrose gradients (in 20mM Tris pH 7.8, 10 mM $MgCl_2$, 100 mM NH_4Cl, 2 mM DTT) and centrifuged at 35,000 rpm (210,000 x *g* at r_{max}) for 3.5 hours instead of 2.5 hours to achieve greater resolution of the pre-30S particles. Gradients were analyzed with a BioComp piston fractionator and UV absorbance traces at 254 nm were recorded with WINDAQ software (DataQ). Additionally, 400 µL fractions from peaks of interest were ethanol precipitated overnight, phenol extracted four times, chloroform extracted twice, and ethanol precipitated a second time prior to rRNA analysis.

3.2.6 Primer extension to map 16S 5' end

Either 2 µg total RNA or 500 ng purified 16S rRNA (1 pmol rRNA) was annealed to 1 pmol ^{32}P-labeled primer **161** (Table A.3). Primers were extended by SuperScript III reverse transcriptase (Invitrogen) at 52.5° C for 30 minutes. Samples were run on an 8% acrylamide gel at 55W for 2-4 hours and exposed to a Phosphorimager screen. Band volumes were quantified with ImageQuant (Molecular Dynamics).

For Total RNA samples from pSpur-transformed cells, values of the four major rRNA species (chromosomally-derived mature rRNA, plasmid-derived mature rRNA, chromosomally-derived immature rRNA, and plasmid-derived immature rRNA) were normalized to the total amount of mature rRNA, as *E. coli* regulate rRNA expression

levels to control for gene dosage an optimize the number of functional ribosomes for the growth conditions (Jinks-Roberston 1983 and Condon 1993).

3.2.7 Northern blot

Northern blots were performed as described (Soper 2013, based on Brown 2004). Glyoxal-treated total RNA (~2 μg) was electrophoresed on a 1.4% 1:1 SeaKem LE:NuSieve GTG agarose gel (Lonza) in 10 mM sodium phosphate pH 7.0 for 16-18 hours at 40 V. After transfer to a Nytran SPC membrane (Whatman), the blot was hybridized overnight at 42° C with 60 pmol ^{32}P-labeled primer **323** (Table A.3). After eight washes of increasing stringency SSC-based buffers, including two high-stringency washes (42°C, 0.1X SSC, 0.1% SDS; Brown 2004), the blot was exposed to a Phosphorimager screen and band volumes were quantified with ImageQuant (Molecular Dynamics).

3.2.8 Generation of assembly factor overexpression vectors

RbfA overexpression from the native promoter was tested using the plasmid p15B-3, a gift from the Noller lab (Dammel 1995). Vectors from the ASKA collection (Kitagawa 2005) – a collection of plasmids with *E. coli* genes under control of the T5-lac IPTG-inducible promoter and *lacI*^{q} repressor – expressing ribosome assembly factors Era, KsgA, RimJ, RimP, RsgA, RsmC, and YbeY were a kind gift from Gloria Culver.

Unfortunately, the ASKA collection vector has a pBR322-derived origin of replication – the same origin of replication as the pLK45 or pSpur vectors – and thus was

incompatible to use to test if overexpression of the factors could rescue the J5/6 mutants. Oligonucleotides **FWD from ASKA** and **REV from ASKA** were designed to amplify the ORF and N-terminal His-tag but not the ASKA C-terminal GFP, Coding fragments amplified by Touchdown PCR were inserted into pD421-RAF (a vector from DNA 2.0 with the T5-lac IPTG-inducible promoter, *lacI*^{q} repressor, and pACYC origin of replication) using a *Sap*I recognition sequence (Table 3.3). Additionally, gene-specific primers **SfiI RbfA FWD, SfiI RbfA REV, SfiI RimM FWD**, and **SfiI RimM REV**, added *Sfi*I recognition sites before and after the RbfA and RimM genes from codon 2 to the 2nd-to-last codon. The ORFs were inserted into the context of the ASKA ORFs (Kitagawa 2005), with a His-tag and a 7 amino acid spacer on the N-terminus and a 5 amino acid spacer on the C-terminus. ORFs were amplified by Touchdown PCR, digested with *Sfi*I, and inserted into pD421-SR digested with *Sfi*I.

3.2.9 Ribosome assembly factor overexpression growths

Saturated overnight cultures of BW25113/pSpur-Triple transformed with a pD421-RAF vector were diluted to OD_{600} = 0.02 in pre-warmed LB with 50 mg/L ampicillin and 50 mg/L kanamycin. Cultures were grown to OD_{600} = 0.2, split into two flasks and each diluted to a calculated OD_{600} = 0.004 in pre-warmed LB with 50 mg/L ampicillin, 50 mg/L kanamycin. Half of the growths were induced with 1 mM IPTG (unless otherwise stated). Cultures were grown for 6 hours. Each hour ~ 0.3 g cell pellets were harvested for protein analysis, and 0.5 ml aliquots were removed and combined with 1 mL RNAprotect for Total RNA analysis (Qiagen). For rRNA processing comparison assays, cultures were grown 3.5 to 4.5 hours until mid-log (OD_{600} = 0.4–0.6).

Table 3.3: **Primer sequences for assembly factor overexpression vectors.** The sequences of the primers used in cloning the ribosome assembly factors are shown. Capital text shows the location of the *Sap*I/*SfiI* recognition sequence. Underlined text is ASKA plasmid specific sequence or ORF specific sequence.

Primer Name	Sequence
Fwd from ASKA	tacacgtacttagtcgctgaaGCTCTTCtatgagaggatctcaccatca
Rev from ASKA	attgacgGCTCTTCtaccctagcggccgcataggcc
SfiI RbfA Fwd	GGCCCTGAGGGCCgcgaaagaatttggtcgc
SfiI RbfA Rev	GGCCGCATAGGCCgtcctccttgctgtcg
SfiI RimM Fwd	GGCCCTGAGGGCCagcaacaactcaccgc
SfiI RimM Rev	GGCCGCATAGGCCaaaaccaggatcccaatct

3.2.10 Small-scale purification of ribosome assembly factors

Cell pellets (~100 mg) were resuspended in 0.5 mL 1 mg/mL lysozyme in Lysis Buffer (50 mM NaH_2PO_4, 300 mM NaCl, 10 mM imidazole, 0.5% (w/v) Tween-20, 10% (w/v) glycerol). Cells were lysed for 30 minutes on ice before the lysate was clarified at 15,000 x *g* for 20 minutes. The supernatant was transferred away from the pellet into a fresh tube (and 20 µL supernatant was saved for SDS-page analysis) before being added to the washed resin from a 50 µL aliquot of 50% Ni-NTA agarose slurry (Qiagen). The lysate and resin were incubated with gentle mixing at 4° C for ~30 minutes. The beads were washed twice with Lysis Buffer and twice with Wash Buffer (Lysis Buffer plus 50 mM imidazole). 10 µL of the washed beads were added to 10 µL 3X SDS Loading Buffer for SDS-page analysis. The ribosome assembly factor was eluted from the remaining Ni-NTA bead with 50 µL Elution Buffer twice (Lysis Buffer plus 250 mM imidazole). Samples of lysate and beads and the intermediate aliquots were combined with 10 µL 3X SDS Loading Buffer, denatured at ~95°C for ~5 minutes and loaded onto a precast 4-20% gel (Mini-PROTEAN TGX Bio-Rad).

3.3 Results

3.3.1 Growth of J5/6 mutants

To test the effect of the mutations in the junction between helices 5 and 6 of the 16S rRNA on bacterial growth, DH1 cells with the temperature-sensitive λ repressor plasmid pCI^{857} were transformed with pLK45 or derivatives containing the J5/6 mutations: G107U, A59,60C and the Triple mutant A59,60C G107U. Cell cultures containing the mutant plasmids grew identically to the culture containing WT pLK45 at 30° C, but grew slightly slower at 42° C when plasmid-derived transcription was permitted (data not shown) showing that expression of the J5/6 mutants is only mildly deleterious in the presence of wild type ribosomes.

I observed a striking difference in growth, however, on spectinomycin plates that select for a Spc^{R} point mutation in the plasmid-encoded 16S rRNA. Diluted cell cultures containing mutant plasmids were non-viable when forced to rely on plasmid-derived ribosomes for protein synthesis (Figure 3.2).

To confirm these results, I transformed the pLK45 derivatives into a Δ7*rrn* strain of *E. coli* with a sucrose-sensitive helper plasmid containing *rrnC* (Δ7*rrn*/pTRNA67, pHK-rrnC^{+}sacB). In the presence of the *rrnC*$^{+}$*sacB* helper plasmid, the cells transformed with the J5/6 Triple mutant grew slightly slower than the cells transformed with wild-type plasmid control (Figure 3.3 A). Upon selecting for the loss of the pHK-rrnC^{+}sacB helper plasmid with sucrose, the cells with WT pLK45 recovered after a few generations, but the cells with mutant pLK45 derivatives did not. Additionally, primer extension analysis of the Spc^{R} point mutation confirmed that very little J5/6 mutant 16S rRNA was

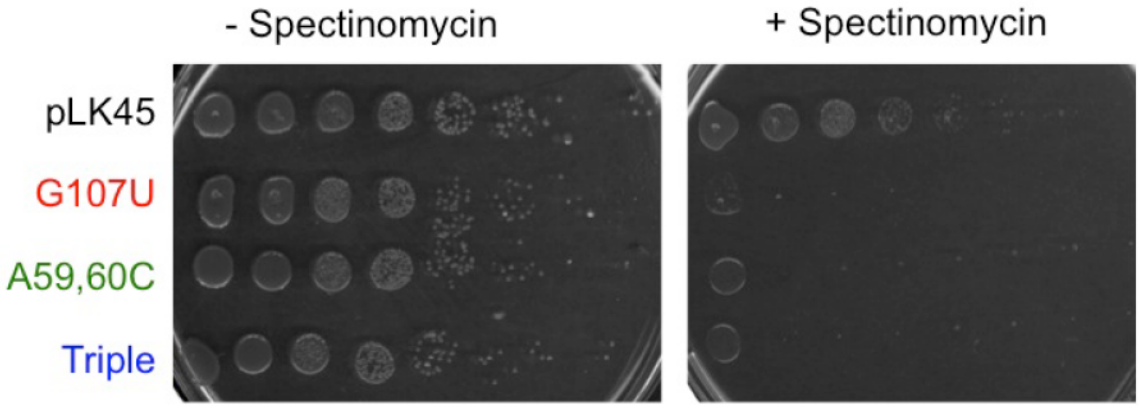

Figure 3.2: **Induction of J5/6 mutants on solid media.** DH1/ pCI^{857} cells transformed with pLK45 or its derivatives (indicated on panel) were grown to mid-log at 30° (permissive conditions). 10-fold serial dilutions were spotted on solid LB agar with or without 10 mg/L spectinomycin and incubated at 42° C (non-permissive). The J5/6 mutants are recessive lethal.

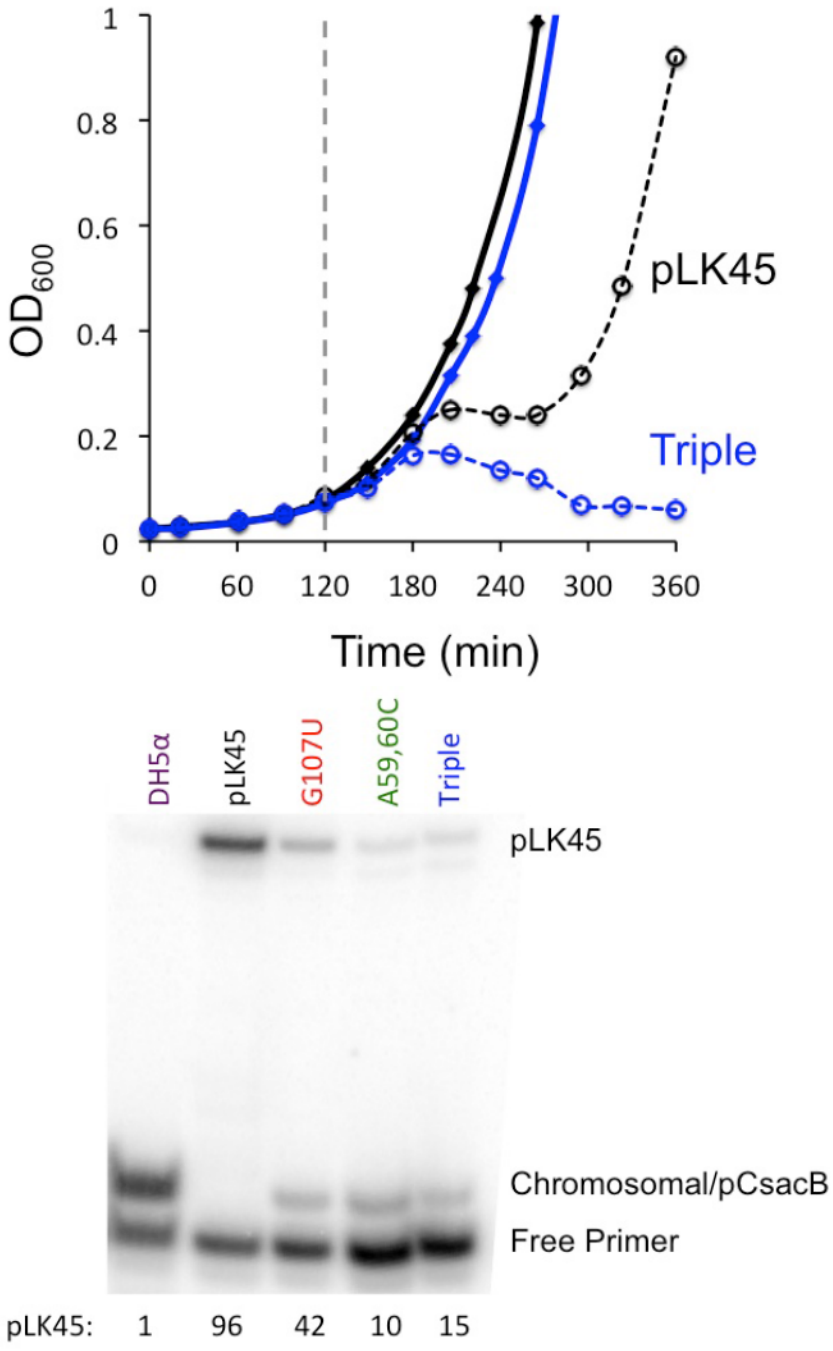

Figure 3.3: **Growth of J5/6 mutants in Δ7*rrn* cells.** A) Growth curves of Δ7*rrn*/pTRNA67, pHK-rrnC^{+}sacB carrying WT pLK45 (black) or pLK45-Triple mutant (blue) were grown at 37° C. After 120 minutes 3% sucrose was added to select for loss of the *rrnC* helper plasmid (dashed lines). B) Primer extension analysis of total RNA from DH5α or from Δ7*rrn*/pTRNA67, pHK-rrnC^{+}sacB cells transformed with pLK45 or derivatives. Cells were grown to mid-log (OD_{600}=0.45-0.6). The proportion of pLK45-derived 16S rRNA is indicated below the gel. J5/6 mutants are unable to support bacterial growth.

found in the Δ7*rrn*/pTRNA67, pHK-rrnC^{+}sacB cells despite the lack of the 7 chromosomal operons (Figure 3.3 B). I therefore concluded that the J5/6 mutants are recessive lethal and cannot support bacterial growth.

3.3.2 Maturation of J5/6 mutant ribosomes

To examine if the J5/6 mutants cannot support growth because of a defect in 30S assembly, polysome profiles were determined by sucrose gradient sedimentation velocity. For these experiments, DH5α cells were transformed with the pLK45 derivatives and grown at 25°, 37°, and 42° C to assay if the assembly of the J5/6 mutants was temperature sensitive.

A polysome profile from DH5α/pLK45 cells showed a large 70S peak and clear 30S and 50S peaks. Analysis of the source and 5' processing of the 16S rRNA revealed a uniform distribution of the plasmid-encoded 16S rRNA and an increase of mature 16S from the lightest fraction of the 30S peak through the heaviest fraction of the 30S peak. There was practically no immature 17S rRNA in the 70S peak fractions. All of this is as expected and serves as a control for the J5/6 mutants.

Polysome profiles from both A59,60C and the Triple mutant strains had pronounced, lighter-than-30S shoulders (Figure 3.4). Analysis of these broad 30S shoulders showed they are enriched in mutant rRNA and immature 17S – especially in the lighter fractions of the 30S peak. Increasing the growth temperature decreased the size of the pre-30S shoulder in relation to the main 30S peak but neither A59,60C nor the Triple mutant rRNA ever made it into the 70S peak. As with Δ7*rrn* strains, the mutant rRNA does not accumulate to the same extent as the WT plasmid-derived rRNA. rRNA

Figure 3.4: **Polysome profiles of J5/6 mutants at three growth temperatures.** Polysome profiles of DH5α /pLK45 (black), DH5α/pLK45-G107U (red), DH5α/pLK45-A59,60C (green) or DH5α/pLK45-Triple (blue) cells grown at 25º, 37º, 42º C. 30S and 70S peaks were fractionated and the 16S rRNA was analyzed for its source and 5' end processing. Both the proportion of plasmid-derived rRNA and bar graphs of the proportion of mature rRNA is indicated below each peak.

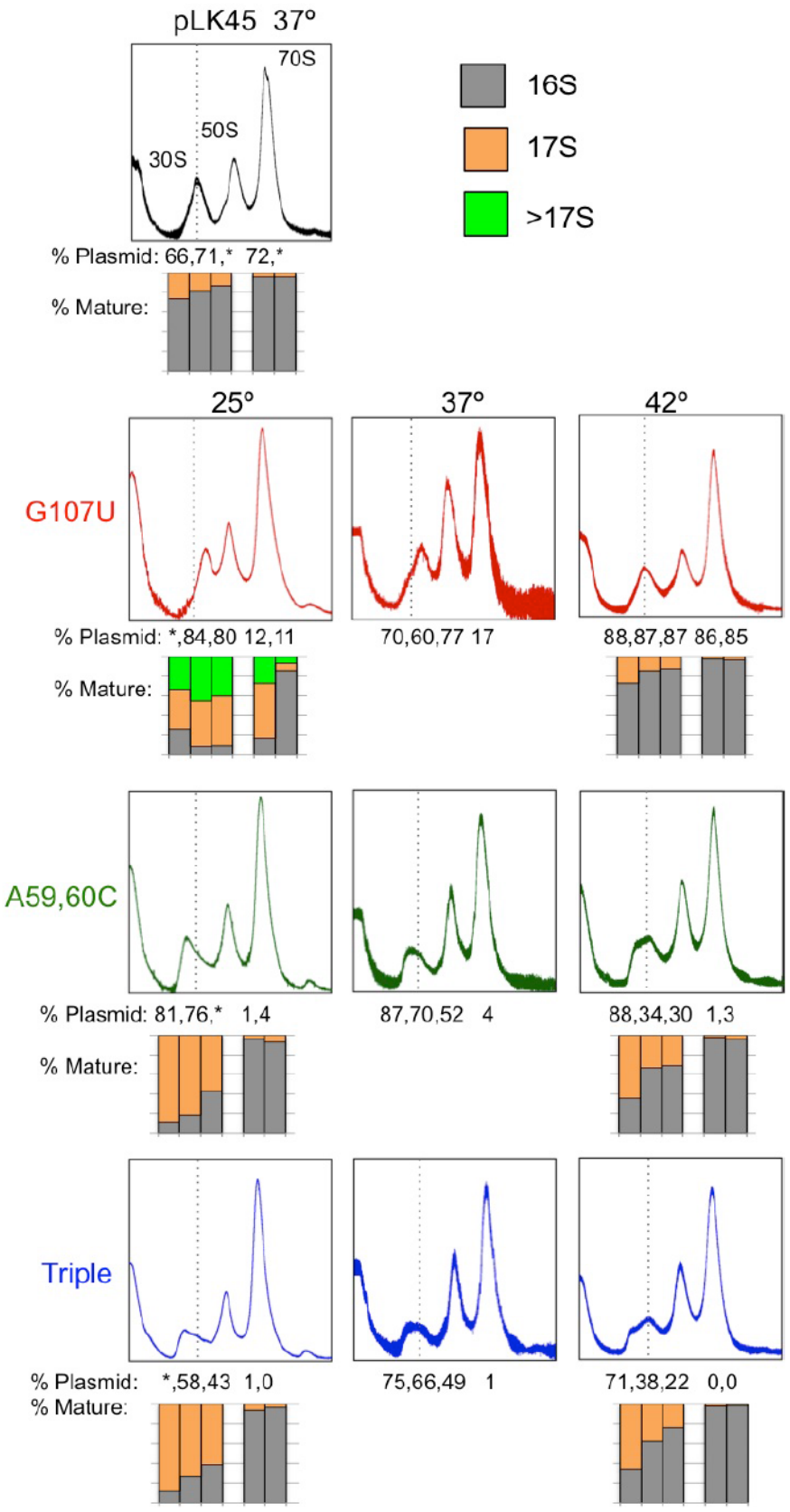
pLK45 37°
70S
50S
30S
16S
17S
>17S
% Plasmid: 66,71,* 72,*
% Mature:
25°
37°
42°
G107U
% Plasmid: *,84,80 12,11
70,60,77 17
88,87,87 86,85
% Mature:
A59,60C
% Plasmid: 81,76,* 1,4
87,70,52 4
88,34,30 1,3
% Mature:
Triple
% Plasmid: *,58,43 1,0
75,66,49 1
71,38,22 0,0
% Mature:

containing these two J5/6 mutants fail to produce functional 30S subunits.

Polysome profiles from cells expressing G107U 16S rRNA exhibited an even more interesting assembly phenotype. At 25º C, the G107U 30S peak was shifted significantly towards heavier fractions. This G107U peak contained mostly mutant rRNA and pre-rRNA with a much longer 5' end than 17S precursor, indicating a lack of cleavage by RNase III. Increasing growth temperatures improved G107U processing, and at 42º C, G107U rRNA entered the 70S peak in similar ratios to the WT pLK45-derived rRNA. A Northern blot of total RNA indicated that this extra-long G107U species is completely unprocessed 35S pre-rRNA (Figure 3.5). The 35S pre-rRNA does not accumulate in MRE600/pSpur-G107U (Figure 3.6) or BW25113/pSpur-G107U strains (Figure 3.7), perhaps because the MS2 hairpin stabilizes an RNase III-processing competent rRNA structure, or because of unknown strain differences.

In order to affinity purify the J5/6 pre-ribosomes, I inserted the mutations into pSpur, a pLK45 derivative with an MS2-hairpin at the tip of helix 6 (Youngman 2005). Serendipitously, the placement of the MS2 hairpin in the pSpur constructs allows for deconvolution of the source and 5' processing of 16S rRNA in one clear primer extension assay due to the 36 nt MS2 insertion (Figure 3.6 A). Polysome profiles from MRE600 cells transformed with pSpur and pSpur derivatives were similar to those from DH5α cells transformed with pLK45 and pLK45 derivatives, with the previously mentioned G107U strain differences (Figure 3.6). The definitive primer extension analysis showed that the immature and the plasmid-derived species were the same. 16S rRNA containing the J5/6 mutants is never fully processed.

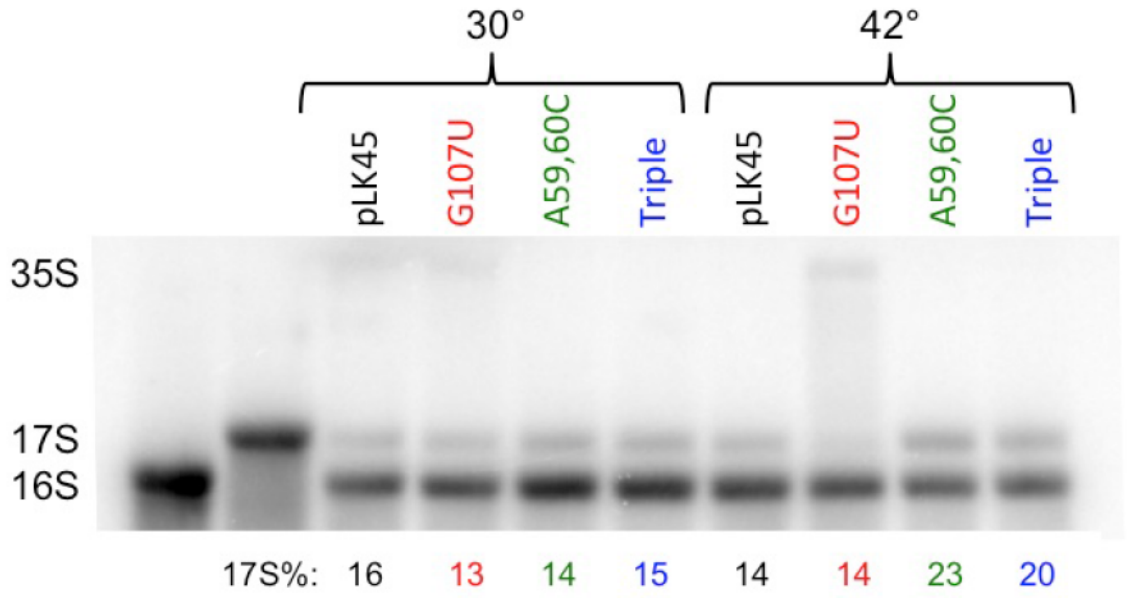

Figure 3.5: **Northern blot of RNA from J5/6 mutants**. Northern blot with total RNA from DH1/ pCI^{857}, pLK45 (black); DH1/ pCI^{857}, pLK45-G107U (red); DH1/ pCI^{857}, pLK45-A59,60C (green); or DH1/ pCI^{857}, pLK45-Triple (blue) grown to mid-log at 30° (permissive, control) or 42° C (non-permissive transcription). Percentage of 17S rRNA species in each lane is indicated below the gel. Cells expressing G107U rRNA have some unprocessed 35S pre-rRNA.

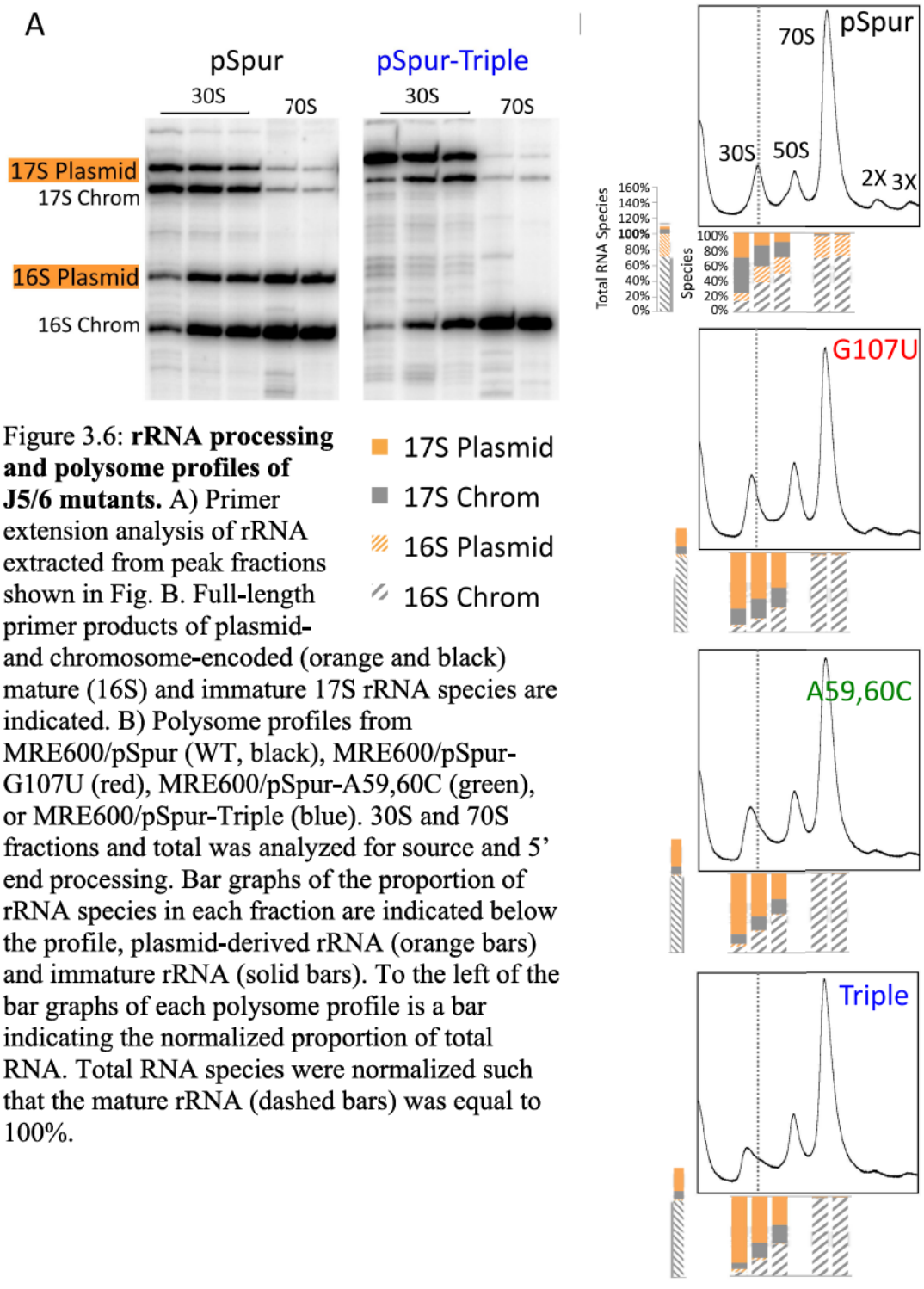

Figure 3.6: **rRNA processing and polysome profiles of J5/6 mutants.** A) Primer extension analysis of rRNA extracted from peak fractions shown in Fig. B. Full-length primer products of plasmid- and chromosome-encoded (orange and black) mature (16S) and immature 17S rRNA species are indicated. B) Polysome profiles from MRE600/pSpur (WT, black), MRE600/pSpur-G107U (red), MRE600/pSpur-A59,60C (green), or MRE600/pSpur-Triple (blue). 30S and 70S fractions and total was analyzed for source and 5' end processing. Bar graphs of the proportion of rRNA species in each fraction are indicated below the profile, plasmid-derived rRNA (orange bars) and immature rRNA (solid bars). To the left of the bar graphs of each polysome profile is a bar indicating the normalized proportion of total RNA. Total RNA species were normalized such that the mature rRNA (dashed bars) was equal to 100%.

3.3.3 The effect of RbfA overexpression on growth and ribosomal maturation of J5/6 mutants

In order to test whether or not RbfA, a ribosome assembly factor with known rRNA folding and processing effects, could aid in the processing of mutant pre-rRNA and the assembly of J5/6 mutant ribosomes, expression of RbfA from the native promoter on a plasmid with ~15 copies per cell was tested in conjunction with expression of J5/6 mutants from pSpur plasmid derivatives. The effect of RbfA expression on bacterial growth rates, processing of total 16S RNA, and the polysome profile was tested.

The lag times and doubling times for growth of the BW25113 parental strain transformed with pSpur derivatives and p15B-3 expressing RbfA were determined at 25º, 37º, and 42º C as described above. The doubling times were insensitive to RbfA overexpression (Table 3.4). There is quite a bit of variation in lag times, but as the lag time is more dependent on the I_0 value and initial fit values, the importance of this variation is unclear (Table 3.5).

In order to test the effect of RbfA expression on mutant pre-rRNA processing, total RNA was extracted from BW25113/pSpur and derivative cells with and without p15B-3 expressing RbfA. Cells were grown at 25º, 37º, and 42º C. The 5' end processing and the source of the 16S rRNA populations was assayed by primer extension. The relative proportion of rRNA species was normalized to the total amount of mature rRNA as rRNA expression levels are regulated to control for gene dosage (Jinks-Roberston 1983 and Condon 1993). RbfA overexpression from the native promoter slightly decreases the accumulation of immature J5/6 rRNA (Figure 3.7). At 37°C the decrease is

Table 3.4: **Doubling times for J5/6 mutants with RbfA overexpression.** Fit doubling times of BW25113 transformed with pSpur derivatives and RbfA overexpression vector (p15B-3). Growth rate data were fit to the four variable equation $y = I_o + Ie^{((t - t_L)/t_D)}$. RbfA overexpression does not significantly change doubling times. Doubling times significantly different from BW25113 are signified in bold text. Errors are from the uncertainty in the fits. Growth of BW25113+EV (pACYC184) only done with pSpur.

		Doubling Time BW25113	Doubling Time + empty vector	Doubling Time + RbfA
BW25113	25° C	82.5 ± 1.6		**97.1 ± 1.4**
	37° C	29.9 ± 0.3		36.8 ± 0.3
	42° C	28.1 ± 0.6		28.2 ± 2
BW25113/pSpur	25° C	84.5 ± 0.8	**98.0 ± 1.3**	99.8 ± 3
	37° C	34.8 ± 1.1	36.6 ± 1.5	37.1 ± 0.4
	42° C	31.2 ± 0.6	**26.9 ± 0.9**	30 ± 2
BW25113/pSpur-G107U	25° C	91.0 ± 0.8		94.7 ± 1.6
	37° C	39.3 ± 0.5		40.8 ± 0.6
	42° C	31.2 ± 0.8		36 ± 3
BW25113/pSpur-A59,60C	25° C	90.8 ± 0.8		97 ± 2
	37° C	38.3 ± 1.0		42.5 ± 0.4
	42° C	31 ± 2		34 ± 3
BW25113/pSpur-Triple	25° C	91.1 ± 1.0		**104 ± 1.2**
	37° C	40.6 ± 0.5		41.5 ± 1.1
	42° C	33.7 ± 1.2		37 ± 2

Table 3.5: **Lag times for J5/6 mutants with RbfA overexpression.** Fit lag times of BW25113 transformed with pSpur derivatives and RbfA overexpression vector (p15B-3). Growth rate data were fit to the four variable equation $y = I_o + Ie^{((t - t_L)/t_D)}$. Lag times vary with RbfA overexpression. Lag times significantly different from BW25113 are signified in bold text. Errors are from the uncertainty in the fits. Growth of BW25113+EV (pACYC184) only done with pSpur.

		Lag Time BW25113	Lag Time + empty vector	Lag Time + RbfA
BW25113	25° C	6 ± 5		9 ± 5
	37° C	5 ± 5		15 ± 5
	42° C	0 ± 5		0 ± 5
BW25113/pSpur	25° C	125 ± 5	**24 ± 5**	28 ± 5
	37° C	46 ± 5	**64 ± 5**	75 ± 5
	42° C	46 ± 5	46 ± 5	40 ± 5
+ pSpur-G107U	25° C	90 ± 5		**53 ± 5**
	37° C	34 ± 5		**117 ± 5**
	42° C	50 ± 5		**25 ± 5**
+ pSpur-A59,60C	25° C	90 ± 5		**27 ± 5**
	37° C	51 ± 5		**140 ± 5**
	42° C	55 ± 5		**32 ± 5**
+ pSpur-Triple	25° C	91 ± 5		**37 ± 5**
	37° C	46 ± 5		**134 ± 5**
	42° C	76 ± 5		75 ± 5

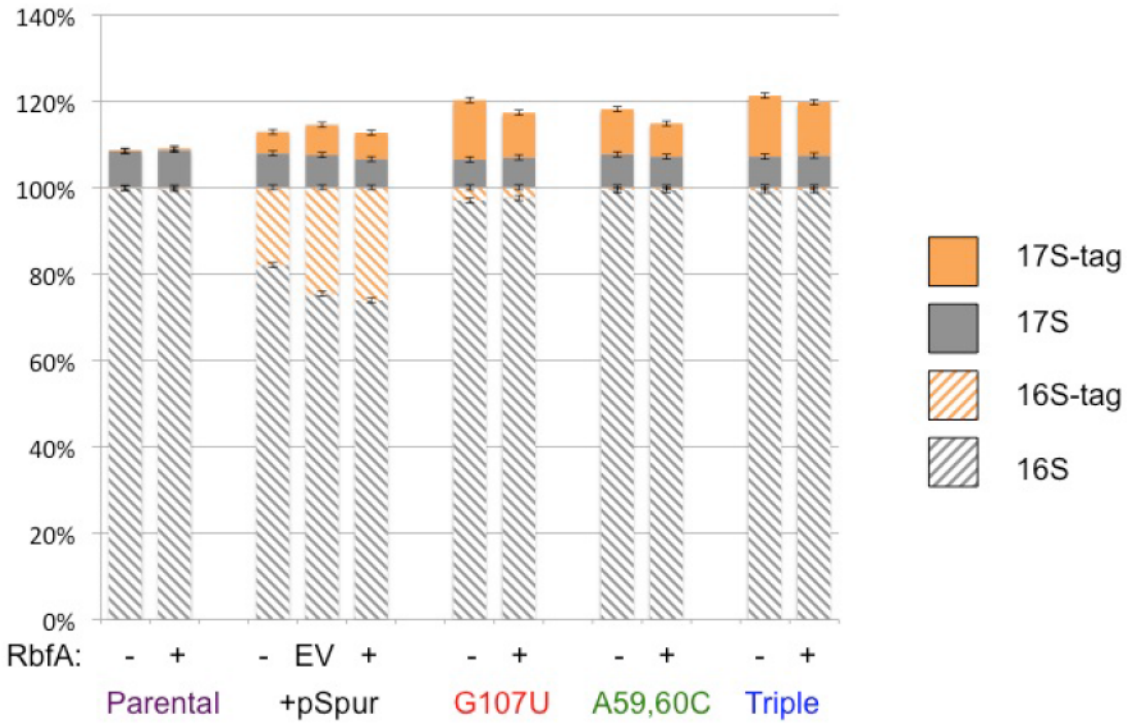

Figure 3.7: **rRNA processing of J5/6 mutants with RbfA overexpression**. 5' end processing and source of 16S rRNA from BW25113 (purple), BW25113/pSpur (black), BW25113/pSpur-G107U (red), BW25113/pSpur-A59,60C (green), or BW25113/pSpur-Triple (blue) with and without p15B-3 (RbfA overexpression vector) grown at 37° C. pCYC-184 derived empty vector (EV) used as p15B-3 control. Bar graphs of plasmid-derived rRNA (orange bars) and immature rRNA (solid bars). Total RNA samples were normalized to the total amount of mature rRNA. Error bars represent the standard deviation of three technical replicates. RbfA overexpression decreases retention of immature mutant rRNA but does not improve processing.

3.4 ± 0.6% for G107U, 2.7 ± 0.6% for A59,60C, and 1.8 ± 0.6% for the Triple mutant. The trend holds for other growth temperatures (data not shown). In contrast, the plasmid-derived rRNA from pSpur can be processed and RbfA overexpression slightly increases the population of mature plasmid-derived rRNA (data not shown).

The rRNA from fractions of analytical sucrose gradients of BW25113/pSpur and BW25113/pSpur-3M with and without p15B-3 was analyzed. The polysome profiles themselves appear unaffected by RbfA overexpression (Figure 3.8). Analysis of the rRNA from the 30s and 70S peaks reveals only tiny differences, well within the error of the assay.

3.3.4 Growth of J5/6 mutants in *ΔrbfA*

In order to probe the effect of ribosome assembly factor RbfA on the mutant pre-ribosomes from another angle, the J5/6 mutant expression plasmids were transformed a *ΔrbfA* strain. Surprisingly, the combination was very deleterious.

Different colonies of *ΔrbfA*/pSpur and *ΔrbfA*/pSpur-Triple have vastly different growth rates (Table 3.6). A long, varied lag time on the order of hours after dilution from saturated cultures was also noticed in another *ΔrbfA* strain, BX41 when transformed with the pSpur derivatives (data not shown). Different colonies of *ΔrbfA*/pSpur and *ΔrbfA*/pSpur-Triple also have vastly different amounts of plasmid-derived rRNA (Table 3.6). The combination of *ΔrbfA* and the J5/6 mutant rRNA is so deleterious that in the fastest growing colonies the amount of J5/6 mutant rRNA is reduced through unknown second-site mutations.

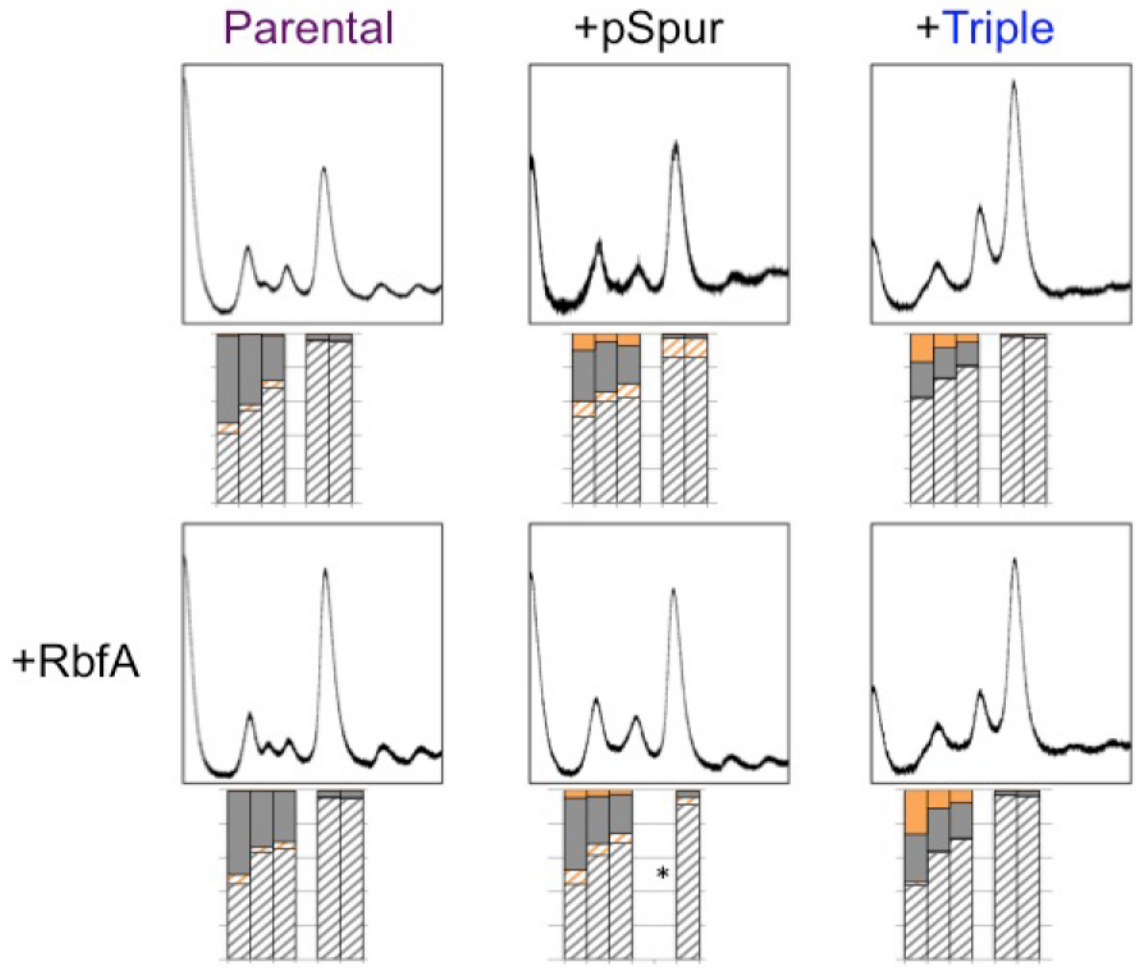

Figure 3.8: **Polysome profiles of J5/6 mutants with RbfA overexpression**. Polysome profiles of BW25113 (Parental; purple), BW25113/pSpur (black), or BW25113/pSpur-Triple (blue) with and without p15B-3 (RbfA overexpression vector) grown at 37º and rRNA from peaks of interest were analyzed. Bar graphs of plasmid-derived rRNA (orange bars) and immature rRNA (solid bars) is indicated below each peak. RbfA overexpression does not improve polysomal localization of mutant rRNA. None of the plasmid-derived rRNA is fully matured to 16S – indicated by the lack of orange dashed bars for the J5/6 mutants. The odd 40S hump in the BW25113 polysomes is found in multiple sources of the parental, does not contain a significant about of 16S or 23S rRNA.

Table 3.6: **Growth rate and proportion of plasmid-derived rRNA of J5/6 mutants in *ΔrbfA*.** Fit lag and doubling times and % plasmid-derived 23S and 16S/17S of *ΔrbfA* cells transformed with pSpur or pSpur-Triple. Growth rate data were fit to the four variable equation $y = I_o + Ie^{((t - t_L)/t_D)}$. Errors are from the uncertainty in the fits. Strains with very low % plasmid-derived rRNA and fast doubling times are indicated in bold text. The combination of *ΔrbfA* with J5/6 mutants is so deleterious that colonies with the least plasmid-derived rRNA grow the fastest.

	Lag Time	Doubling Time	Plasmid-derived 23S	Plasmid-derived 16S+17S
pSpur 3/5/14	110 ± 10	71 ± 2	18 %	18%
pSpur -1 12/3/14	60 ± 10	72 ± 3	25 %	54%
pSpur -2 12/3/14	73 ± 10	66 ± 2	24 %	54%
pSpur -3 12/3/14	61 ± 10	71 ± 4	24 %	52%
Triple 3/5/14	171 ± 10	**65.3 ± 0.7**	**2 %**	**2%**
Triple -1 12/3/14	54 ± 10	100 ± 2	17 %	25%
Triple -2 12/3/14	65 ± 10	**67.2 ± 0.8**	**4 %**	**5%**
Triple -3 12/3/14	81 ± 10	90.4 ± 1.8	27 %	30%

3.3.5 The effect of ribosome assembly factor overexpression on growth and ribosomal maturation of J5/6 mutants

Since the studies on RbfA were less informative than expected, a variety of assembly factors were tested to see if the results could help me elucidate the roadblock to maturation that affected the J5/6 mutants. Due to the low copy number nature of this plasmid, the IPTG induction of ribosome assembly factors was modest, and maximal with 1 mM IPTG after 4 hours (Figure 3.9). Comparison of the purified Era-His protein to the lysate control (to control for cell density) indicates optimal protein expression at 4, 5, and 6 hours post-induction for the 1 mM and 4 mM IPTG time courses. A 4 or 5 hour induction also produced a maximal retention of immature mutant plasmid-derived species. The decrease in chromosomally-derived 17S at some time points is due to the OD at which the samples were harvested. Only the 1 hour, 3 hour, and 4 hour growths were from mid-log cells due to experimental limitations.

Once the optimal induction conditions were determined, a selection of the ribosome assembly factor overexpression library were grown to an OD of 0.2, induced and diluted, grown ~ 4 hours until mid-log and harvested. Induction of ribosome assembly factors had little to no effect on bacterial growth rate (data not shown). Four hours of 1 mM IPTG induction of Era produced a 1.6% increase in the retention of immature mutant plasmid-derived species (Figure 3.10). RsgA induction increased retention by 1.9%. RimP induction decreased the retention by 4.6%. RsmC induction decreased the retention by 1.9%, and KsgA induction decreased the retention by 2.8%.

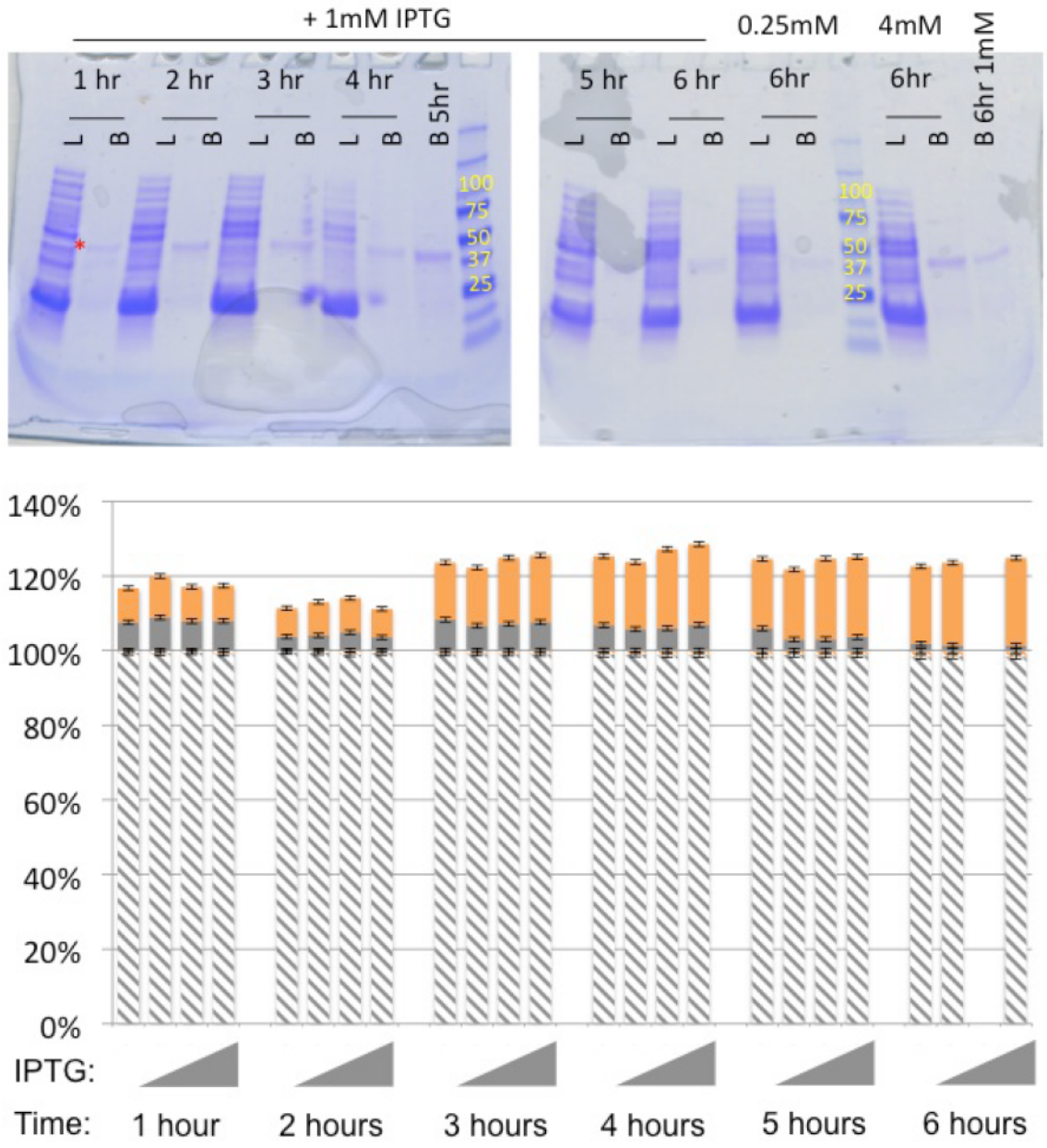

Figure 3.9: **IPTG induction time course of Era**. A) SDS-page gel of fractions from a small-scale Ni-NTA purification, Era-His is 36 kDa (red asterisk). Lysate (L) and protein bound to Ni-NTA beads (B) Labeled. Maximal induction of His-tagged ribosome assembly factors occurs after 4 hours. Yellow numbers indicate the molecular weight of the protein marker. B) 5' end processing and source of 16S rRNA from BW25113/pSpur-Triple, pD421-Era IPTG induction time course. IPTG concentration ranges from 0 mM to 4 mM. Bar graph of total RNA indicating plasmid-derived rRNA (orange bars) and immature rRNA (solid bars). Maximal effect of induced ribosome assembly factors occurs after 4 hours.

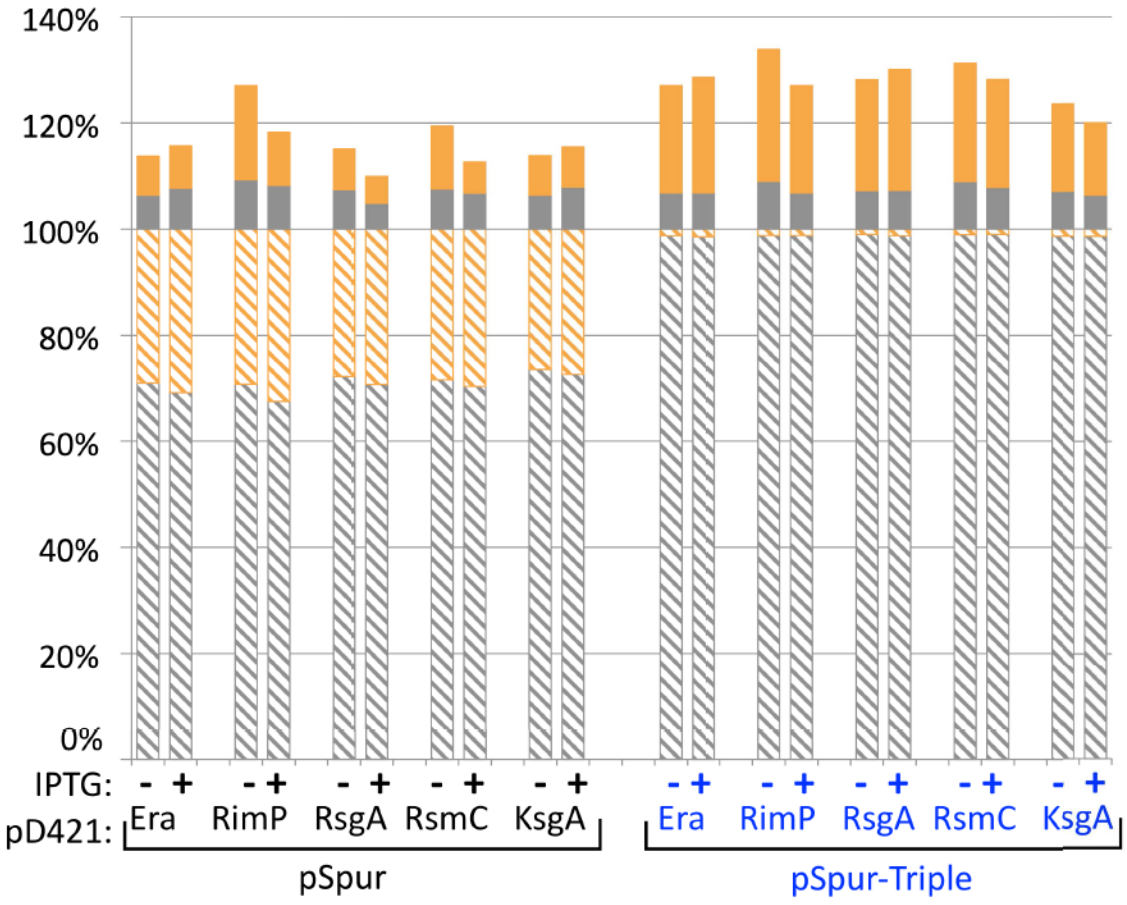

Figure 3.10: **rRNA processing of J5/6 mutant rRNA with ribosome assembly factor overexpression**. 5' end processing and source 16S rRNA from BW25113/pSpur and BW25113/pSpur-Triple (blue) cells transformed with a pD421-RAF plasmid were diluted to OD_{600} = 0.02 from a saturated overnight growth, grown to OD_{600} = 0.2, diluted into LB with and without 1 mM IPTG and grown 3.5 to 4.5 hours until mid-log (OD_{600} = 0.45-0.6). Bar graphs of plasmid-derived rRNA (orange bars) and immature rRNA (solid bars). Overexpression of Ribosome Assembly Factors produces modest changes in the amount of immature plasmid-derived rRNA retained but does not aid in maturation the J5/6 mutants.

3.4 Discussion

3.4.1 The J5/6 mutant ribosomes do not mature

E. coli strains with plasmid-derived J5/6 mutant rRNA grow slightly slower than those harboring the WT plasmids pLK45 or pSpur. This growth defect is rather mild. On the other hand, regardless of whether the chromosomally-derived rRNA is selected against due to the presence of spectinomycin or if the only wild-type copy of rRNA is on a helper plasmid and selected against due to sucrose sensitivity, once the J5/6 mutant rRNA is alone, bacterial growth stalls. All three of the J5/6 mutants are recessive lethal and non-functional.

Since ribosome assembly is so important and can proceed through a variety of pathways with redundancies and assembly factors, it is rare that an assembly defect is so pronounced. Many only have cold-sensitive phenotypes. Even six small ribosomal proteins: S17 and S20, two 5' domain primary binding proteins; S15, a central domain primary binding protein; S6, a central domain secondary binding protein; and S9 and S13, two 3' domain secondary proteins, are non-essential for life and thus 30S ribosome biogenesis (Bubunenko 2007). I find the fact that one, two, or three single nucleotide mutations – G107U, A59,60C, and A50,60C G107U (Triple) – in the junction of helices 5 and 6 can be more deleterious than the deletion of S20 or S17, two r-proteins directly involved in the restructuring of that junction to be particularly noteworthy.

The A59,60C and the Triple mutants stall at the 17S-containing assembly platform stage. Though an increase in growth temperature can decrease the size of the lighter pre-30S shoulder, it is not sufficient to allow the mutant ribosomes to become mature and be recognized by a 50S subunit and enter the 70S pool.

The completely unprocessed 30S-containing pre-rRNA G107U species – previously only seen in E. coli lacking RNase III (Srivastava 1990) – is novel. Previously discovered ribosome assembly intermediates tend to be lighter than the complete 30S – such as the 21S RI and the 26S RI* from *in vitro* assembly (Held 1973b), the 21S neomycin-induced particle (Foster 2008), the 21S and 27S *in vivo* pulse-chase assembly intermediates (Lindahl 1975), and *in vivo* assembly intermediates discovered by sucrose gradient purification followed by quantitative mass spectrometry (Chen 2013).

One possibility for the temperature-dependent inhibition of RNase III processing for the G107U mutant is that the single point mutation affects the relative stability of various RNA secondary structures and only with extra thermal energy can the correct RNase III recognition helix be formed (Figure 3.11). RNA secondary structure prediction models (Mathews 2004) of the 16S 5' domain with the leader show both a leader•helix 6, leader•helix 3 structure and a native-like structure with a native helix 6 and helix 3. These two structures are equally probable for the WT sequence (8 out of the top 20 models for both structures); however, for G107U, the leader•helix 6, leader•helix 3 structure is significantly more likely (13 out of the top 20 models, while the native structure is only represented 3 times out of the top 20 models. The leader is known to interact with helices 3 and 6 via oligonucleotide hybridization assays and UV-crosslinking studies (Pardon 1995, Besancon 1999). The addition of the MS2 hairpin to

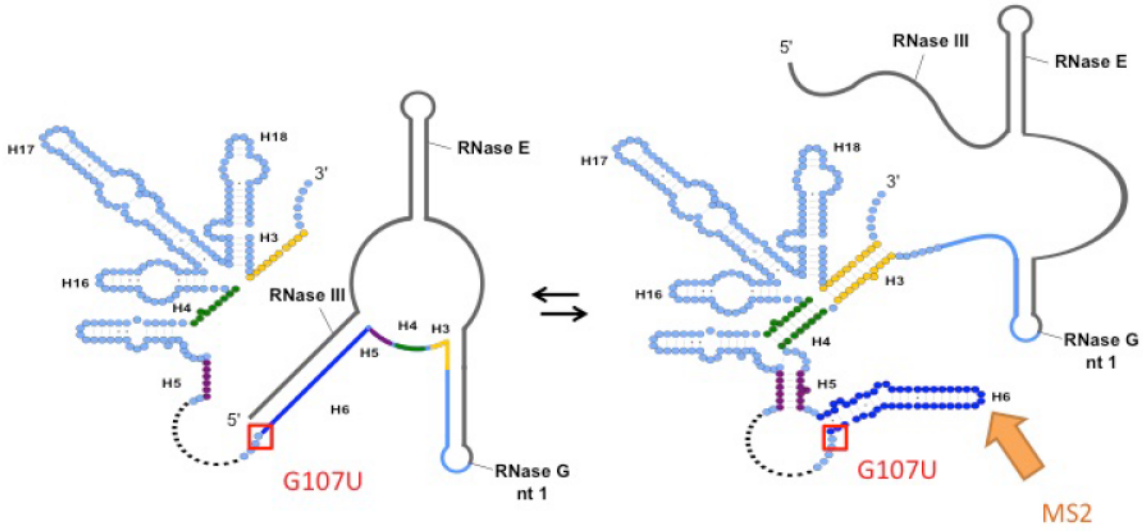

Figure 3.11: **Structural models of the 16S 5' domain with leader.** Two RNA secondary structural models for the 16S 5' domain with the full rRNA leader. The dynamic helices, 3, 4, 5, and 6, are color-coded. The pre-16S leader is in grey and the rest of 5' domain is in light blue. Sites of nucleolytic processing and key helices are labeled. The lower sub-domain (helices 7-14) is indicated by a dashed line. The location of the G107U mutation and the MS2 insertion are indicated by a red box and orange arrow respectively.

the tip of helix 6 could stabilize the correct leader structure and enable RNase III processing, as I have not detected 35S-containing species from MRE600/pSpur-G107U or BW25113/pSpur-G107U strains. Whether the possible misfolding effect of the G107U mutant has anything to do with theJ5/6 ribosome biogenesis defect has not yet been determined.

3.4.2 Expression of RbfA decreases accumulation of immature J5/6 rRNA

Overexpression of RbfA from its native promoter decreases the retention of immature mutant 17S pre-rRNA. Overexpression of RbfA increases the amount of mature plasmid-derived RNA for the pSpur WT. This indicates that RbfA does help WT pre-RNA mature, as expected, but the J5/6 mutants cannot be matured. RbfA overexpression might help to tag the immature mutant ribosomes for degradation, or it might help them overcome an assembly roadblock only to enter a state where they are more easily degraded. A cryo-EM structure of RbfA complexed to 30S ribosomes shows that RbfA binds to the neck region of the 30S and displaces helix 44 and 45 (Datta 2007), this could make the 3' end more accessible to exonucleases.

The combination of *ΔrbfA* and the J5/6 Triple mutant is quite deleterious. The fastest growing colonies reduce the amount of J5/6 mutant rRNA through unknown second-site mutations. This suggests the possibility of increased toxicity of immature ribosomes in the absence of RbfA. Why the J5/6 mutants are assembly-incompetent and so toxic in the absence of a ribosome assembly factor is an open question. Whether this

synthetic toxicity is unique to *ΔrbfA* or if the J5/6 mutants would be just as toxic in other ribosome assembly factor deletion strains is worth investigation.

3.4.3 Ribosome assembly factors cannot rescue J5/6 mutants

Overexpression of Era and RsgA slightly increases the retention of J5/6 17S pre-rRNA. RsmC overexpression slightly decreases the retention of mutant immature rRNA while KsgA and RimP overexpression decreases the retention a bit more.

Cryo-EM structures exist for Era, RbfA, RsgA, and KsgA and they mostly localize to the same neck area, but have largely non-overlapping binding sites (Figure 3.12). Era binds between the head and the platform (Sharma 2005) while RbfA displaces helices 44 and 45 to bind at the pivotal junction between the four domains (Datta 2007). Both RbfA and Era interact with helix 28 and they could both be present at the same time, though the KH domain from Era would not be likely to contact helix 45 if RbfA is displacing it. Era is an early-binding ribosome assembly factor (Bunner 2010) as is RbfA (Soper 2103). RsgA is dependent on the presence of RbfA to bind with the 30S subunit (Goto 2011). RsgA's OB domain interacts with the 30S platform, specifically helices 23 and 24, and the zinc-finger domain interacts with helix 44 (Jomaa 2011). Both Era and RsgA are involved in 3' end processing, but there is no overlap in their binding sites (Jomaa 2011). RsgA is involved in the release of RbfA, especially the C-terminal alpha helix, but a potentially incredibly informative co-structure with both RsgA and RbfA bound to the 30S subunit has not been solved yet (Jeganathan 2015). KsgA binds in

basically the same location as RbfA and RsgA – contacting helices 24, 27, and 45 while displacing helix 44 – and thus cannot act until late (Boehringer 2012). Though at this time there is not a structure of RimP complexed with 30S ribosomes, one can hypothesize that it is near the central pseudoknot and the r-proteins S12 and S5, in the same general neck area as RbfA, RsgA, and KsgA (Sashital 2014).

All of the assembly factors tested increased the amount of plasmid-derived WT 16S. There does not appear to be a simple temporal delineation between when ribosome assembly factors act and whether the immature J5/6 mutants are protected or degraded. Era, which is known to bind early and work late, increases the amount of mutant 17S pre-rRNA retained while RbfA decreases it. RsgA, which works after RbfA, increases the amount retained and the late RimP and KsgA, which is known to work after RbfA, decrease the amount retained.

Another possibility is that assembly factors that destabilize the 4-domain junction decrease the retention of mutant 17S pre-rRNA and assembly factors that stabilize the 4-domain junction increase the retention of mutant 17S pre-rRNA. RbfA and KsgA displace helix 44 and they both decrease the retention of mutant 17S pre-rRNA. Era and RsgA both contact the 3' minor domain but do not displace helix 44 and they both increase the retention of mutant 17S pre-rRNA. Interestingly, RimP overexpression has the strongest effect on J5/6 mutants as it reduces the amount of retained 17S rRNA from 23% to 19% (normalized to the total amount of mature rRNA) and it acts directly to stabilize the central pseudoknot. Regardless of the reasons for immature mutant ribosome retention or degradation, the J5/6 mutants still cannot be matured.

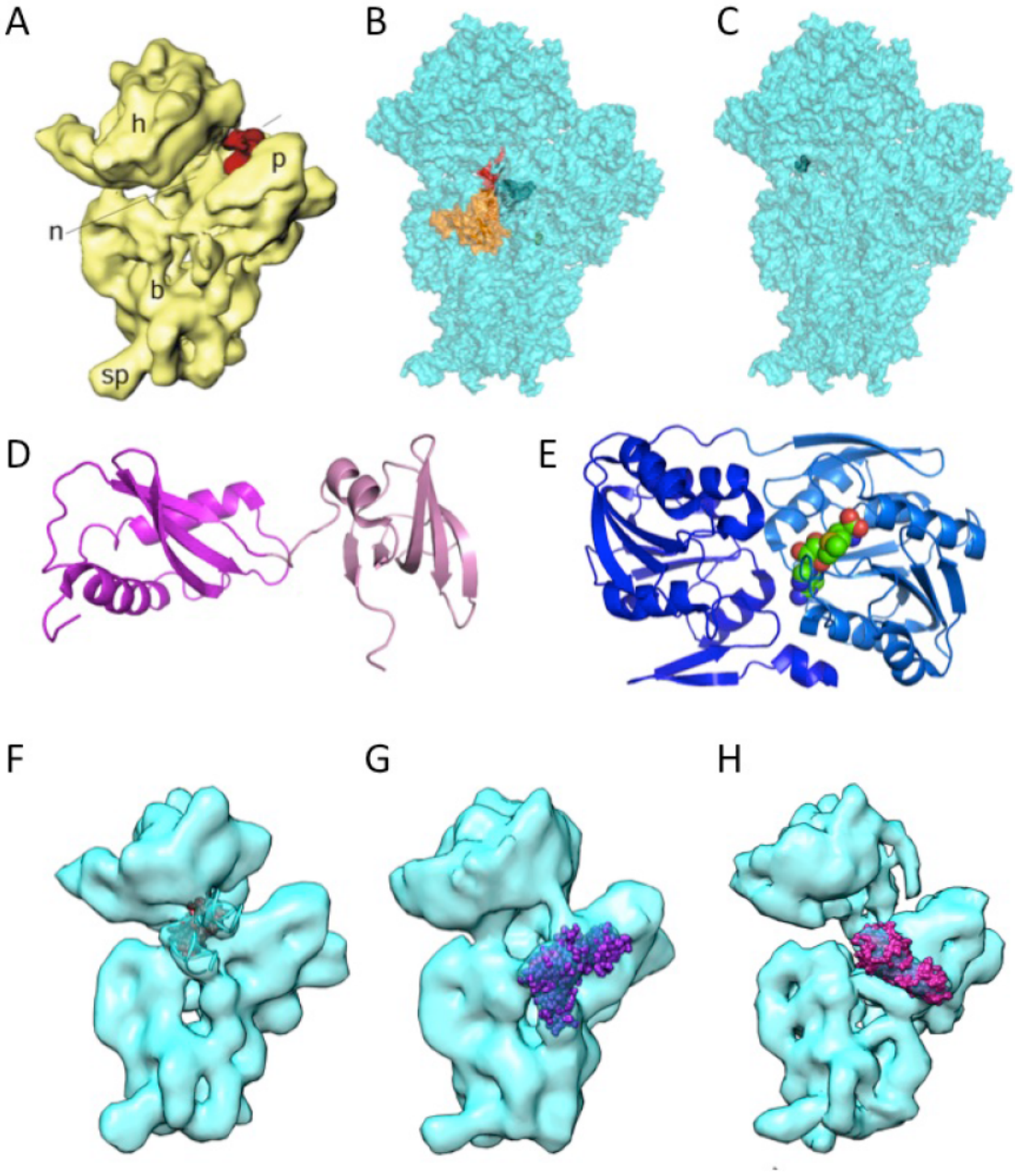

Figure 3.12: **Ribosome assembly factors.** Interface views of A) Cryo-EM map of Era (red) in complex with S1 depleted 30S subunit, figure from Sharma 2005 B) 30S crystal structure with RimP primary interaction partners S5 (red), S12 (orange) and central pseudoknot (black spheres). C) 30S crystal structure with RsmC methylation substrate G1207 in lab spheres. Crystal structures of D) RimP N-terminal domain in magenta, C-terminal domain in pink PDB 1IB8. E) RsmC N-terminal domain in blue, C-terminal domain in light blue, SAM in green spheres PDB 3DMF. F) Cryo-EM map of RbfA (brick red) bound to 30S ribosome EMD 1413. G) RsgA (purple) with GMPPNP bound to 30S subunit EMD1895 H) KsgA (red-purple) bound to 30S subunit EMD 2017. All cryo-EM map contour levels are as recommended by authors.

Chapter 4: Structure of the J5/6 Triple mutant 30S head domain

4.1 Introduction

Since the mutations in the junction between helices 5 and 6 of the 16S rRNA completely block maturation of the pre-16S rRNA and fail to produce functional 30S ribosomes *in vivo*, but *in vitro* structural probing of the 5' domain where the mutations are located revealed only moderate and local perturbations, I wanted *in vivo* structural information on these immature mutant ribosomes in order to gain greater insight into the importance of the J5/6 region during ribosome biogenesis.

In vivo hydroxyl radical footprinting is a method for determining the solvent accessibility of the RNA backbone, and was developed in our lab (Adilakshmi 2006, Adilakshmi 2009). This powerful method works well on even non-uniform and difficult-to-isolate species, such as pre-30S particles (Soper 2013).

Hydroxyl radical footprinting is sensitive to RNA tertiary structure and RNA-protein interactions because these interactions protect the RNA backbone from solvent and the reactive species (Latham 1989). Additionally, this reaction does not depend on the identity of the nucleobase, so it is sequence independent, unlike many other footprinting techniques such as DMS or kethoxal (Tullius 2005). These aspects make hydroxyl radical footprinting ideal for ribosome structure studies (Adilakshmi 2006, Adilakshmi 2009).

In vitro, hydroxyl radicals are commonly generated by the Fenton reaction in which iron(II)-EDTA reduces hydrogen peroxide to •OH (Tullius 2005). Hydroxyl radicals can be produced inside living cells by bombarding cells with ionizing radiation, which abstracts an electron from water and ultimately generates short-lived hydroxyl radicals (Klassen 1987).

$$H_2O \xrightarrow{\text{Ionizing radiation}} H_2O^+ + e^-_{aq} \xrightarrow{H_2O} H_3O^+ + \bullet OH + e^-_{aq}$$

The hydroxyl radical oxidizes nucleobases, sugars, and protein side chains within the cell, but when it reacts with the ribose of the RNA backbone it results in oxidative degradation of the ribose and the release of the nucleobase (Hertzberg 1984). This produces a pause one nucleotide 3' of the attack when assayed by primer extension. A high flux synchrotron X-ray beam can generate a decent signal in less than 100 milliseconds (Adilakshmi 2009).

I used a synchrotron-generated X-ray beam to generate hydroxyl radicals *in vivo* to probe the structure of immature 30S subunits stalled by my J5/6 mutations (Figure 4.1 for workflow). Initial attempts to purify the mutant ribosomes from irradiated samples using an MS2 affinity tag in the 16S rRNA proved unsuccessful. Attempts to determine the r-protein complement of the mutant ribosomes, which would have shed some light on the state at which the J5/6 mutants were stalled, was also unsuccessful. Allele-specific primer extension on total RNA, however, was successful.

I discovered that the 3' major domain of the J5/6 Triple mutant rRNA is solvent exposed at helices 35-37 and is cleaved at helix 2. This region forms the neck of the 30S ribosome – an interface between the head and the platform that forms late during assembly. Exposure of this region suggests that late r-protein S2 and the native tertiary

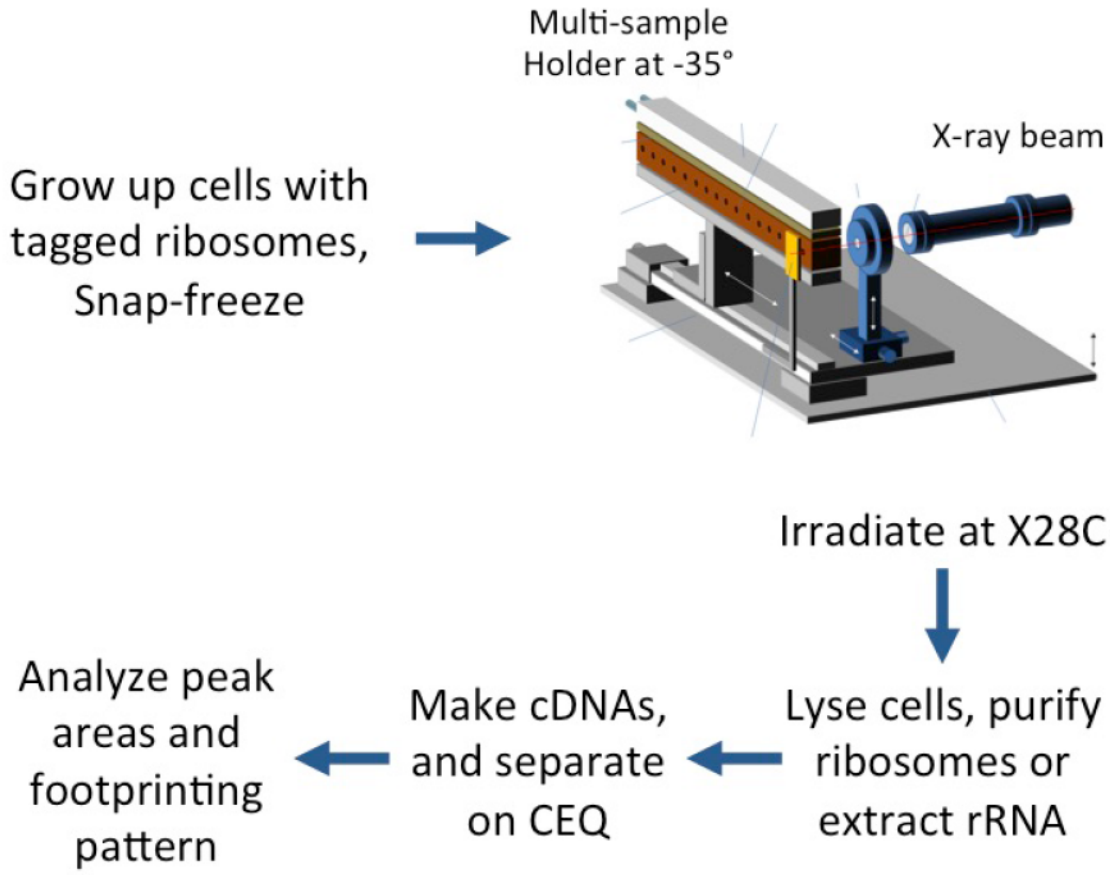

Figure 4.1: ***In vivo* hydroxyl radical footprinting workflow**. Diagram of *in vivo* hydroxyl radical footprinting method. Diagram of X28C multi-sample holder courtesy of S. Gupta (Adilakshmi 2009).

interactions with other domains of the 30S ribosome are not present in the J5/6 Triple mutant. This suggests that the J5/6 region is critical for proper assembly of even the far away 3' major domain.

In vitro structural information on the J5/6 mutants suggest that they destabilize the native conformation of helix 3 (Chapter 2), which is important for forming the central pseudoknot and permitting long-range native domain-domain interactions (Ramaswamy 2009b). *In vivo* hydroxyl radical footprinting on the J5/6 mutants provides further evidence for this long-range destabilization of the central pseudoknot and a possible explanation for the complete inability of J5/6 mutant ribosomes to mature.

4.2 Materials and Methods

4.2.1 MS2-MBP protein purification

MS2-MBP was prepared as previously described (Youngman 2005, R. Green, personal communication) with several amendments to reduce co-purification of even minimal amounts of ribonucleases. BL21(DE3) Gold (Invitrogen) cells transformed with pMal-MBP-MS2-His (a gift from U. Maivali) were grown to mid-log (OD_{600} = 0.5) at 37°C in 1 L LB and expression of MBP-MS2-His was induced with 1mM IPTG for an additional 3-4 hours at 37°C. The culture was harvested by centrifugation and stored at -20°C until use.

A cell pellet from ½ to ⅓ of a 1 L growth (less cell mass was determined to be better for avoiding overloading the HisTrap column) was resuspended in 20 mL Lysis Buffer (50 mM NaH_2PO_4 pH 8.0, 300 mM NaCl, 0.5% Tween20, 10% glycerol, 10 mM imidazole, 6 mM β-mercaptoethanol) (Batey 2007). Cells were lysed on a Emulsiflex using standard laboratory protocols and the cellular debris were pelleted twice at 10,000 x *g* for 20 min, before the supernatant was loaded onto a 5 mL HisTrap column equilibrated with Ni^{2+} following standard protocols (GE Healthcare). After lysis, care was taken to eliminate the introduction of ribonucleases; all solutions were made in baked glassware with ribonuclease-free water. The column was washed with at least 12 column volumes of Wash Buffer (Lysis Buffer plus 50 mM imidazole) before MBP-MS2-His was eluted with Elution Buffer (Lysis Buffer with 250 mM imidazole).

Protein fractions were identified by SDS-PAGE prior to overnight dialysis into low salt buffer (25 mM MES pH 6.0, 25 mM NaCl). Dialyzed protein was loaded onto an

Uno S6 column (Bio-Rad) and eluted with a non-uniform NaCl gradient. Using a BioRad BioLogic system a gradient of 6-mL 0-100 mM NaCl, 30-mL 100-300 mM NaCl, and 42-mL 300-1000 mM NaCl was used (in MES pH 6.0). Fractions were tested for ribonuclease activity against uniformly ^{32}P- labeled RNA at 37°C for 30 minutes in HKM2 (8mM K-Hepes, pH 7.5, 33 mM KCl, 0.1 mM EDTA, 2 mM $MgCl_2$) and analyzed on an 8% polycrylamide gel in 1X TBE. Fractions with MBP-MS2-His and no detectible ribonuclease activity activity were pooled and dialyzed into Storage Buffer (20 mM Tris pH 7.5 at 4°C, 150 mM NaCl, 0.02% sodium azide, 20% glycerol) prior to storage at -80°C.

4.2.2 Small-scale ribosome purification

Ribosome affinity purifications were performed as previously described (Youngman 2005, Maivali 2011) but with several modifications to the volumes and wash steps for small, high-purity samples. 300 µL amylose beads (600 µL of resin in 20% ethanol, NEB) was transferred to a disposable column (Sigma-Aldrich) and washed twice with 3 column volumes of Column Buffer (20 mM Tris pH 7.5, 0.2 M NaCl, 1 mM EDTA) and then washed twice with 3 column volumes of Binding Buffer (20 mM Tris pH 7.5, 100 mM NH_4Cl, 10 mM $MgCl_2$). Beads were resuspended in 400 µL Binding Buffer and 100 µL 7 mg/mL MS2-MBP in Storage Buffer was added. MS2-MBP was bound to the amylose resin during a 20-minute incubation with vigorous shaking at 4°C. Excess MS2-MBP was removed with two additions of 3 column volumes of Binding Buffer.

A 50 µL cell pellet (irradiated or not) was resuspended in 300 µL lysozyme buffer (10 mM Tris pH 7.8, 15 mM $MgCl_2$, 1 mg/mL lysozyme). The mixture was incubated at room temperature for 5 minutes prior to the addition of 15 µL 10% deoxycholate, vortex mixing and clarification by centrifugation at 13,000 x *g* for 20 min. The clarified lysate was added to washed MS2-MBP-amylose beads, along with 200 units of rRNasin (Promega). The mixture was further incubated at 4°C with vigorous shaking for 30 minutes. 100 µL 200 mM vanadyl ribonucleoside complex was also an effective inhibitor of ribonuclease activity but proved more difficult to effectively remove. Beads were washed four times with 3 column volumes of Binding Buffer warmed to 37°C, MS2-tagged ribosomes were eluted twice with 2 column volumes of Elution Buffer (Binding Buffer with 12 mM maltose). For rRNA analysis by primer extension, the r-proteins immediately removed by the addition of 1% SDS, two phenol extractions, two chloroform extractions, and ethanol precipitation with 0.3 M sodium acetate and glycogen to improve yield.

4.2.3 Primer extension to map 16S 5' end

Primer extensions to determine 5' end maturity and % plasmid-derived rRNA were performed as described in Chapter 3.

4.2.4 Isolation of r-proteins for mass spectrometry

Isolation of r-proteins from immature, mutant ribosomes was performed as described (Spedding 1990) with minor modifications. The 260:280 absorbance ratio for

the MS2-MBP-purified ribosomes were measure, and then used to determine the excess MS2-MBP. Given the A260:280 = 0.58 for my MS2-MBP preparation and the A260:280 = 2.0 for purified 30S ribosomes, the percentage of excess MS2-MBP can be calculated using:

$$\%P = 100 - (11.16^* R_{260/280} - 6.32)/(2.16 - R_{260/280})$$

in which %P is the percentage of the purified ribosome mixture that is MS2-MBP and $R_{260/280}$ is the absorbance ratio for the sample (Glasel 1995). The A260 value was then very crudely corrected by scaling the absorbance at 260 by the calculated concentration of actual ribosomes using:

$$A260_{corr} = A260_{obs}*(100-\%P/100)$$

in which %P is the percentage of protein as calculated above and the $A260_{obs}$ it the observed absorbance 260 nm. Once the absorbance at 260 nm was calculated, 300-500 A260 units of ribosomes were mixed vigorously with 2 volumes ice cold glacial acetic acid. The rRNA was precipitated and the rRNA pellet re-extracted. The r-protein rich supernatants were combined in an acetone-resistant tube and precipitated with 5-10 volumes ice cold acetone overnight at -20°C. The r-protein pellets were washed with acetone, dried under vacuum, and stored at -80°C until they were shipped to the Limbach lab for mass spectrometric analysis. Analyses of two independent preparations could only detect the MS2-MBP pull-down protein, and no r-proteins.

4.2.5 *In vivo* footprinting

MRE600 (RNase I-) cells transformed with pSpur and pSpur J5/6 derivatives were prepared as previously described (Adilakshmi 2009). Briefly, cultures were grown

at 37°C to mid log (OD_{600} 0.4-0.6), then rapidly chilled, harvested by centrifugation, washed once in 10 mM Tris-HCl, pH 7.5, 1 mM $MgCl_2$, then resuspended in minimal buffer. 5 µL aliquots were partitioned into 0.2 mL PCR tubes (BrandTech #781305 to fit in the X28C multi-sample holder) and snap-frozen in a dry ice/ethanol bath. Cell pellet were stored at -80°C and shipped on dry ice.

Frozen samples were exposed to a synchrotron X-ray beam in a pre-chilled multi-sample holder on a motorized stage (X28C, National Synchrotron Light Source at Brookhaven National Laboratory) A macro was used to control the movement of the multi-sample holder with respect to the X-ray beam and to correct for the ~0.05 mm deviations in X and Y position of the sample. An interfaced UniBlitz electronic shutter was used to achieve high precision and accuracy of irradiation times.

Proper irradiation dosage to generate sufficient hydroxyl radicals but still maintain single-hit kinetics was determined by a dose response to be between 25 and 100 ms depending on the trip (Adilakshmi 2009). For RNA analysis, cell pellets were resuspended in 500 µL RNAprotect bacteria Reagent (Qiagen) and total RNA extracted with the RNeasy Mini prep kit (Qiagen).

4.2.6 Analysis of footprinting data

Gels were quantified using SAFA (Das 2005) to obtain band intensity and thus the reactivity of each nucleotide. The results were adjusted for loading variation by selecting a strong band with minimal variation between lanes (see Figure 4.4, cyan stars). Each lane was normalized using these strong, invariant bands, caused by RT pauses, likely due to rRNA sequence or structure of high stability. After normalization, the

nucleotide intensities for the 3 technical replicates were averaged. The error bars indicate the standard deviation of the triplicates. For a few nucleotides (>5%) one of the three band intensities was quite different from the others and was discarded. Further processing of these data is outlined in the results section.

4.3 Results

4.3.1 Specific primer extension of plasmid-derived rRNA

In order to probe the structure of the J5/6 mutant pre-30S particles, I initially attempted to affinity purify the mutant ribosomes from samples of irradiated MRE600 cells transformed with pSpur and J5/6 mutant derivatives. I adapted the initial Youngman (2005) protocol for the small samples used in X-ray footprinting. Ribosomes purified in this manner had very little contaminating chromosomal-derived ribosomes, however, they did show indications of RNA degradation due to co-purifying ribonucleases (Figure 4.2).

Many methods were attempted to eliminate or reduce this degradation, as it would produce high background for hydroxyl radical footprinting experiments. Due to the technical limitations of single-hit kinetics with the hydroxyl radical footprinting, the footprinting signal is low to begin with, which makes co-purification of cellular ribonucleases quite detrimental. However, I was unsuccessful at reducing the ribonuclease degradation to acceptable levels.

Other optimization steps, such as improving the quantity of purified ribosomes without sacrificing purity, were more successful. Reapplying the flow-through from the purification to fresh MS2-MBP-amlyose beads increased the recovery of tagged ribosomes (data not shown).

Since I was unsuccessful at reducing the ribonuclease degradation in the affinity purified ribosomes to acceptable levels, I designed and tested several allele-specific primers (Table 4.1). Unfortunately, I was unable to prime reverse transcription from the

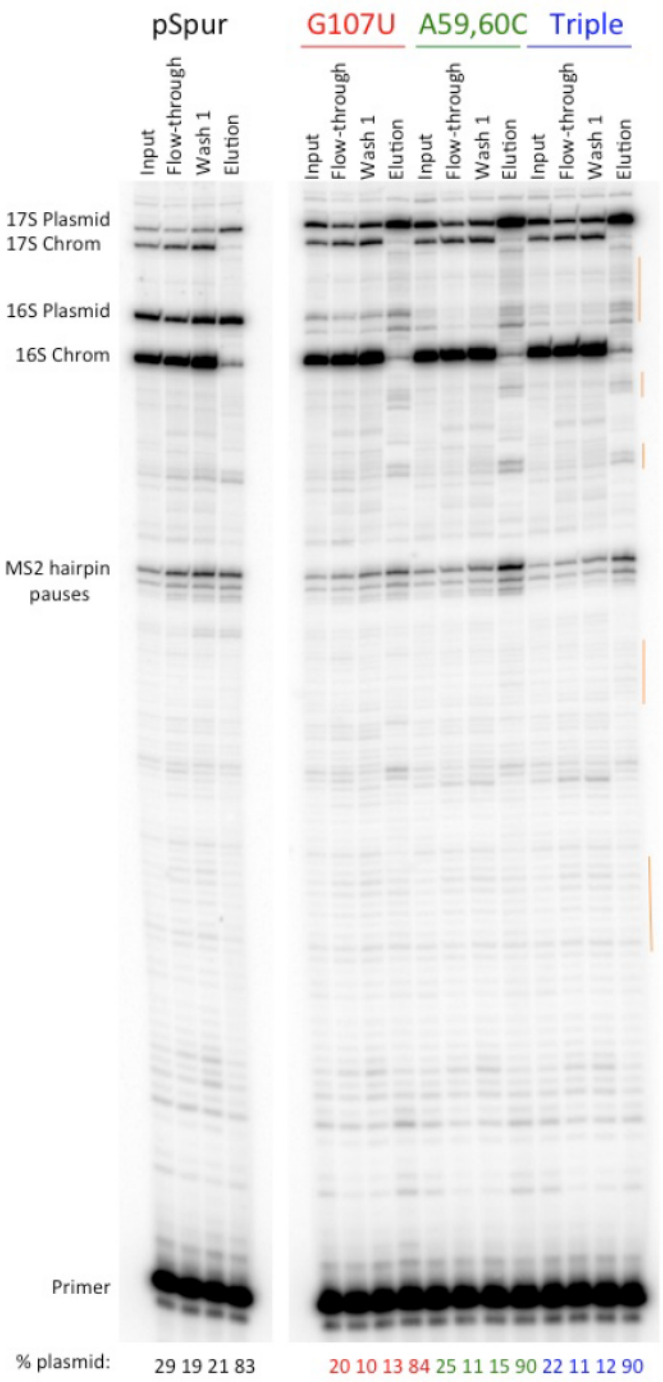

Figure 4.2: **Primer extension of rRNA from small-scale ribosome purifications.** rRNA was extracted from fractions at various stages of a test purification from MRE600/pSpur (black), MRE600/pSpur-G107U (red), MRE600/pSpur-A59,60C (green), or MRE600/pSpur-Triple (blue) cells. ^{32}P-labeled primer 161 was annealed and extended (Table A.3). Fraction of plasmid-derived rRNA in each lane are indicated below the gel. Input rRNA had between 30-20% plasmid-derived rRNA, which was depleted in the flow-through and wash fractions. The elution fractions were between 85-90% pure with some rRNA degradation (vertical orange lines). Major cDNA products are indicated on the side.

Table 4.1: **Primers designed for allele-specific primer extension**. Uppercase letters denote allele-specific residues

Name	Sequence
MS2-1	gcaaagaagACTAGTAAAGATGGG
MS2-2	gCAAAGAAGACTAGTAAAGATGGG
MS2-3	CCTCATCAAAACTAGTcttcttcc
MS2-4	cttcttcctgttaccgttcg
MS2-5	gcatgtgttaggcctgc
Spc^R allele specific primer	ggccatgatgacttgacA

MS2 hairpin, likely because of the stability of the hairpin secondary structure (Figure 4.3). However, extension of a primer designed to anneal with Spc^R point mutation C1192U at the very 5' end proved to be quite allele-specific (similar to Power 1993, Table 4.1, Figure 4.3 A). I used this allele-specific Spc^R primer to selectively analyze the footprinting pattern of the J5/6 mutant pre-30S particles.

4.3.2 Hydroxyl radical footprinting of the 30S head domain

In order to determine the structure of the 3' domain of the J5/6 mutant pre-30S particles I used allele-specific primer extension on total RNA purified from irradiated MRE600 *E. coli* cells transformed with pSpur and pSpur-Triple. Extension of a primer covering the Spc^R point mutation was used to selectively analyze the footprinting pattern of the plasmid-encoded rRNA. The cleavage patterns were read out by primer extension followed by slab gel electrophoresis (Figure 4.4). Band intensity and thus the reactivity of each nucleotide was quantified by SAFA. The non-irradiated samples had a low background, except for a few invariable pauses (Figure 4.5), and a very strong pause at A918 in the Triple mutant, which will be further discussed below. Footprinting results from the Triple mutant were compared to those from the pSpur WT. In many regions the relative exposures in the Triple mutant were similar to those in WT (Figure 4.6 B); however, the helix 35-37 region was quite exposed in the mutant relative to the wild type (Figure 4.6 A). Six nucleotides, including A918 of the central pseudoknot had strong pauses in the Triple mutant rRNA with and without irradiation.

In order to clearly identify structural differences in the Triple mutant pre-30S ribosomes, I calculated the ratios of nucleotide accessibilities of the Triple mutant

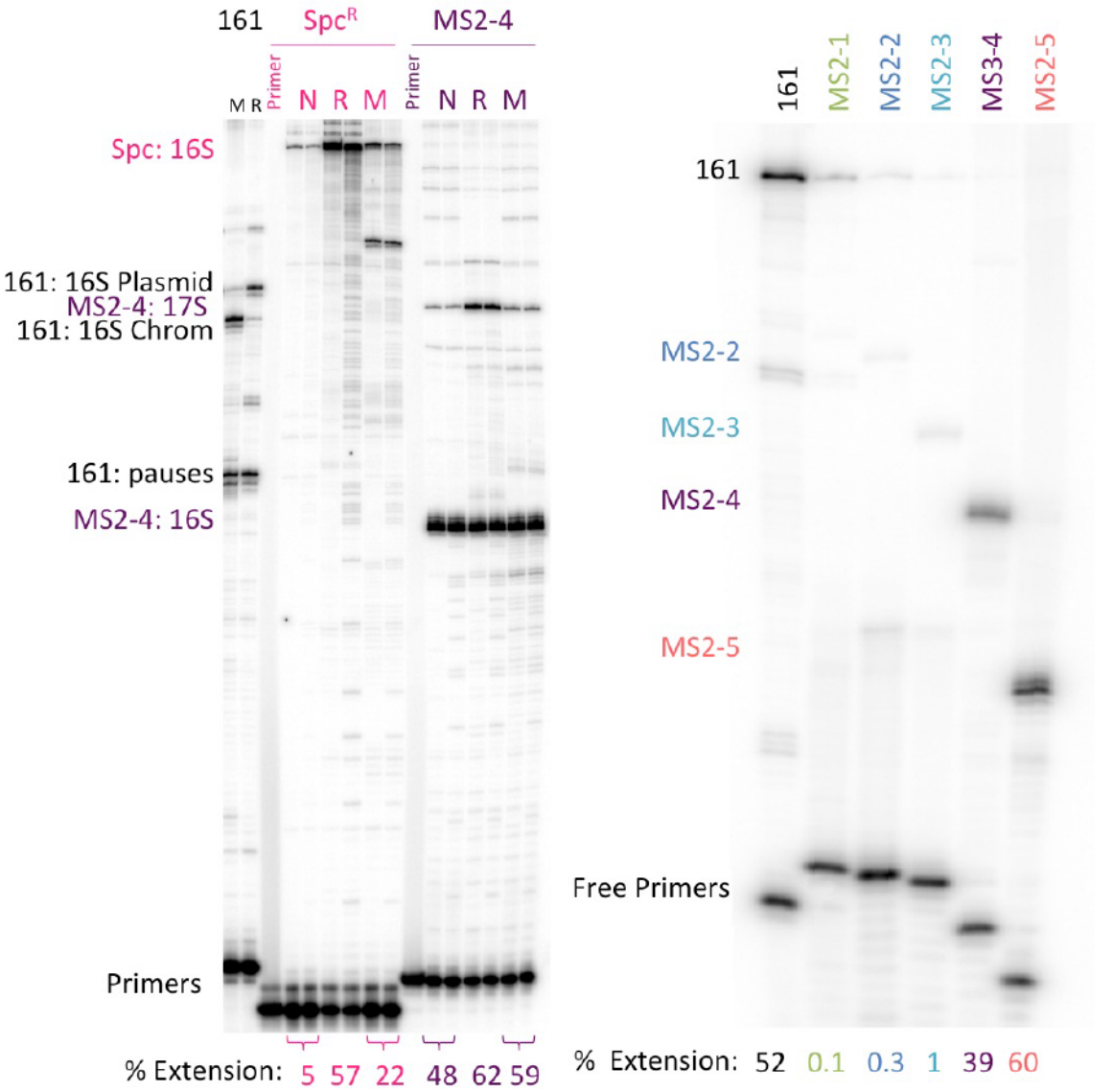

Figure 4.3: **Allele-specific primer extension tests.** A) Primer extension to test allele-specific primers. For lanes labeled "M" the primer extension with ^{32}P-labeled primer was performed on 2 µg total RNA from MRE600/pSpur cells. For lanes labeled "R" the primer extension was performed on 500 ng affinity purified tagged ribosomes, with some carryover of chromosomal RNA. For lanes labeled "N" the primer extension was performed on 2 µg total RNA from WT MRE600 cells not transformed with any plasmids. Primer labeled at top, and color-coded, sequences are in Table 4.1 (or A.3 for control primer 161). Major cDNA products are indicated on the side. The fraction of primer actual extended is indicated below the gel. B) Primer extension to test MS2-hairpin primers. ^{32}P-labeled primers were annealed to *in vitro* transcribed 5' domain RNA with the helix 6 MS2 hairpin extension. The fraction of primer extended is indicated below the gel. Primers MS2-4 and MS2-5 were able to be extended, but were not allele-specific.

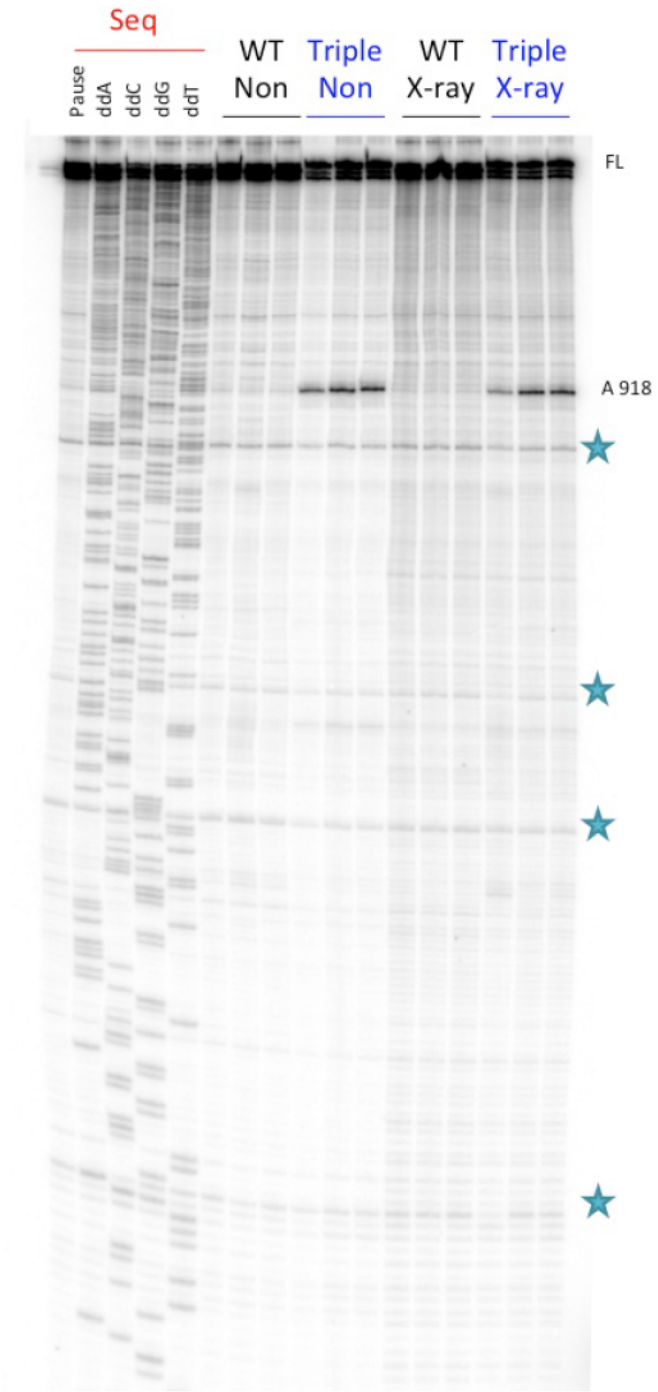

Figure 4.4: **Primer extension slab gel on rRNA from irradiated and non-irradiated cells.** Lanes 1-5 are the dideoxy sequencing ladders, and a pause lane to correct for reverse transcriptase pausing. Lanes 6-8 are primer extensions on total RNA extracted from MRE600/pSpur cells that were shipped to Brookhaven National Laboratory but not irradiated. Lanes 9-11 are primer extensions on total RNA extracted from non-irradiated MRE600/pSpur-Triple cells. Lanes 12-14 are MRE600/pSpur cells that were irradiated for 25 ms to achieve 75% full length 16S rRNA. Lanes 15-17 are irradiated MRE600/pSpur-Triple cells. Major cDNA products are labeled on the side, and invariable pauses used for data scaling are indicated by blue stars.

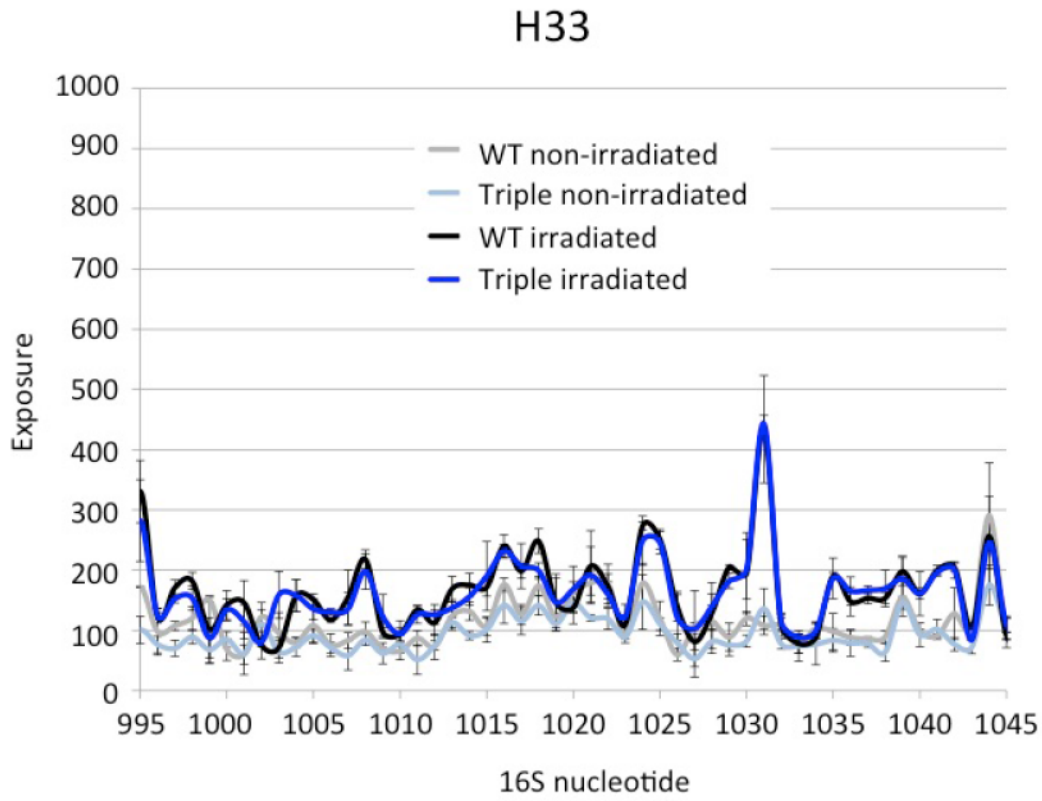

Figure 4.5: **Hydroxyl radical footprinting results for helix 33.** Plot for the 16S 1065-1115 nucleotide (helices 35-37) region comparing irradiated (dark) and non-irradiated (light) WT (black/grey) and Triple mutant (blue) rRNA. Y-axis values are the average adjusted reactivity for each nucleotide. Notice the low background for the WT and Triple mutant non-irradiated samples. Error bars indicate standard deviation between 3 technical replicates.

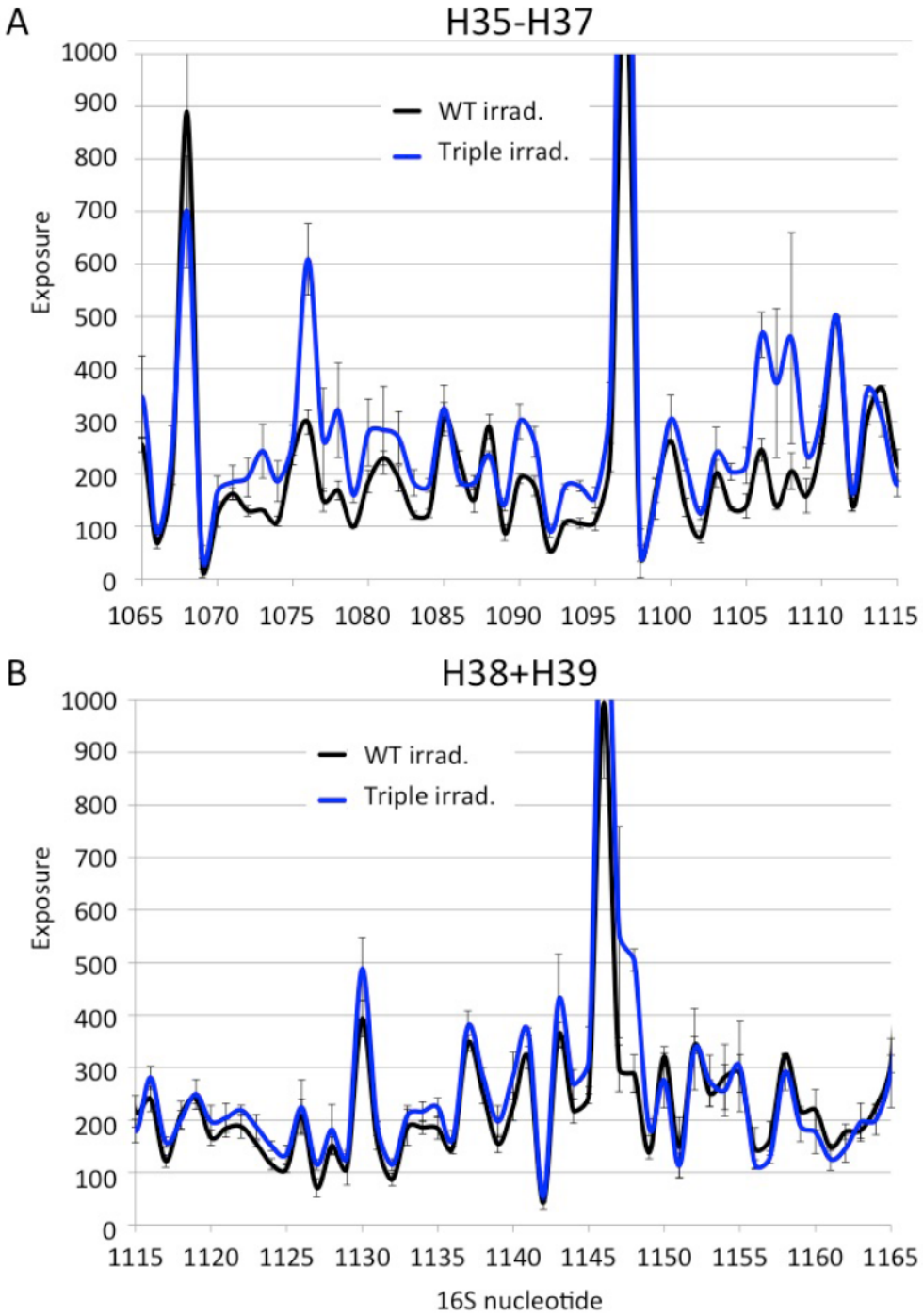

Figure 4.6: **Sample hydroxyl radical footprinting data.** Plot comparing WT (black/grey) and Triple mutant (blue) rRNA Y-axis values are the average adjusted nucleotide reactivities for each nucleotide. Error bars indicate standard deviation between 3 technical replicates. A) Plot for the 16S 1065-1115 nucleotide (helices 35-37) region. Note the differences between WT and 3M can be seen 1070-1083 of helices 35 and 36 as well as 1090-1093 of helix 37 and 1106-1110 of helix 35. B) Plot for the 16S 1100-1145 nucleotide (helices 38-39) region. Note the similarities between the Triple mutant and WT in this region.

compared to the WT pSpur control. The ratios of the exposure in Triple mutant over the WT for each nucleotide were plotted on a histogram and the protection and exposure bins were empirically determined (Figure 4.7). Nucleotides with altered solvent accessibility in the J5/6 Triple mutant were mapped onto the 16S secondary structure and the tertiary structure of the 16S rRNA in the 30S ribosome (Figure 4.8 and 4.9).

The most perturbed regions of those covered by my assay are helix 36 and helix 2, which form the "neck" of the 30S ribosome. Helix 36 reaches down the back of the 30S particle and interacts with the minor groove of A16, U17, C18, A19 (hydrogen bonding and some ribose zippering too) and packs against H25 forming the binding site for the tertiary r-protein S2. Many of the protected residues (see helix 33) are in non-A form helices, or kinks in the crystal structure, indicating that these kinks could protect the backbone from the solvent, and they are not – or at least less – present in the Triple mutant. Exposures of the helix 2 and helix 36 regions have been seen in other *in vivo* probing experiments of immature ribosomes (Soper 2013, McGinnis 2015).

4.3.3 Cleavage of the Central Pseudoknot of J5/6 Triple mutant ribosomes

My observation of the strong radiation-independent reverse transcriptase pause at A918 in the Triple mutant rRNA was quite intriguing. Nucleotide A918 is a part of the central pseudoknot, a vital structure that forms late during assembly and is required for translational activity (Besancon 1999, Brink 1993). This strong pause could be due to cleavage of the phosphodiester backbone, or a modification of the nucleotide. Since, to

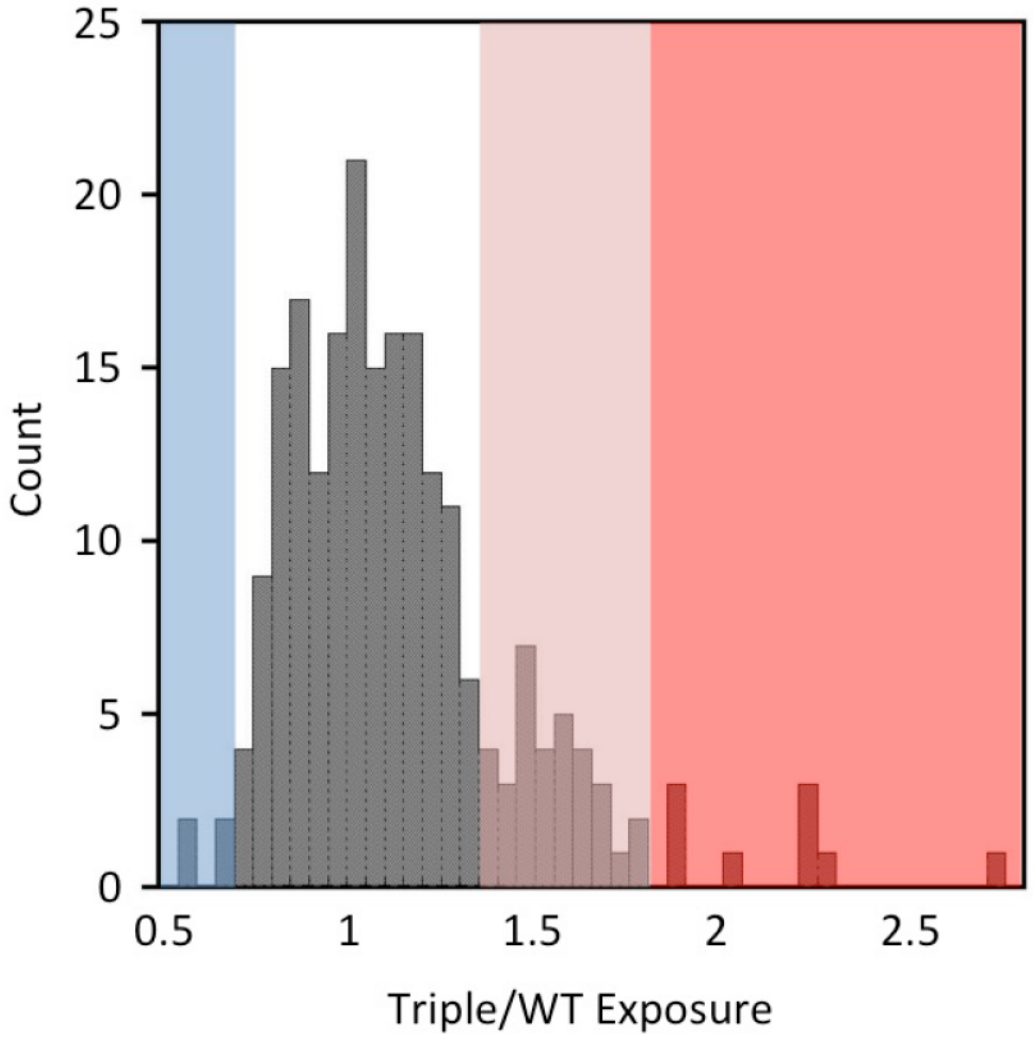

Figure 4.7: **Histogram of Triple mutant/WT ratios of nucleotide exposure**. For each nucleotide the ratio of the exposure in Triple mutant over the WT was calculated. Ratios greater than one represent nucleotides more exposed in the mutant while ratios less than one represent nucleotides protected in the mutant. These ratios were plotted on a histogram and empirical cut-off values were selected for perturbation clusters.

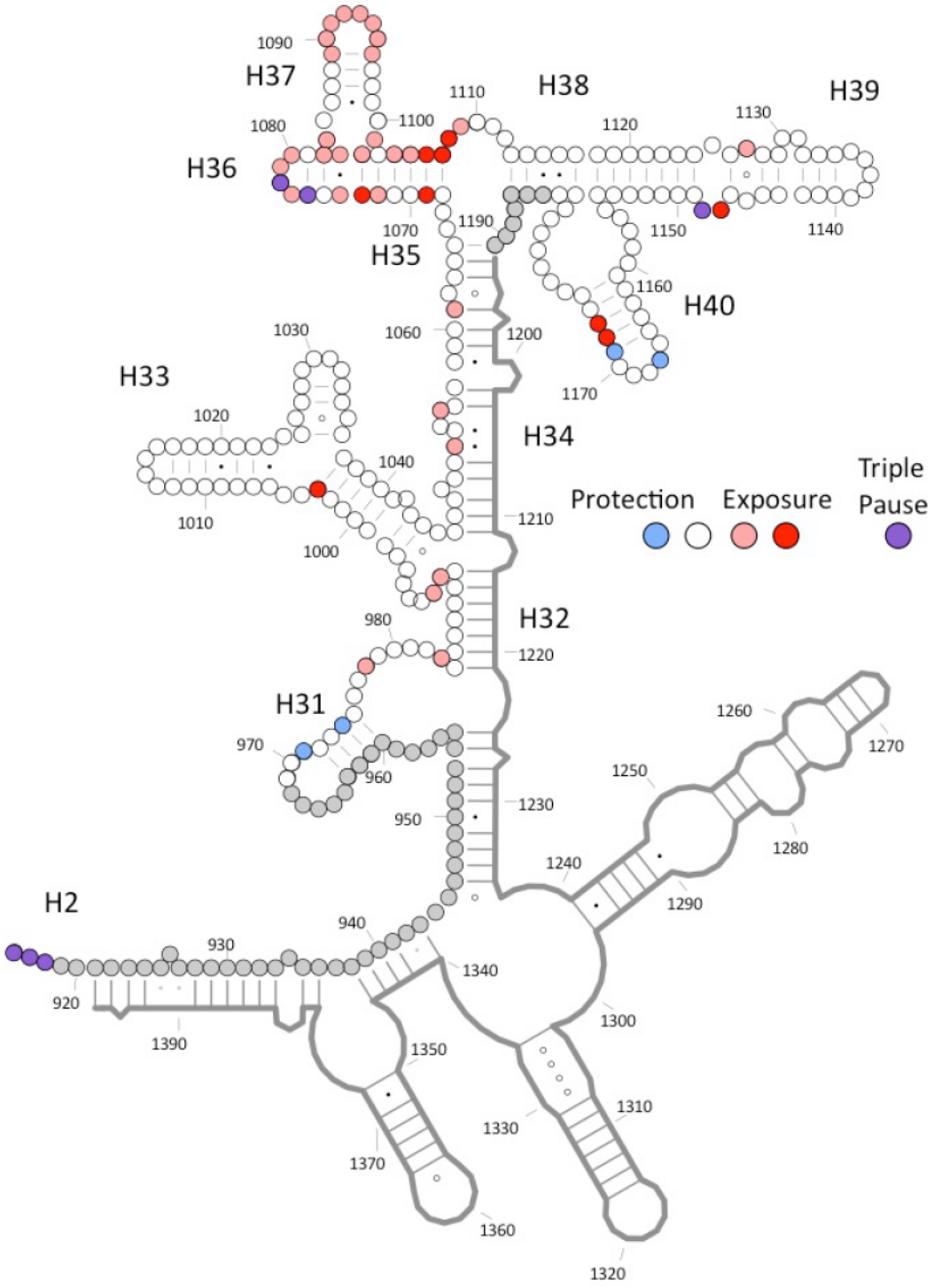

Figure 4.8: ***In vivo* footprinting results of J5/6 Triple mutant.** Nucleotides with altered exposure in the J5/6 Triple mutant are mapped onto the 16S 3' major domain secondary structure. Nucleotides with ratios less than 0.75 are blue, nucleotides with ratios between 1.4-1.8 are light red, nucleotides with exposure ratios greater than 1.8 are red. Residues with strong pauses in the non-irradiated and irradiated Triple mutant are purple. Light grey residues: data not available. Key helices and residues are labeled.

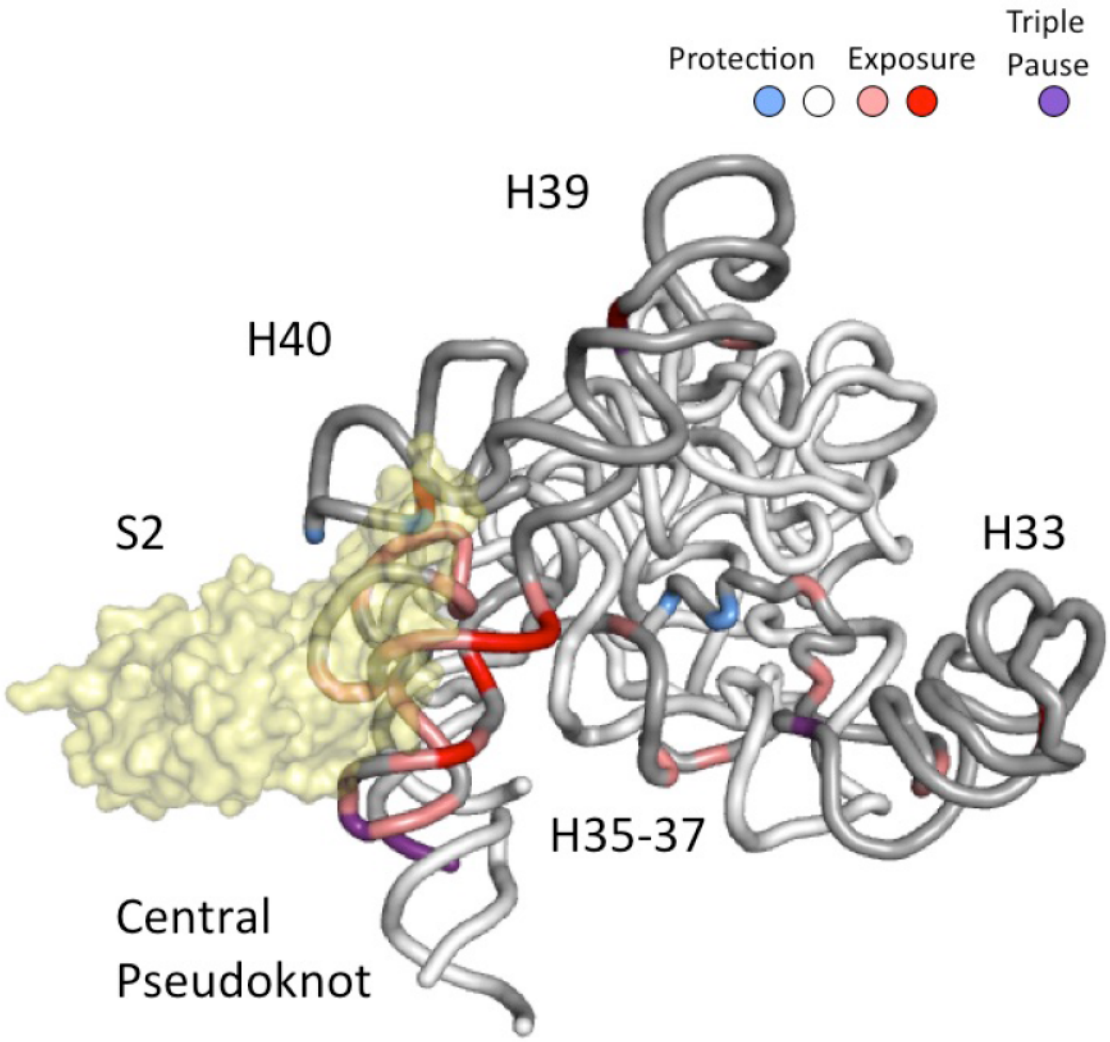

Figure 4.9: ***In vivo* footprinting results of J5/6 Triple mutant.** Nucleotides with altered exposure in the J5/6 Triple mutant are mapped onto the three-dimensional structure of the solvent face of the head domain colored as in Figure 4.7 and 4.8. Key helices are labeled and S2 is yellow.

my knowledge, there is no evidence of this nucleotide being modified and more evidence of cleavage occurring in this region, I believe this is a more reasonable explanation. A Northern blot with probes that hybridize to either side of the proposed site of cleavage (Basturea 2011) which may clear show cleaved rRNA species, or r-protein occupancy from quantitative mass spectrometry of affinity purified pre-ribosomes may be able to definitively prove the radiation-independent pause is due to cleavage of the rRNA.

Work from the Williamson lab showed that ribosome assembly factor RimP was critical for central pseudoknot formation (Sashital 2014). The central pseudoknot is not formed in more than 40% of *ΔrimP* ribosomes, which also show an abundance of "floppy head" particles by negative-stain EM density (Sashital 2014). RimP has no enzymatic activity and the functional interactions of RimP are unclear, but RimP does accelerate the binding of 5' domain/central pseudoknot proteins S5 and S12 (Bunner 2010). I was interested to see if an overexpression of RimP could reduce the central pseudoknot reverse transcriptase pause or cleavage detected above.

Induction of RimP in cells transformed with the Triple mutant reduced the cleavage of the central pseudoknot at A918 from 30% to 19% (Figure 4.10). Another ribosome assembly factor RbfA did not affect the cleavage of the central pseudoknot. In addition, there is a strain-dependent difference in the amount of cleavage at A918. Ribosomes from MRE600/Triple cells are ~15% cleaved at A918 while ribosomes from BW25113/Triple cells are ~30% cleaved (compare Figure 4.4 and 4.10). The explanation for this strain difference is unknown.

This reduction of central pseudoknot cleavage upon RimP overexpression is coupled with a 5% decrease in the amount of immature mutant 16S rRNA that

Figure 4.10: **Cleavage of the Central Pseudoknot of J5/6 Triple mutant ribosomes.** Allele-specific primer extension analysis of rRNA extracted from BW25113 cells. Cells with pSpur-Triple (blue) have a large portion of independent 3' domains as indicated by primer extensions stops due to a cleavage at A918. IPTG induction of RimP reduces this cleavage in the pSpur-Triple mutant cells. Fraction of transcripts stopped at A918 over full length and cleaved transcripts for each strain indicated below the gel.

accumulates (Figure 3.11). As the mechanism for RimP ribosome assembly activity has not been determined, how RimP could act to reduce cleavage at the central pseudoknot while also decreasing accumulation or increasing turnover is difficult to conceptualize.

It is likely this cleavage is the same endonucleolytic cleavage near the central pseudoknot detected by Basturea et al (2011). In the absence of the nucleases that normally degrade rRNA decay intermediates (RNase II, RNase R and PNPase) rRNA fragments corresponding to the 3' head domain and the 5' small subunit body and platform portion could be detected (Basturea 2011). During glucose starvation, the 5' ~900 nt fragment could not be detected due to rapid degradation, possibly by RNase PH, but the head fragment could still be detected by Northern blot (Basturea 2011). If the central pseudoknot of the J5/6 Triple mutant is accessible to a quality-control ribonuclease, is unclear what prevents complete removal of the possible 3' head domain.

4.4 Discussion

4.4.1 J5/6 Triple mutant has an immature head

The helix 5-6 junction is surprisingly critical for proper ribosome assembly. Mutations to this region produce ribosomes that are unable to fully assemble and are stalled in a 17S-containing complex. Somehow the J5/6 mutants are able to perturb the structural interactions of the solvent face of the neck. This is illustrated by a hydroxyl radical footprinting pattern with pronounced exposures on helices 2, 35-37 and the binding site for the late r-protein S2 (Figure 4.8).

The coexistent exposure of helix 36 and cleavage of helix 2 indicates that the head domain is not properly oriented in the J5/6 Triple mutant ribosomes. It is interesting that mutations in the center of the body domain could have such far-reaching affects on the neck. One hypothesis is that the J5/6 Triple mutant could interfere with the proper domain-domain orientations that reinforce the central pseudoknot through helix-helix interactions. Proper orientation of helix 5, 6, and 15 could be communicated via helices 4 and 3 to the central pseudoknot and from there to the rest of the ribosome. Helix 21 of the central domain wraps around the 'back' of the 5' body and contacts S17, and could also be impacted by a misassembled 5' domain.

Correlation of the exposures of helix 36, the proposed lack of S2, and the cleavage of the central pseudoknot make me wonder if the J5/6 mutants could stall the ribosomes in a Group II intermediate stage with a fully formed 30S body and platform but an "unanchored" head domain (Sashital 2014). Further structural information for the rest of the mutant ribosome could resolve this question and illuminate possible perturbed

helix-helix interactions, aberrant helix packing or long-range interactions, or other structural clues for why point mutations at the junction of helices 5 and 6 could have such a pronounced phenotype and be completely unable to be fully assembled and processed.

The r-protein complement for these pre-ribosomes is an open question that the Woodson lab in collaboration with the Limbach lab is working to answer. Knowing which r-proteins are in low abundance in the J5/6 mutant ribosome would shed some light on the point at which the J5/6 mutant ribosomes are stalled and may be able to elucidate the early stages of ribosome biogenesis. Due to the exposures of the neck region revealed by in vivo hydroxyl radical footprinting, I suspect S2, as well as other r-proteins that stabilize the neck (S5, S12, and S3) would be missing or in low abundance.

Overexpression of RimP, a ribosome assembly factor with an as of yet poorly understood role in ribosome biogenesis can reduce the central pseudoknot cleavage exhibited by the J5/6 Triple mutant. RimP is known to accelerate the binding of 5' domain/central pseudoknot proteins S5 and S12 (Bunner 2010), thus is has a well-supported role in stabilizing the neck of the 30S ribosome.

Chapter 5: Conclusions

5.1 The J5/6 region is critical for 30S biogenesis

Ribosome assembly is a complex and as-of-yet incompletely understood process. The intricate interplay of co-transcriptional rRNA folding, r-protein-guided rRNA conformational changes, and nucleolytic rRNA processing to yield a functional ribosome is aided by protein co-factors. The initial goal for my thesis was to see how mutations to the junction between helices 5 and 6 affected ribosome assembly in an attempt to catch a glimpse at an early assembly intermediate.

To our surprise, the *in vivo* phenotypes for all three J5/6 mutants were quite severe. The J5/6 mutants are recessive lethal. Neither selecting for an Spc^R point mutation in the plasmid-encoded 16S rRNA nor selecting for the loss of a pHK-rrnC$^+$sacB helper plasmid in a Δ7*rrn E. coli* strain led to bacterial growth (Powers 1990, Asai 1999). Further study revealed that the J5/6 mutants never complete the late-stage nucleolytic processing to produce the mature 16S rRNA, and never entered the 70S polysome peak. It is still an open debate in the field whether 50S subunit joining and a mock round of translation is required for final rRNA processing, or if rRNA processing is required for the 50S subunit to be able to bind (Karbstein 2013, Deutscher 2009, Li 1999). Regardless, the J5/6 mutant ribosomes are stalled prior to this point in biogenesis.

Neither a change in growth temperature – a common technique in the field to relieve rRNA misfolding kinetic assembly traps (Traub 1969, Dammel 1993) – nor overexpression of known ribosome assembly factors led to an improvement rRNA processing and ribosome maturation. Such a hard block on ribosome assembly was unexpected. The complete inability of the J5/6 mutants to be processed suggests that they possess a very high barrier to proper assembly. Perhaps the J5/6 mutations completely block the re-arrangement of rRNA helices or utter fail at properly timed release of a ribosome assembly factor.

To my knowledge, a complete failure of ribosome assembly has not been seen before; though the assembly of rRNA mutants has not really been studied. To date, only one other study has looked at the rRNA processing and polysome profiles of a rRNA mutant, and the assembly defects of this mutant were partial at 37° C (Dammel 1993). Other studies have looked at the proportion of mutant rRNA in 30S and 70S peaks as well as *in vivo* translational activity and miscoding of a heterogeneous population of mutant and chromosomal ribosomes has been determined (Gagnon 2006) or the mutant rRNA accumulation and temperature or antibiotic sensitivity/resistance of rRNA mutants (Douthwaite 1989, Triman 1989, Powers 1991) but not at ribosome assembly. Some of these mutants did not accumulate, or were only found in the 30S peak, but the root cause of this was not explored. Other rRNA mutations such as G530U abolish 30S ribosome activity (Powers 1990) and yet are not degraded (Paier 2015).

Overexpression of some known ribosome assembly factors led to an increase in the accumulation of mutant 17S rRNA, and other factors decreased the accumulation of mutant 17S rRNA. The cause for this variation is unknown, but perhaps assembly factors

that displace helix 44 somehow improve turnover of mutant ribosomes and assembly factors that do not displace helix 44, yet bind to the neck, somehow protect the immature ribosomes. The most pronounced effect was from overexpression of RimP, an assembly factor known for improving central pseudoknot formation and speeding up S5 and S12 binding (Sashital 2014, Bunner 2010), decreased the amount of mutant 17S rRNA from 23% to 19%, and also reduced the cleavage of the central pseudoknot in the J5/6 Triple mutant from 30% to 19%.

Exploration of the structure of the 3' head domain of the J5/6 Triple mutant pre-30S ribosome using allele-specific primer extension on *in vivo* hydroxyl radical footprinted rRNA revealed solvent exposures to helices 35-37 and a strong nucleolytic (non-irradiation) cleavage at the central pseudoknot. Exposure of helices 35-37 suggests that late r-protein S2 and the native tertiary interactions with other domains of the 30S ribosome are not present in the J5/6 Triple mutant, which has been seen before, but to a lesser extend likely indicated a greater proportion of particles with perturbed head domains in the J5/6 mutants than in assembly factor deletion strains or immature WT 30S particles (Soper 2013, McGinnis 2015). The helix 2 cleavage indicates that the critical central pseudoknot is not formed, which has been frequently in immature or non-functional ribosomes (Moazed 1986b, Besancon 1999, Soper 2013). Both quality-control and starvation ribosome degradation pathways feature a cleavage at this helix, though the identity of the ribonuclease and the purpose of the endonucleolytic cleavage are both unknown (Basturea 2011). The significance of the J5/6 mutant ribosomes also exhibiting this cleavage has not yet been determined.

Insight into how the J5/6 mutations could destabilize the central pseudoknot, inhibit native domain-domain interactions, and ultimately block ribosome maturation comes from *in vitro* assembly studies. Generally speaking, the *in vitro* assembly abnormalities I detected were modest and local; however, the J5/6 mutants destabilize the native conformation of helix 3 – as assayed by Helix 3-S4 ensemble FRET – even in the presence of S16. S16 is a very important secondary r-protein that packs helix 15 against the junction between helices 5 and 6, globally stabilizes the 5' domain, and flips a conformational switch at helix 3, which subsequently permits the formation of the central pseudoknot (Ramaswamy 2009b).

How, precisely the J5/6 mutations destabilize the native conformation of helix 3 is an open question. The mutations were selected to destabilize a proposed metastable assembly intermediate featuring a Right Angle motif (Grabow 2012) without interfering with the final state. In theory the mutations should make helix 15 stacking against the minor groove of helix 6 more favorable, if in fact the competing structure is a Right Angle motif. However, if the mutations do interfere with helix 15 stacking, this interference would likely be communicated to the central pseudoknot via the conformation of helix 4 and 3.

More specifically the J5/6 mutations should conserve the interactions of the N-terminus of S20 with the major groove of helix 5. Specifically, Lys 4 hydrogen bonding with the 2' hydroxyl of A60, Arg 9 hydrogen bonding with O6 of G107, and Asn 2 interacting with the backbone of G331 should be completely conserved in the J5/6 mutants (Schuwirth 2005). The mutations should also not hinder the tertiary interaction

of helix 13 G331 base stacking with A59 too badly. However, unintended consequences of the mutations are entirely likely.

EMSA co-localization assays between Cy5-labeled S20 and Cy3-labeled primer annealed to 5'dom-h3 rRNA shows a loss of high-affinity binding of S20 to the J5/6 mutants. SHAPE chemical probing of the J5/6 mutant 5' domains shows local increases in reactivity/flexibility of helix 13 and the J5/6 region in rRNA the absence of r-proteins. These perturbations are largely corrected by the addition of the primary r-proteins S4, S17, and S20 in the case of helix 13, and the addition of the primary r-proteins as well as S16 in the case of the J5/6 region. The SHAPE chemical probing shows no perturbations to the S16 binding site on helices 17 and 15; however, the SHAPE assays were performed with great excess of r-proteins so they could represent the r-proteins 'final state', not the actual *in vivo* dynamic equilibrium state.

Combining all of the *in vitro* and *in vivo* data, I propose some models for the structure of the stalled J5/6 ribosomes (Figure 5.1). All three structural models feature helices 35-37 that are exposed to solvent, an unformed central pseudoknot, and are lacking r-proteins S5, S12, S2, S3, and S21. They differ in the extent to which the J5/6 mutations destabilize the 5' domain. In one, the N-terminus of S20 is unstructured, helix 6 might be forming a Right Angle motif with helix 5 and displaces helix 15, and S16 may not be present. Though cryo- or negative stain EM structures of pre-30S ribosomes have frequently seen a displaced helix 44, and missing or 'floppy' head domains, none of the currently available structures exhibit a perturbed 5' domain (Mulder 2010, Jomaa 2011, Guo 2011, Boehringer 2012, Leong 2013, Yang 2014). If the J5/6 mutants adopt this structure, it would be an exciting first.

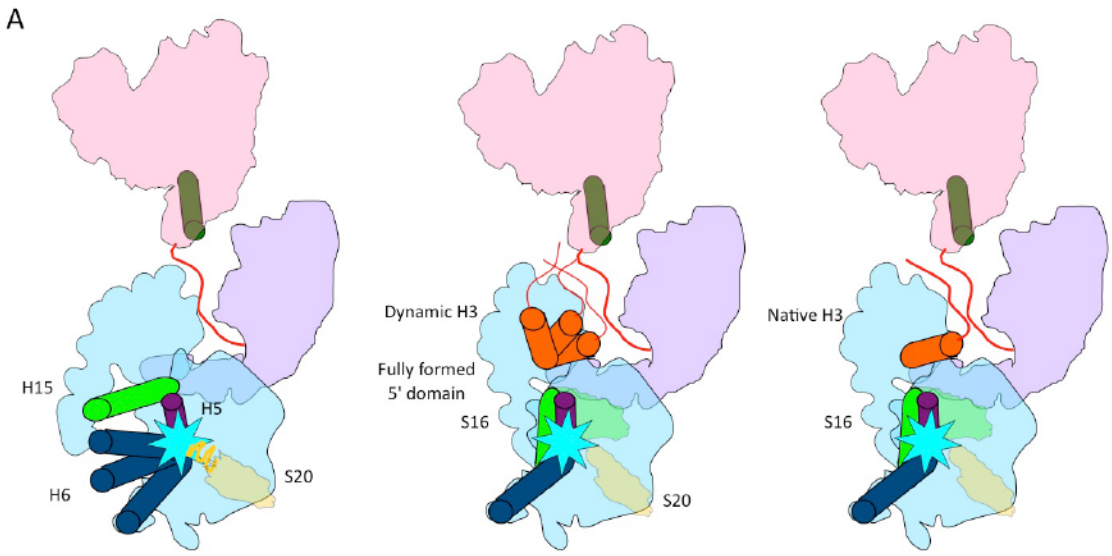

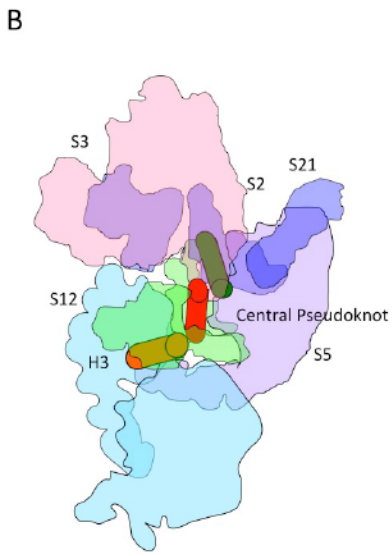

Figure 5.1: **Models for the structure of the J5/6 mutant ribosome.** A) Three possible structural models for J5/6 Triple mutant. 16S rRNA domains are colored as in Figure 1.1 (5' domain is pale cyan, central domain is lilac, 3' major domain is rose). The 3' minor domain is omitted for clarity. All three models lack the central pseudoknot (red) and feature exposed helices 35-37 (green cylinder). Key r-proteins S20 (yellow), S16 (green) and helices (H3, H5, H6, H15) and their proposed structures are indicated in colored cylinders. The three models differ in the structure of the helix 5/6 junction (cyan star) and the orientation of helix 15 and helix 3. B) A structural model of a native 30S for comparison. Helix 3 (orange) is in the native conformation, the central pseudoknot (red) is formed, helices 35-37 are protected, secondary r-proteins S5, S12 (green) and tertiary r-proteins S2, S3, S21 (blue) are at full occupancy.

In another structural model, the 5' domain is fully structured, S16 is at full occupancy, but helix 3 is dynamic, not locked into its native conformation. In the third, helix 3 is in the native conformation, but the central pseudoknot is not formed for some other reason. The occupancy of S12 would be able to differentiate between these models as it's binding site is only formed if helix 3 is in the native conformation (Stern 1988b). The origin of the reverse transcriptase pause at A918 is likely due to endonucleolytic cleavage, but these models do not depict a cleavage of the unformed central pseudoknot, which RimP overexpression partially suppresses.

5.2 Future directions

My work on the J5/6 mutants inspired one open question: what do the immature J5/6 mutant ribosomes look like? This could be answered by further troubleshooting to reduce the ribonuclease contamination and background in the affinity purification method to a level compatible with the low signal of *in vivo* hydroxyl radical footprinting. By exploring if other domain-domain interaction surfaces are exposed to solvent, we could learn more about the stage of ribosome assembly at which the J5/6 mutants are stalled. My current hypothesis is that they look somewhat like the Class II 'floppy head' particles identified by Sashital et al (2014) but further work is needed to confirm this hypothesis. It is also possible that due to the nucleolytic cleavage at the central pseudoknot, a proportion of the J5/6 mutants exist as independent 3' head domains and 5' body-platforms, though these species were not detected in analytical sucrose gradients, so they could not be a large proportion.

Determining the solvent exposure of the J5/6 region, S20 binding site, and helix 15 could also provide insight as to why the J5/6 mutant ribosomes are so completely stalled, but due to the fact that they can reach a near-30S sedimentation coefficient, a completely misassembled 5' domain is unlikely. Though the sedimentation coefficient is dependent upon a particle's shape in addition to its mass, it is unlikely the J5/6 mutant ribosomes could have a drastically misassembled 5' body domain and still sediment the same. Other things we could learn from a complete footprint include if some other r-protein binding sites are vacant, the structure of helix 44, and regions of rRNA misfolding.

Mass spectrometry on the r-protein occupancy of affinity purified J5/6 mutant ribosomes could also help determine the structure of the J5/6 mutants and if they are stalled in a Class II 'floppy-head' particle stage. If the J5/6 mutants are stalled in a Class II-like state, they should be missing S5, S12, S21, S3 and S2, but should contain near stoichiometric levels of at least the 3' domain primary r-protein S7 if not also secondary r-proteins S9, S19, and S13. However, if the central pseudoknot cleavage of the J5/6 mutants leads to dissociation of the 3' head from the 5' body and platform, then S7, S9, S19 and S13 should be less abundant. Either way, due to the *in vivo* hydroxyl radical footprinting data of the J5/6 mutant 3' domain, I expect S3 and likely S2 will have low occupancy. Since a S20 deletion is viable, it would be interesting to see the occupancy of S20 in the J5/6 mutant ribosomes (Bubunenko 2007).

It would also be quite informative if associated ribosome assembly factors could be identified by mass spectrometry. This could provide insight as to when these assembly factors bind or function, and may be able to answer why overexpression of some factors

led to an increase in retained mutant 17S rRNA and other factors led to a depletion of mutant 17S rRNA. Identification of novel possible assembly factors could provide insight into the ribosome assembly process, and suggest further ribosome assembly factor overexpression experiments.

Another method to attempt to identify novel assembly factors that act upon the J5/6 mutant would be to identify high-copy number suppressors on Spc plates that select for plasmid-encoded 16S rRNA. Care would need to be taken to ensure that the suppressors are bona fide suppressors and not revertants or mutations that improve spectinomycin resistance for chromosomally-derived ribosomes.

Along the same lines, it would be interesting to see if other assembly factor deletions are as deleterious to the J5/6 mutants as *ΔrbfA*. I believe the phenotype of *ΔrimP* would be particularly interesting. The structural phenotype of the J5/6 mutants is (possibly) similar to that of *ΔrimP* ribosomes, so either the combination could be practically silent, or catastrophically toxic.

My work on the J5/6 mutants inspired another pressing question: are the stalled pre-ribosomes on path? One way to answer this question would be to identify an assembly factor that ameliorates the J5/6 mutant phenotype and then co-incubate the purified stalled J5/6 mutant ribosomes with an extract with that factor and watch the ribosomes mature. One first-level read-out of this would be to watch the 17S rRNA be processed in the presence of this extract (like in Gupta 2014 and others). Watching the J5/6 mutant ribosomes gain translational activity after *in vitro* treatment with said purified factor or extract would be very compelling. If the J5/6 mutants can never be

fixed, then the biological relevance of the observations derived from the J5/6 mutants would be cast into question.

Further *in vitro* studies attempting to tease apart why these mutations are so deleterious to assembly and how they disrupt the native conformation of helix 3 could be useful. Possible experiments include studying how the kinetics of helix 3 conformational change for the J5/6 mutants using single molecule FRET, and further exploring the binding affinity of S20 for the J5/6 mutant 5' domain rRNAs under various conditions with various other r-proteins.

Appendixes

Table A.1 **Bacterial strains used in this work.**

	Genotype
DH1/ pCI^{857}	F^{-} *glnV44 recA1 endA1 gyrA96 thi1 hsdR17 ((rK^{-} mK^{+}) relA1/* pCI^{857}
SQZ10	F- *ara* Δ*lac thi* Δ(*purDH-rrnE-metA*) *polA1 zih*::Tn*10* Δ(*rrsB-gltT-rrlB*)*101* Δ(*rrsH-ileV-alaV-rrlH*)*103* Δ(*rrsG-gltW-rrlG*)*30*::*lacZ* $^{+}$ *polA* $^{+}$Δ(*rrsA-ileT-alaT-rrlA*)*34* Δ(*rrsD-ileU-alaU-rrlD*)*25*::*cat* $^{+}$ Δ(*rrsC-gltU-rrlC*)*15*::*cat* $^{+}$ *ilv* $^{+}$/pTRNA67, pHK-rrnC^{+} sacB (Tsumeaki 1999, Zaporojets 2003)
DH5α	F- *endA1 hsdR17 (rK^{-} mK^{+}) glnV44 thi-1 recA1 gyrA* relA1 *Δ(lacIZYA-argF)U169 deoR (φ80dlacΔ(lacZ)M15)*
MRE600	F- *rna*
BW25113	*Δ(araD-araB)567 ΔlacZ4787*(::rrnB-3) *λ- rph*-1 *Δ(rhaD-rhaB)568 hsdR514*
JM3136	BW25113 *ΔrbfA779*::kan (Baba 2006)

Table A.2: **Plasmids used in this work.**

pRNA1	pUC-derived plasmid with T7 RNA polymerase transcribe-able 5' domain of the 16S rRNA with EcoRI linearization site (Adilakshmi 2005)
MCR-Topo	pCR2.1-Topo kit derived plasmid with ~1kb mutant rRNA segments (Invitrogen)
pRNA5	pUC-derived plasmid with T7 RNA polymerase transcribe-able 16S rRNA with XbaI linearization site
pLK45	pBR322-derived plasmid with full *rrnB* operon with U1192 and G2058 plasmid-specific Spc^R and Ery^R point mutations downstream from the λ-promoter (Powers 1990)
pSpur	pLK45 derivative with an MS2-hairpin inserted at the tip of helix 6 (Youngman 2005)
pCI^{857}	p15A-based plasmid containing the temperature-sensitive cI857 allele of the λ repressor gene (Remaut 1983)
pTRNA67	pACYC-derived plasmid with *rrn* encoded tRNA sequences downstream from the *tac* promoter (Zaporojets 2003)
pHK-$rrnC^+$ *sacB*	pSC101-derived plasmid with the *rrnC* operon and a Km-*sacB* cassette (Zaporojets 2003)
p15B-3	pACYC184-derived plasmid with *rbfA* gene and promoter (Dammel 1995)
pCA24N	Base plasmid for the ASKA collection, a pBR322-derived plasmid with a Histidine- and GFP-tagged *E. coli* gene under control of the T5-lac promoter and $lacI^q$ repressor (Kitagawa 2005)
pD421	pACYC184-derived plasmid with T5-lac promoter and $lacI^q$ repressor (DNA 2.0)

Table A.3: **Primers used for primer extension in this work**. Numbered primers are named for the 16S nucleotide that anneals to the 3' end of the primer.

	Sequence
16S plasmid origin primer	gggccatgatgacttga (Triman 1989)
23S plasmid origin primer	aaaggttcacggggtctt (Zhang 1995)
161	gcggtattagctaccgt (Moazed 1986a)
323	agtctggaccgtgtctc (Moazed 1986a)
1199	tcgtaagggccatgatg (Moazed 1986a)
1486	ggttaccttgttacgacttcacccc (Moazed 1986a)
Spc^R allele specific primer	ggccatgatgacttgacA

Bibliography

Adilakshmi T, Ramaswamy P, Woodson SA. 2005. Protein-independent folding pathway of the 16S rRNA 5' domain. *Journal of Molecular Biology* **351:**508-519.

Adilakshmi T, Lease RA, Woodson SA. 2006. Hydroxyl radical footprinting in vivo: mapping macromolecular structures with synchrotron radiation. *Nucleic Acids Research* **34:** e64.

Adilakshmi T, Bellur DL, Woodson SA. 2008. Concurrent nucleation of 16S folding and induced fit in 30S ribosome assembly. *Nature* **455:**1268-1272.

Adilakshmi T, Soper SFC, Woodson SA. 2009. Structural analysis of RNA in living cells by in vivo synchrotron X-ray footprinting. Methods in Enzmology **468:**239-258.

Albrechtsen B, Ross BM, Squires C, Squires CL. 1991. Transcriptional termination sequence at the end of the Escherichia coli ribosomal RNA G operon: complez terminators and antitermination. *Nucleic Acids Research* **19:**1845-1852.

Al-Hashimi HM. Walter NG. 2008. RNA dynamics: it is about time. *Current Opinion in Structural Biology* **18:**321-329.

Andersen N, Douthwaite S. 2006. YebU is a m5C methyltransferase specific for 16 S rRNA nucleotide 1407. *Journal of Molecular Biology* **359:**777-786.

Anton BP, Saleh L, Benner JS, Raleigh EA, Kasif S, Roberts RJ. 2008. RimO, a MiaB-like enzyme, methylthiolates the universally conserved Asp88 residue of ribosomal protein S12 in Escherichia coli. *Proceedings of the National Academy of Sciences of USA* **105:**1826-1831.

Armache JP, Anger AM, Márquez V, Franckenberg S, Fröhlich T, Villa E, Berninghausen O, Thomm M, Arnold GJ, Beckmann R, Wilson DN. 2013. Promiscuous behaviour of archaeal ribosomal proteins: implications for eukaryotic ribosome evolution. *Nucleic Acids Research* **41:** 1284-1293.

Arnold RJ, Reilly JP. 1999. Observation of Escherichia coli ribosomal proteins and their posttranslational modifications by mass spectrometry. *Analytical Biochemistry* **269:**105-122.

Artsimovitch I, Patlan V, Sekine SI, Vassylyeva MN, Hosaka T, Ochi K, Yokoyama S, and Vassylyev DG. 2004. Structural Basis for Transcription Regulation by Alarmone ppGpp. *Cell* **117:**299-310.

Asai T, Zaporojets D, Squires C, Squires CL. 1999. An Escherichia coli strain with all chromosomal rRNA operons inactivated: Complete exchange of rRNA genes between bacteria. *Proceedings of the National Academy of Sciences of USA* **96:**1971-1976.

Attardi G, Huang PC, Kabat S. 1965. Recognition of ribosomal RNA sites in DNA. I. Analysis of the E. coli system. *Proceedings of the National Academy of Sciences of USA* **53:**1490-1498.

Baba T, Ara T, Hasegawa M, Takai Y, Okumura Y, Baba M, Datsenko KA, Tomita M, Wanner BL, Mori H. 2006. Construction of *Escherichia coli* K-12 in-frame, single-gene knockout mutants: the Keio collection. *Molecular Systems Biology* **2:**2006.0008.

Basturea G, Deutscher M. 2007. Substrate specificity and properties of the Escherichia coli 16S rRNA methyltransferase, RsmE. *RNA* **13:**1969-1976.

Basturea G, Zundel MA, Deutscher M. 2010. Degradation of ribosomal RNA during starvation: Comparison to quality control during steady-state growth and a role for RNase PH. *RNA* **17:** 338-345.

Basturea G, Dague DR, Deutscher M, Rudd KE. 2012. YhiQ Is RsmJ, the Methyltransferase Responsible for Methylation of G1516 in 16S rRNA of E. coli. *Journal of Molecular Biology* **415:**16-21.

Batey RT, Kieft JS. 2007. Improved native affinity purification of RNA. *RNA* **13:**1384-1389.

Behrouzi R, Roh JH, KilburnD, Briber RM, Woodson SA. 2012. Cooperative Tertiary Interaction Network Guides RNA Folding. *Cell* **149:**348-357.

Bellur DL, Woodson SA. 2009. A minimized rRNA-binding site for ribosomal protein S4 and its implications for 30S assembly. *Nucleic Acids Research* **37:**1886-1896.

Belotserkovsky JM, Dabbs ER, Isaksson LA. 2011. Mutations in 16S rRNA that suppress cold-sensitive initiation factor 1 affect ribosomal subunit association. *Federation of European Biochemical Societies Journal* **278:**3508-3517.

Ben-Shem A, Jenner L, Yusupova G, Yusupov M. 2010. Crystal structure of the eukaryotic ribosome. *Science* **330:** 1203-1209.

Berg KL, Squires C, Squires CL. 1989. Ribosomal RNA operon anti-termination: Function of leader and spacer region Box B-Box A sequences and their conservation in diverse microorganisms. *Journal of Molecular Biology* **209:**345-358.

Besancon W, Wagner R. 1999. Characterization of transient RNA-RNA interactions important for the facilitated structure formation of bacterial ribosomal 16S rRNA.

Nucleic Acids Research **27:**4353-4362.

Bessarab DA, Kaberdin VR, Wei CL, Liou GG, Lin-Chao S. 1998. RNA components of Escherichia coli degradosome: evidence for rRNA decay. *Proceedings of the National Academy of Sciences of USA* **95:** 3157-3161.

Bjoerk GR. 1985. E. coli Ribosomal Protein Operons: The case of the misplaced genes. *Cell* **42:**7-8

Boehringer D, O'Farrell HC, Rife JP, Ban N. 2012. Structural insights into methyltransferase KsgA function in 30S ribosomal subunit biogenesis. *The Journal of Biological Chemistry* **287**:10453–10459.

Bram RJ, Young RA, Steitz JA. 1980. The ribonuclease III site flanking 23S sequences in the 30S ribosomal precursor RNA of E. coli. *Cell* **19:**393–401.

Brink MF, Verbeet MP, de Boer HA. 1993. Formation of the central pseudoknot in 16S rRNA is essential for initiation of translation. *The EMBO Journal* **12:**3987-3996.

Brosius J, Palmer ML, Kennedy PJ, Noller HF. 1978. Complete nucleotide sequence of a 16S ribosomal RNA gene from Escherichia coli. *Proceedings of the National Academy of Sciences of USA* **75:**4801-4805.

Brosius J, Dull TJ, Noller HF. 1980. Complete nucleotide sequence of a 23S ribosomal RNA gene from Escherichia coli. *Proceedings of the National Academy of Sciences of USA* **77:**201-204.

Brown T, Mackey K, Du TT. 2004. Analysis of RNA by Northern and Slot Blot Hybridization. *Current Protocols in Molecular Biology* **67:**4.9:1-19.

Brunschede H, Dove TL, Bremer H. 1977. Establishment of exponential growth after a nutritional shift-up in Escherichia coli B/r: accumulation of deoxyribonucleic acid,

ribonucleic acid, and protein. *Journal of Bacteriology* **129:** 1020-1033.

Bubunenko M, Baker T, Court DL. 2007. Essentiality of ribosomal and transcription antitermination proteins analyzed by systemic gene replacement in Escherichia coli. *Journal of Bacteriology* **189:**2844-2853.

Bunner AE, Nord S, Wikström PM, Williamson JR. 2010. The effect of ribosome assembly cofactors on in vitro 30S subunit reconstitution. *Journal of Molecular Biology* **398**:1–7.

Bylund GO, Persson BC, Lundberg LAC, Wikstrom PM. 1997. A novel ribosome associated protein is important for efficient translation in Escherichia coli. *Journal of Bacteriology* **179:**4567-4574.

Bylund GO, Wipemo LC, Lundberg LAC, Wikstrom PM. 1998. RimM and RbfA are essential for efficient processing of 16S rRNA in Escherichia coli. *Journal of Bacteriology* **180:**73–82.

Campbell TL, Brown ED. 2008. Genetic interaction screens with ordered overexpression and deletion clone sets implicate the Escherichia coli GTPase YjeQ in late ribosome biogenesis. *Journal of Bacteriology* **190:**2537–2545.

Cashel M, Kalbacher B. 1970. The control of ribonucleic acid synthesis in Escherichia coli. V. Characterization of a nucleotide associated with the stringent response. *Journal of Biological Chemistry* **245:**2309-2318.

Cate JH, Gooding AR, Podell E, Zhou K, Golden BL, Szewczak AA, Kundrot CE, Cech TR, Doudna JA.1996. RNA tertiary structure mediation by adenosine platforms. *Science* **273:**1696-1699.

Cerretti DP, Mattheakis LC, Kearney KR, Vu L, Nomura M. 1988. Translational

regulation of the spc operon in Escherichia coli. Identification and structural analysis of the target site for S8 repressor protein. *Journal of Molecular Biology* **204:**309-329.

Chen R, Chen-Schmeisser U. 1977. Isopeptide linkage between N-alpha-monomethylalanine and lysine in ribosomal protein S11 from Escherichia coli. *Proceedings of the National Academy of Sciences of USA* **74:**4905-4908.

Chen SS, Williamson JR. 2013. Characterization of the ribosome biogenesis landscape in *E. coli* using quantitative mass spectrometry. *Journal of Molecular Biology* **425:**767–779.

Chen X, Court DL, Ji X. 1999. Crystal structure of ERA: a GTPase-dependent cell cycle regulator containing an RNA binding motif. *Proceedings of the National Academy of Sciences of USA* **96:** 8396-8401.

Chworos A, Severcan I, Koyfman AY, Weinkam P, Oroudjev E, Hansma HG, Jaeger L. 2004. Building programmable jigsaw puzzles with RNA. *Science* **306:** 2068-2072.

Condon C, French S, Squires C, Squires CL. 1993. Depletion of functional ribosomal RNA operons in Escherichia coli causes increased expression of the remaining intact copies. *The EMBO Journal* **12:**4305-4315.

Condon C, Squires C, Squires CL. 1995. Control of rRNA Transcription in Escherichia coli. *Microbiological Reviews* **59:**623-645.

Connolly K, Rife JP, Culver G. 2008. Mechanistic insight into the ribosome biogenesis functions of the ancient protein KsgA. *Molecular Microbiology* **70**:1062-1075.

Connolly K, Culver G. 2013. Overexpression of RbfA in the absence of the KsgA checkpoint results in impaired translation initiation. *Molecular Microbiology*

87:968-981.

Craven GR, Voynow P, Hardy SJ, Kurland CG. The ribosomal proteins of Escherichia coli. II. Chemical and physical characterization of the 30S ribosomal proteins. *Biochemistry* **8:**2906-2915.

Daigle DM, Brown ED. 2004. Studies of the interaction of Escherichia coli YjeQ with the ribosome in vitro. *Journal of Bacteriology* **186:**1381-1387.

Dammel CS, Noller HF. 1993. A cold-sensitive mutation in 16S rRNA provides evidence for helical switching in ribosome assembly. *Genes & Development* **7:**660-670.

Dammel CS, Noller HF. 1995. Suppression of a cold-sensitive mutation in 16S rRNA by overexpression of a novel ribosome-binding factor, RbfA. *Genes & Development* **9:**626–637.

David CL, Keener J, Aswad DW. 1999. Isoaspartate in ribosomal protein S11 of Escherichia coli. *Journal of Bacteriology* **181:**2872-2877.

Davies BW, Köhrer C, Jacob AI, Simmons LA, Zhu J, Aleman LM, Rajbhandary UL, Walker GC. 2010. Role of Escherichia coli YbeY, a highly conserved protein, in rRNA processing. *Molecular Microbiology* **78**:506-518.

Davies J, Gorini L, Davis BD. 1965. Misreading of RNA codewords induced by aminoglycoside antibiotics. *Molecular Pharmacology* **1:** 93-106.

Das R, Laederach A, Pearlman SM, Herschlag D, Altman RB. 2005. SAFA: semi-automated footprinting analysis software for high-throughput quantification of nucleic acid footprinting experiments. *RNA* **11:**344-54.

Dean D, Yates JL, Nomura M. 1981. Escherichia coli ribosomal protein S8 feedback

regulates part of spc operon. *Nature* **289:**89-91.

Demirci H, Gregory ST, Dahlberg AE, Jogl G. 2008. Crystal structure of the Thermus thermophilus 16 S rRNA methyltransferase RsmC in complex with cofactor and substrate guanosine. *The Journal of Biological Chemistry* **283:**26548-26556.

Datta PP, Wilson DN, Kawazoe W, Swami NK, Kaminishi T, Sharam MR, Booth TM, Takemoto C, Fucini P, Yokoyama S, Agrawal RK. 2007. Strucutral aspects of RbfA action during small ribosomal subunit assembly. *Molecular Cell* **28:**434-445.

de Boer HA, Gilbert SF, Nomura M. 1979. DNA sequences of promoter regions for rRNA operons rrnE and rrnA in E. coli. *Cell* **17:**201-209.

Dennis PP, Bremer H. 1973. Regulation of ribonucleic acid synthesis in Escherichia coli B-r: an analysis of a shift-up. 1. Ribosomal RNA chain growth rates. *Journal of Molecular Biology* **75:**145-159.

Dennis PP, Ehrenberg M, Fange D, Bremer H. 2009. Varying rate of RNA chain elongation during rrn transcription in Escherichia coli. *Journal of Bacteriology* **191:**3740-3746.

Deutscher MP. 2009. Maturation and degradation of ribosomal RNA in bacteria. *Progress in Molecular Biology and Translational Science* **85:**369-391.

Doolittle WF, Pace NR. 1971. Transcriptional organization of the ribosomal RNA cistrons in Escherichia coli. *Proceedings of the National Academy of Sciences of USA* **68:**1786-1790.

Dorywalska M, Blanchard SC, Gonzalez RL, Kim HD, Chu S, Puglisi JD. 2005. Site-specific labeling of the ribosome for single-molecule spectroscopy. *Nucleic Acids*

Research **33:**182-189.

Douthwaite S, Powers T, Lee JY, Noller HF. 1989. Defining the structural requirements for a helix in 23 S ribosomal RNA that confers erythromycin resistance. *Journal of Molecular Biology* **209:** 655-665.

Dunn JJ, Studier FW. 1973. T7 early RNAs and Escherichia coli ribosomal RNAs are cut from large precursors in vivo by ribonuclease III. *Proceedings of the National Academy of Sciences of USA* **70:**3296–3300.

Dutca LM, Culver GM. 2008. Assembly of the 5' and 3' minor domains of 16S ribosomal RNA as monitored by tethered probing from ribosomal protein S20. *Journal of Molecular Biology* **376:**92-108.

Ehrenberg M, Bremer H, Dennis PP. 2013. Medium-dependent control of the bacterial growth rate. *Biochimie* **95:**643-658.

Fallon AM, Jinks CS, Strycharz GD, Nomura M. 1979. Regulation of ribosomal protein synthesis in Escherichia coli by selective mRNA inactivation. *Proceedings of the National Academy of Sciences of USA* **76:**3411-3415.

Foster C, Champney WS. 2008. Characterization of a 30S ribosomal subunit assembly intermediate found in Escherichia coli cells growing with neomycin or paromomycin. *Archives of Microbiology* **189:**441–49.

Gagnon MG, Steinberg SV. 2002. GU receptors of double helices mediate tRNA movement in the ribosome. *RNA* **8:**873-877.

Gagnon MG, Mukhopadhyay A, Steinberg SV. 2006. Close packing of helices 3 and 12 of 16 S rRNA is required for the normal ribosome function. *The Journal of Biological Chemistry* **281:**39349-39357.

Gagnon MG, Boutorine YI, Steinberg SV. 2010. Recurrent RNA motifs as probes for studying RNA-protein interactions in the ribosome. *Nucleic Acids Research* **38:**3441-3453.

Gegenheimer P, Apirion D. 1975. Escherichia coli ribosomal ribonucleic acids are not cut from an intact precursor molecule. *The Journal of Biological Chemistry* **250:**2407-2409.

Glasel JA. 1995. Validity of nucleic acid purities monitored by 260nm/280nm absorbance ratios. *Biotechniques* **18:**62-63.

Glaser G, Cashel M. 1979. In vitro transcripts from the rrn B ribosomal RNA cistron originate from two tandem promoters. *Cell* **16:**111-21.

Glaser G, Sarmientos P, Cashel M. 1983. Functional interrelationship between two tandem E. coli ribosomal RNA promoters. *Nature* **302:**74-76.

Goto S, Kato S, Kimura T, Muto A, Himeno H. 2011. RsgA releases RbfA from 30S ribosome during a late stage of ribosome biosynthesis. *The EMBO Journal* **30:**104-114.

Grabow WW, Zhuang Z, Swank ZN, Shea JE, Jaeger L. 2012. The Right Angle (RA) motif: a prevalent ribosomal RNA structural pattern found in Group I introns. *Journal of Molecular Biology* **424:**54-67.

Greber BJ, Bieri P, Leibundgut M, Leitner A, Aebersold R, Boehringer D, Ban N. 2015. Ribosome. The complete structure of the 55S mammalian mitochondrial ribosome. *Science* **348:** 303-308.

Guo Q, Yuan Y, Xu Y, Feng B, Liu L, Chen K, Sun M, Yang Z, Lei J, Gao N. 2011. Structural basis for the function of a small GTPase RsgA on the 30S ribosomal

subunit maturation revealed by cryoelectron microscopy. *Proceedings of the National Academy of Sciences of USA* **108:**13100-13105.

Gupta N, Culver GM. 2014. Multiple in vivo pathways for Escherichia coli small ribosomal subunit assembly occur on one pre-rRNA. *Nature Structural & Molecular Biology* **21:**937-943.

Haseltine WA, Block R, Gilbert W, Weber K. 1972. MSI and MSII made on ribosome in idling step of protein synthesis. *Nature* **238:**381-384.

Held WA, Mizushima S, Nomura M. 1973a. Reconstitution of Escherichia coli 30S ribosomal subunits from purified molecular components. *The Journal of Biological Chemistry* **248:**5720-5730.

Held WA, Nomura M. 1973b. Rate-determining step in the reconstitution of Escherichia coli 30S ribosomal subunits. *Biochemistry* **12:**3273-3281.

Held WA, Ballou B, Mizushima S, Nomura M. 1974. Assembly mapping of 30S ribosomal proteins from Escherichia coli: further studies. *The Journal of Biological Chemistry* **249:**3103-3111.

Hernandez VJ, Bremer H. 1991. Escherichia coli ppGpp synthetase II activity requires spoT. *The Journal of Biological Chemistry* **266:**5995-5999.

Hertzberg RP, Dervan PB. 1984. Cleavage of DNA with methidiumpropyl- EDTA-iron(II): Reaction conditions and product analyses. *Biochemistry* **23:** 3934-3945.

Hitz H, Schafer D, Wittmann-Liebold B. 1975. Primary structure of ribosomal protein S6 from the wild type and a mutant of Escherichia coli. *FEBS Letters* **65:**259-262.

Holmes KL, Culver GM. 2004. Mapping structural differences between 30S ribosomal subunit assembly intermediates. *Nature Structural & Molecular Biology* **11:**179-

186.

Inoue K, Alsina J, Chen J, Inouye M. 2003. Suppression of defective ribosome assembly in a rbfA deletion mutant by overexpression of Era, an essential GTPase in Escherichia coli. *Molecular Microbiology* **48:**1005-1016

Isono K, Isono S. 1980. Ribosomal protein modification in Escherichia coli. II. Studies of a mutant lacking the N-terminal acetylation of protein S18. *Molecular and General Genetics* **177:**645-651.

Janda I, Kitakawa M, Isono K. 1985. Gene rpmF for ribosomal protein L32 and gene rimJ for a ribosomal protein acetylating enzyme are located near pyrC (23.4 min) in Escherichia coli. *Molecular and General Genetics* **201:** 433-436.

Jagannathan I, Culver GM. 2003. Assembly of the central domain of the 30S ribosomal subunit: roles for the primary binding ribosomal proteins S15 and S8. *Journal of Molecular Biology* **330:** 373-383.

Jeganathan A, Razi A, Thurlow B, Ortega J. 2015. The C-terminal helix in the YjeQ zinc-finger domain catalyzes the release of RbfA during 30S ribosome subunit assembly. *RNA* **21:** 1203-1216.

Jinks-Roberts S, Gourse RL, Nomura M. 1983. Expression of rRNA and tRNA genes in Escherichia coli: evidence for feedback regulation by products of rRNA operons. *Cell* **33:** 865-876.

Jacob AI, Köhrer C, Davies BW, RajBhandary UL, Walker GC. 2013. Conserved bacterial RNase YbeY plays key roles in 70S ribosome quality control and 16S rRNA maturation. *Molecular Cell* **49:** 427-438.

Jomaa A, Stewart G, Martín-Benito J, Zielke R, Campbell TL, Maddock JR, Brown ED,

Ortega J. 2011. Understanding ribosome assembly: the structure of in vivo assembled immature 30S subunits revealed by cryo-electron microscopy. *RNA* **17:**697-709.

Kaberdina AC, Szaflarski W, Nierhaus KH, Moll I. 2009. An unexpected type of ribosomes induced by kasugamycin: a look into ancestral times of protein synthesis? *Molecular Cell* **33:** 227-236.

Kaczanowska M, Rydén-Aulin M. 2007. Ribosome Biogenesis and the Translation Process in Escherichia coli. *Microbiology and Molecular Biology Reviews* **71:**477-494.

Kang WK, Icho T, Isono S, Kitakawa M, Isono K. 1989. Characterization of the gene rimK responsible for the addition of glutamic acid residues to the C-terminus of ribosomal protein S6 in Escherichia coli K12. *Molecular and General Genetics* **217:**281-288.

Karbstein K. 2013. Quality control mechanisms during ribosome maturation. *Trends in Cell Biology* **23:**242-250.

Keener J, Nomura M. 1996. Regulation of ribosome synthesis. *In* F. C. Neidhardt (ed.), *Escherichia coli* and *Salmonella:* cellular and molecular biology, 2nd ed. ASM Press, Washington, DC. 1417-1431.

Kelley T, Culver GM. 2008. Suppression of a cold-sensitive mutation in ribosomal protein S5 reveals a role for RimJ in ribosome biogenesis. *Molecular Microbiology* **68:**1547-1559.

Kenerley ME, Morgan EA, Post L, Lindahl L, Nomura M.. 1977. Characterization of hybrid plasmids carrying individual ribosomal ribonucleic acid transcription units

of Escherichia coli. *Journal of Bacteriology* **13:**931-949.

Kim H, Abeysirigunawarden SC, Chen K, Mayerle M, Ragunathan K, Luthey-Schulten Z, Ha T, Woodson SA. 2014. Protein-guided RNA dynamics during early ribosome assembly. *Nature* **506:**334-338.

Kimura S, Suzuki T. 2010. Fine-tuning of the ribosomal decoding center by conserved methyl-modifications in the Escherichia coli 16S rRNA. *Nucleic Acids Research* **38:**1341-1352.

Kitagawa M, Ara T, Arifuzzaman M, Ioka-Nakamichi T, Inamoto E, Toyonaga H, Mori H. 2005. Complete set of ORF clones of Escherichia coli ASKA library (A Complete Set of E. coli K-12 ORF Archive): Unique Resources for Biological Research. *DNA Research* **12:** 291-299.

Kjeldgaard NO. 1961. The kinetics of ribonucleic acid- and protein formation in Salmonella typhimurium during the transition between different states of balanced growth. *Biochimica et Biophysica Acta* **49:**64-76.

Klassen, NV. 1987. Primary products in radiation chemistry. *In* I. Farhataziz and M. A. J. Rodgers, eds. Radiation Chemistry: Principles and Applications VCH Publishers, New York 29-61.

Klein DJ, Schmeing TM, Moore PB, Steitz TA. 2001. The kink-turn: A new RNA secondary structure motif. *The EMBO Journal* **20:**4214-4221.

Krzyzosiak W, Denman R, Nurse K, Hellmann W, Boublik M, Gehrke CW, Agris PF, Ofengand J. 1987. In vitro synthesis of 16S ribosomal RNA containing single base changes and assembly into a functional 30S ribosome. *Biochemistry* **26:** 2353-2364.

Latham JA, Cech TR. 1989. Defining the inside and outside of a catalytic RNA molecule. *Science* **245:**276-282.

Leong V, Kent M, Jomaa A, Ortega J. 2013. Escherichia coli rimM and yjeQ null strains accumulate immature 30S subunits of similar structure and protein complement. *RNA* **19:**798-802.

Lewicki BTU, Margus T, Remme J, Nierhaus KH. 1993. Coupling of rRNA transcription and Ribosomal assembly in vivo: Formation of active ribosomal subunit in Escherichia coli requires transcription of rRNA genes by host RNA polymerase which cannot be replaced by bacteriophage T7 RNA polymerase. *Journal of Molecular Biology* **231:**581-593.

Li SC, Squires CL, Squires C. 1984. Antitermination of E. coli rRNA transcription is caused by a control region segment containing lambda nut-like sequences. *Cell* **38:**851-860.

Li Z, Pandit S, Deutscher MP. 1999. RNase G (CafA protein) and RNase E are both required for the 5' maturation of 16S ribosomal RNA *The EMBO Journal* **18:**2878-2885.

Liang ST, Xu YC, Dennis P, Bremer H. 2000. mRNA Composition and Control of Bacterial Gene Expression. *Journal of Bacteriology* **182:**3037-3044.

Liiv A, Remme J. 2004. Importance of transient structure during post-transcriptional refolding of the pre-23S rRNA and ribosomal large subunit assembly. *Journal of Molecular Biology* **342:**725-741.

Lindahl L. 1975. Intermediates and time kinetics of the in vivo assembly of Escherichia coli ribosomes. *Journal of Molecular Biology* **92:**15-37.

Littlefield JW, Keller EB, Gross J, Zamecnik PC. Studies on cytoplasmic ribonucleoprotein particles from the liver of the rat. *Journal of Biological Chemistry* **217:**111-123.

Loevgren JM, Wikstrom PM. 2001. Hybrid protein between ribosomal protein S16 and RimM of Escherichia coli retains the ribosome maturation function of both proteins. *Journal of Bacteriology* **183:**5352-5357.

Loevgren JM, Bylund GO, Srivastava MK, Lundberg LAC, Persson OP, Wikstrom PM. 2004. The PRC-barrel domain of the ribosome maturation protein RimM mediates binding to ribosomal protein S19 in the 30S ribosomal subunits. *RNA* **10:**1798-1812.

Lu Q, Inouye M. 1998. The gene for 16S rRNA methyltransferase (ksgA) functions as a multicopy suppressor for a cold-sensitive mutant of era, an essential RAS-like GTP-binding protein in Escherichia coli. *Journal of Bacteriology* **180:**5243-5246.

Maiväli Ü, Paier A, Tenson T. 2013. When stable RNA becomes unstable: the degradation of ribosomes in bacteria and beyond. *Biological Chemistry* **394:**845-855.

Matelska D, Purta E, PanMek S, Boniecki MJ, Bujnicki JM, Dunin-Horkawicz S. 2013. S6:S18 ribosomal protein complex interacts with a structural motif present in its own mRNA *RNA* **19:**1341-1348.

Mathews DH, Disney MD, Childs J., Schroeder SJ, Zuker M, Turner DH. 2004. Incorporating chemical modification constraints into a dynamic programming algorithm for prediction of RNA secondary structure. *Proceedings of the National Academy of Sciences of USA* **101:**7287-7292.

Mayerle M, Bellur DL, Woodson SA. 2011. Slow formation of stable complexes during coincubation of minimal rRNA and ribosomal protein S4. *Journal of Molecular Biology* **412:**453-465.

Mayerle M, Woodson SA. 2013. Specific contacts between protein S4 and ribosomal RNA are required at multiple stages of ribosome assembly. *RNA* **19:**574-585.

McGinnis JL, Liu Q, Lavender CA, Devaraj A, McClory SP, Fredrick K, Weeks KM. 2015. In-cell SHAPE reveals that free 30S ribosome subunits are in the inactive state. *Proceedings of the National Academy of Sciences of USA* **112:** 2425-2430.

Meng W, Belyaeva T, Savery NJ, Busby SJ, Ross WE, Gaal T, Gourse RL, Thomas MS. 2001. UP element-dependent transcription at the Escherichia coli rrnB P1 promoter: positional requirements and role of the RNA polymerase alpha subunit linker. *Nucleic Acids Research* **29:**4166-4178.

Merianos HJ, Wang J, Moore PB. 2004.The structure of a ribosomal protein S8/*spc* operon mRNA complex. *RNA* **10:**954-964.

Moazed D, Stern S, Noller HF. 1986. Rapid chemical probing of conformation in 16S ribosomal RNA and 30S ribosomal subunits using primer extension. *Journal of Molecular Biology* **187:**399-416.

Moazed D, Van Stolk BJ, Douthwaite S, Noller HF. 1986b. Interconversion of active and inactive 30 S ribosomal subunits is accompanied by a conformational change in the decoding region of 16 S rRNA. *Journal of Molecular Biology* **191:** 483-493.

Mora G, Donner D, Thammana P, Lutter L, Kurland CG, Craven GR. Purification and characterization of 50S ribosomal proteins of Escherichia coli. *Molecular and general genetics* **112:**229-242.

Morgan EA. 1986. Antitermination mechanisms in rRNA operons of Escherichia coli. *Journal of Bacteriology* **168:**1-5.

Mulder AM, Yoshioka C, Beck AH, Bunner AE, Milligan RA, Potter CS, Carragher B, Williamson JR. 2010. Visualizing ribosome biogenesis: parallel assembly pathways for the 30S subunit. *Science* **330:**673-677.

Murray KD, Bremer H. 1996. Control of spot-dependent ppGpp synthesis and degradation in Escherichia coli. *Journal of Molecular Biology* **259:**41-57.

Nesterchuk MV, Sergiev PV, Dontsova OA. 2011. Posttranslational modifications of ribosomal proteins in Escherichia coli. *Acta Naturae* **3:**22-33.

Ninnemann O, Koch C, Kahmann R. 1992. The E.coli fis promoter is subject to stringent control and autoregulation. *The EMBO Journal* **11:**1075-1083.

Nissen P, Ippolito JA, Ban N, Moore PB, Steitz TA. 2001. RNA tertiary interactions in the large ribosomal subunit: the A-minor motif. *Proceedings of the National Academy of Sciences of USA* **98:**4899-4903.

Noller HF, Kop J, Wheaton V, Brosius J, Gutell RR, Kopylov AM, Dohme F, Herr W, Stahl DA, Gupta R, Waese CR. 1981. Secondary structure model for 23S ribosomal RNA. *Nucleic Acids Research* **9:**6167-6189.

Noller HF. 1991. Ribosomal RNA and Translation. *Annual Reviews in Biochemistry* **60:** 191-227.

Nord S, Bhatt MJ, Tükenmez H, Farabaugh PJ Wikstroem PM. 2015. Mutations of ribosomal protein S5 suppress a defect in late-30S ribosomal subunit biogenesis caused by lack of the RbfA biogenesis factor. *RNA* **21:**1-15.

Nord S, Bylund GO, Lovgren JM, Wikstroem PM. 2009. The RimP protein is important

for maturation of the 30S ribosomal subunit. *Journal of Molecular Biology* **386:**742-753.

Nowotny V, Nierhaus KH. 1988. Assembly of the 30S subunit from Escherichia coli ribosomes occurs via two assembly domains which are initiated by S4 and S7. *Biochemistry* **27:**7051-7055.

Okamoto S, Tamaru A, Nakajima C, Nishimura K, Tanaka Y, Tokuyama S, Suzuki Y, Ochi K. 2007. Loss of a conserved 7-methylguanosine modification in 16S rRNA confers low-level streptomycin resistance in bacteria. *Molecular Microbiology* **63:**1096-1106.

Olson ER, Flamm EL, Friedman DI. 1982. Analysis of nutR: A region of phage lambda required for antitermination of transcription. *Cell* **31:**61-70.

Olsson MO, Isaksson LA. 1979. Analysis of rpsD mutations in Escherichia coli. III. Effects of rpsD mutations on expression of some ribosomal protein genes. *Molecular and general genetics* **169:**271-278.

Paier A, Leppik M, Soosaar A, Tenson T, Maiväli Ü. 2015. The effects of disruptions in ribosomal active sites and in intersubunit contacts on ribosomal degradation in Escherichia coli. *Scientific Reports* **5:**7712.

Pan J, Thirumalai D, Woodson SA. 1997. Folding of RNA involves parallel pathways. *Journal of Molecular Biology* **273:**7-13.

Pardee AB, Prestidge LS. 1956. The dependence of nucleic acid synthesis on the presence of amino acids in Escherichia coli. *Journal of Bacteriology* **71:**677-683.

Pardon B, Wagner R. 1995. The Escherichia coli ribosomal RNA leader nut region interacts specifically with mature 16S RNA. *Nucleic Acids Research* **23:**932-941.

Paul BJ, Barker MM, Ross W, Schneider DA, Webb C, Foster JW, Gourse RL. 2004 DksA: a critical component of the transcription initiation machinery that potentiates the regulation of rRNA promoters by ppGpp and the initiating NTP. *Cell* **118:**311-322.

Piir K, Paier A, Liiv A, Tenson T, Maiväli U. Ribosome degradation in growing bacteria. *EMBO Reports* **12:**458-462.

Poot RA, Jeeninga RE, Pleij CW, van Duin J. 1997. Acetylation of ribosomal protein S5 affected by defects in the central pseudoknot in 16S ribosomal RNA? *FEBS Letters* **401:**175-179.

Powers T, Noller HF. 1990. Dominant lethal mutation in a conserved loop in 16S rRNA. *Proceedings of the National Academy of Sciences of USA* **87**:1042-1046.

Powers T, Noller HF. 1991. A functional pseudoknot in 16S ribosomal RNA. *The EMBO Journal* **10:** 2203-2214.

Powers T, Noller HF. 1993. Allele-specific structure probing of plasmid-derived 16S ribosomal RNA from Escherichia coli. *Gene* **123:** 75-80.

Ramaswamy P, Woodson SA. 2009a. Global stabilization of rRNA structure by ribosomal proteins S4, S17, and S20. *Journal of Molecular Biology* **392:**666-677.

Ramaswamy P, Woodson SA. 2009b. S16 throws a conformation switch during assembly of 30S 5' domain. *Nature Structural & Molecular Biology* **16:**438-445.

Remaut E, Tsao H, Fiers W. 1983. Improved plasmid vectors with a thermoinducible expression and temperature-regulated runaway replication. *Gene* **22:**103-113.

Roberts RB (ed.) 1958. *Microsomal particles and protein synthesis.* Pergamon Press, New York. vii-viii.

Robertson HD, Webster RE, Zinder ND. 1968. Purification and properties of ribonuclease III from Escherichia coli. *The Journal of Biological Chemistry* **243:**82-91.

Ron EZ, Kohler RE, Davis BD. 1966. Polysomes extracted from Escherichia coli by freeze-thaw-lysozyme lysis. *Science* **153:**1119-1120.

Rook MS, Treiber DK, Williamson JR. 1998. Fast folding mutants of the Tetrahymena group I ribozyme reveal a rugged folding energy landscape. *Journal of Molecular Biology* **281:**609-620.

Ross W, Thompson JF, Newlands JT, Gourse RL. 1990. E.coli Fis protein activates ribosomal RNA transcription in vitro and in vivo. *The EMBO Journal* **9:**3733-3742.

Ross W, Gosink KK, Salomon J, Igarashi K, Zou C, Ishihama A, Severinov K, Gourse RL. 1993. A third recognition element in bacterial promoters: DNA binding by the alpha subunit of RNA polymerase. *Science* **262:**1407-1413.

Roy-Chaudhuri B, Kirthi N, Kelley T, Culver GM. 2008. Suppression of a cold-sensitive mutation in ribosomal protein S5 reveals a role for RimJ in ribosome biogenesis. *Molecular Microbiology* **68:**1547-1559.

Sashital DG, Greeman CA, Lyumkis D, Potter CS, Carragher B, Williamson JR. 2014. A combined quantitative mass spectrometry and electron microscopy analysis of ribosomal 30S subunit assembly in E. coli. *Elife* **3:**e04491.

Sayed A, Matsuyama SI, Inouye M. 1999. Era, an essential Escherichia coli small G-protein, binds to the 30S ribosomal subunit. *Biochemical and Biophysical Research Communications* **264:**51-54.

Schlax PJ, Xavier KA, Gluick TC, Draper DE. 2001. Translational repression of the Escherichia coli α operon mRNA: Importance of an mRNA conformational switch and a ternary entrapment complex. *The Journal of Biological Chemistry* **276:**38494-38501.

Schuwirth BS, Borovinskaya MA, Hau CW, Zhang W, Vila-Sanjurjo A, Holton JM, Cate JH. 2005. Structures of the Bacterial Ribosome at 3.5 Å Resolution. *Science* **310:**827-834.

Sharma MR, Barat C, Wilson DN, Booth TM, Kawazoe M, Hori-Takemoto C, Shirouzu M, Yokoyama S, Fucini P, Agrawal1 RK. 2005. Interaction of Era with the 30S Ribosomal Subunit: Implications for 30S Subunit Assembly. *Molecular Cell* **18:**319-329.

Shajani Z, Sykes MT, Williamson JR. 2011. Assembly of Bacteria Ribosomes. *Annual Review of Biochemistry* **80:**28.1-28.26.

Shine J, Dalgarno L. 1974. The 3'-terminal sequence of Escherichia coli 16S ribosomal RNA: complementarity to nonsense triplets and ribosome binding sites. *Proceedings of the National Academy of Sciences of USA* **71:**1342-1346.

Siekevitz P, Zamecnik PC. 1981. Ribosomes and protein synthesis. *Journal of Cell Biology* **91:**53s-65s.

Siiback T, Remme J. 2010. Subribosomal particle analysis reveals the stages of bacterial ribosome assembly at which rRNA nucleotides are modified. *RNA* **16:**2023-2032.

Sonenberg N, Wilchek M, Zamir A. 1975. Identification of a region in 23S rRNA located at the peptidyl transferase center. *Proceedings of the National Academy of Sciences of USA* **72:**4332-4336.

Soper SFC, Dator RP, Limbach PA, Woodson SA. 2013. In vivo X-ray footprinting of pre-30S ribo- somes reveals chaperone-dependent remodeling of late assembly intermediates. *Molecular Cell* **52**:506-516.

Spedding G. 1990. Ribosomes and protein synthesis: A practical approach. *Oxford University Press.*

Spedding G, Gluick TC, Draper DE. 1993. Ribosome initiation complex formation with the pseudoknotted alpha operon messenger RNA. *Journal of Molecular Biology* **229:**609-622.

Srivastava AK, Schlessinger D. 1990. Mechanism and regulation of bacterial ribosomal RNA processing. *Annual Reviews of Microbiology* **44:**105-129.

Steen KA, Rice GM, Weeks KM. 2012. Fingerprinting noncanonical and tertiary RNA structures by differential SHAPE reactivity. *Journal of the American Chemical Society* **134:** 13160-13163.

Stern S, Changchien LM, Craven GR, Noller HF. 1988a. Interaction of proteins S16, S17 and S20 with 16 S ribosomal RNA. *Journal of Molecular Biology* **200:** 291-299.

Stern S, Powers T, Changchien LM, Noller HF. 1988b. Interaction of ribosomal proteins S5, S6, S11, S12, S18 and S21 with 16 S rRNA. *Journal of Molecular Biology* **201:** 683-695.

Stern S, Weiser B, Noller HF. 1988c. Model for the three-dimensional folding of 16 S ribosomal RNA. *Journal of Molecular Biology* **204:** 447-481.

Stern S, Powers T, Changchien LM, Noller HF. 1989. RNA-Protein Interactions in 30S Ribosomal Subunits: Folding and Function of 16S rRNA. *Science* **244:**783-790.

Sulthana S, Deutscher MP. 2013. Multiple exoribonucleases catalyze maturation of the 3' terminus of 16S ribosomal RNA (rRNA). *The Journal of Biological Chemistry* **288:**12574-12579.

Suzuki S, Tatsuguchi A, Matsumoto E, Kawazoe M, Kaminishi T, Shirouzu M, Muto Y, Takemoto C, Yokoyama S. 2007. Structural characterization of the ribosome maturation protein, RimM. *Journal of Bacteriology* **189:**6397-6406.

Sykes MT, Shajani Z, Sperling E, Beck AH, Williamson JR. 2010. Quantitative proteomic analysis of ribosome assembly and turnover in vivo. *Journal of Molecular Biology* **403:**331-345.

Takiff HE, Chen SM, Court DL. 1989. Genetic analysis of the rnc operon of Escherichia coli. *Journal of Bacteriology* **171:**2581-2590.

Talkington MWT, Siuzdak G, Williamson JR. 2005. An assembly landscape for the 30S ribosomal subunit. *Nature* **438:**628-632.

Theissen G, Thelen L, Wagner R. 1993. Some base substitutions in the leader of an Escherichia coli ribosomal RNA operon affect the structure and function of ribosomes: Evidence for a transient scaffold function of the rRNA leader. *Journal of Molecular Biology* **223:**203-218.

Tissieres A, Watson JD. 1958. Ribonucleoprotein particles from Escherichia coli. *Nature* **182:**778-780.

Torres M, Condon C, Balada JM, Squires C, Squires CL. 2001. Ribosomal protein S4 is a transcription factor with properties remarkably similar to NusA, a protein involved in both non-ribosomal and ribosomal RNA antitermination. *The EMBO Journal* **20:**3811-3820.

Traub P, Nomura M. 1969. Structure and function of Escherichia coli ribosomes. VI. Mechanism of assembly of 30 s ribosomes studied in vitro. *Journal of Molecular Biology* **40:** 391-413.

Triman K, Becker E, Dammel C, Katz J, Mori H, Douthwaite S, Yapijakis C, Yoast S, Noller HF. 1989. Isolation of temperature-sensitive mutants of 16S rRNA in Escherichia coli. *Journal of Molecular Biology* **209:**645-653.

Tscherne JS, Nurse K, Popienick P, and Ofengand J. 1999. Purification, cloning, and characterization of the 16 S RNA m 2G1207 methyltransferase from Escherichia coli. *The Journal of Biological Chemistry* **274**:924-929.

Tu C, Zhou X, Tropea JE, Austin BP, Waugh DS, Court DL, Ji X. 2009. Structure of ERA in complex with the 3' end of 16S rRNA: implications for ribosome biogenesis. *Proceedings of the National Academy of Sciences of USA* **106:** 14843-14848.

Tu C, Zhou X, Tarasov SG, Tropea JE, Austin BP, Waugh DS, Court DL, Ji X. 2011. The Era GTPase recognizes the GAUCACCUCC sequence and binds helix 45 near the 3′ end of 16S rRNA. *Proceedings of the National Academy of Sciences of USA* **108:** 10156-10161.

Tullius TD, Greenbaum JA. 2005. Mapping nucleic acid structure by hydroxyl radical cleavage. *Current Opinions Chemical Biology* **9:**127-134.

Vasa SM, Guex N, Wilkinson KA, Weeks KM, Giddings MC. 2008. ShapeFinder: A software system for high-throughput quantitative analysis of nucleic acid reactivity information resolved by capillary electrophoresis. *RNA* **14:**1979-1990.

Vetting MW, de Carvalho LPS, Roderick SL, Blanchard JS. 2005. A novel dimeric

structure of the RimL N^{α}-acetyltransferase from Salmonella typhimurium. *The Journal of Biological Chemistry* **280:**22108-22114.

Voorhees RM, Fernández IS, Scheres SH, Hegde RS. 2014. Structure of the mammalian ribosome-Sec61 complex to 3.4 Å resolution. *Cell* **157:** 1632-1643.

Wagner R, Gassen HG. 1975. On the covalent binding of mRNA models to the part of the 16 S RNA which is located in the mrna binding site of the 30 S ribosome. *Biochemical and Biophysical Research Communications* **65:**519-529.

Weisser M, Voigts-Hoffmann F, Rabl J, Leibundgut M, Ban N. 2013. The crystal structure of the eukaryotic 40S ribosomal subunit in complex with eIF1 and eIF1A. *Nature Structural and Molecular Biology* **20:** 1015-1017.

Wikstroem PM, Lind LK, Berg DE, Bjoerk GR. 1992. Importance of mRNA folding and start codon accessibility in the expression of genes in a ribosomal protein operon of Escherichia coli. *Journal of Molecular Biology* **224:**949-966.

Wikstroem PM, Bystroem AS, Bjoerk GR. 1988. Non-autogenous control of ribosomal protein synthesis from the *trmD* operon in Escherichia coli. *Journal of Molecular Biology* **203:**141-152.

Wilkinson KA, Merino EJ, & Weeks KM. 2006. Selective 2'-hydroxyl acylation analyzed by primer extension (SHAPE): quantitative RNA structure analysis at single nucleotide resolution. *Nature Protocols* **1:**1610-1616.

Wilson DN, Nierhaus KH. 2007. The weird and wonderful world of bacterial ribosome regulation. *Critical Reviews in Biochemistry and Molecular Biology* **42:**187-219.

Wimberly BT, Brodersen DE, Clemons WM Jr, Morgan-Warren RJ, Carter AP, Vonrhein C, Hartsch T, Ramakrishnan V. 2000. Structure of the 30S ribosomal

subunit. *Nature* **407:**327-339.

Wittmann-Liebold B, Greuer B. 1978. The primary structure of protein S5 from the small subunit of the Escherichia coli ribosome. *FEBS Letters* **95:**91-98.

Woese CR, Fox GE, Zablen L, Uchida T, Bonen L, Pechman K, Lewis BJ, Stahl D. 1975. Conservation of primary structure in 16S ribosomal RNA. *Nature* **254:**83-86.

Woodson SA. 2011. RNA folding pathways and the self-assembly of ribosomes. *Accounts of Chemical Research* **44:**1312-1319.

Woolstenhulme CJ, Hill WE. 2009. The genesis of ribosome structure: how a protein generates RNA structure in real time. *Journal of Molecular Biology* **392:** 645-656.

Xia B, Ke H, Shinde U, Inouye M. 2003. The role of RbfA in 16S rRNA processing and cell growth at low temperature in Escherichia coli. *Journal of Molecular Biology* **332:**575-584.

Yang Z, Guo Q, Goto S, Chen Y, Li N, Yan K, Zhang Y, Muto A, Deng H, Himeno H, Lei J, Gao N. 2014. Structural insights into the assembly of the 30S ribosomal subunit in vivo: functional role of S5 and location of the 17S rRNA precursor sequence. *Protein Cell* **5:**394-407.

Yu L, Gunasekera AH, Mack J, Olejniczak ET, Chovan LE, Ruan X, Towne DL, Lerner CG, Fesik SW. 2001. Solution Structure and Function of a Conserved Protein SP14.3 Encoded by an Essential Streptococcus pneumoniae Gene. *Journal of Molecular Biology* **311:** 593-604.

Young RA, Steitz JA. 1978. Complementary sequences 1700 nucleotides apart form a ribonuclease III cleavage site in Escherichia coli ribosomal precursor RNA. *Proceedings of the National Academy of Sciences of USA* **75:**3593-3597.

Youngman EM, Green R. 2005. Affinity purification of in vivo-assembled ribosomes for in vitro biochemical analysis. *Methods* **36:**305-312.

Zaporojets D, French S, Squires CL. 2003. Products transcribed from rearranged rrn genes from Escherichia coli can assemble to form functional ribosomes. *Journal of Bacteriology* **185:**6921-6927.

Zarrinkar PP, Williamson JR. 1994. Kinetic intermediates in RNA folding. *Science* **265:**918-924.

Zhang F, Ramsay ES, Woodson SA. 1995. In vivo facilitation of Tetrahymena group I intron splicing in Escherichia coli pre-ribosomal RNA. *RNA* **1:**284-292.

Zhi H, Wang X, Cabrera JE, Johnson RC, Jin DJ. 2003. Fis stabilizes the interaction between RNA polymerase and the ribosomal promoter rrnB P1, leading to transcriptional activation. *Journal of Biological Chemistry* **278:**47340-47349.

Curriculum Vitae

Mollie Rappe

(970) 779-1017 **@mollie_rappe**
mollie.rappe@gmail.com **mollierappe**

Born: 23rd February, 1987
Location: Boulder, Colorado, U.S.A

Education

Johns Hopkins University — Baltimore, MD
Ph.D. in Molecular Biophysics — expected summer 2015
Effects of mutations in the junction between helices 5 and 6 of the 16S rRNA upon 30S biogenesis
Dr. Sarah A. Woodson

Fort Lewis College — Durango, CO
B.S. in Biochemistry, math minor; *summa cum laude* — 2005–2009

Research Experience

Johns Hopkins University — May 2010–present

- Presented posters at three international meetings and numerous internal events. Clearly illustrated my research. One presentation led to two new collaborations.
- Proofread and edited coworkers' job talks and cover letters.
- Assisted coworkers in constructing coherent narratives for meetings and presentations.
- Taught coworkers and collaborators specialized techniques and wrote technical protocols.
- Searched for, evaluated, and comprehended peer-reviewed literature on a regular basis.
- Used a variety of techniques from cell biology, molecular biology, biochemistry, and biophysics to assay rRNA mutants in vivo and in vitro.
- Designed and troubleshot a new biophysical technique to isolate *in vivo* footprinted RNA mutants to look at residue-level structural changes during early ribosome assembly.

Bloomberg School of Public Health — Spring 2010

- Examined the RNA specificity of CasE — a RNA cleaving member of the trendy and powerful CRISPR complex — using a variety of biochemical techniques.

Johns Hopkins University — Winter 2009

- Investigated the binding specificity of various biologically-relevant S4 mutants to their minimal binding domain by fluorescence.

Johns Hopkins University — Fall 2009

- Determined thermodynamic stabilities of the group I intron and a mutant.

Research Experience cont.

Fort Lewis College 2008–2009

- Began initial biochemical and phenotypic screens on yeast lacking various HDACs or HATs. Epigenetics is vital for understanding the basis of cell differentiation and cancer.

IBM Almaden Summer 2008

- Characterized polymer films for photo-nanoimprint lithography — a promising method of fabricating nanoscale silicon chips.

Fort Lewis College 2007–2008

- Performed initial metabolomic screens on a widespread, environmentally-important but under-studied soil bacterium *Acidobacterium capsulatum*.

Montana State University Summer 2007

- Crystallized and began X-ray diffraction studies on a novel protein from *Sulfolobus* Spindle-shaped Virus — a virus that survives in volcanic hot spring archaea.

Teaching Experience

Johns Hopkins University *Lab Mentor* Fall 2011–present

- Principally instructed 3 rotating graduate students as well as helped 10 new graduate students and postdocs with laboratory skills and operational protocols.

Johns Hopkins University *Teaching Assistant* Fall 2010

- Taught 30 graduate and undergraduate students Python programing, graded weekly homework assignments, and held exam help sessions for Proteins and Nucleic Acids.

Fort Lewis College *Teaching Assistant* Spring 2006–2009

- Answered questions, assisted with instrumentation and software, and ensured the safety of 24 General and Organic Chemistry students. Involved in revamping the pre-lab quizzes.

Fort Lewis College *Resident Assistant* 2006–2007

- Enforced university policy, monitored and counseled a university residence hall floor of 45 ethnically-diverse freshman students.
- Planned and implemented between 12 and 15 educational programs a semester and produced monthly fun and informative bulletin boards.

Presentations and Meetings

DCSWA Professional Development Day, 2015 — Scholarship recipient
19th Annual RNA Society Meeting, 2014 — Poster presentation
Ribosomes Conference, 2013 — Poster presentation
9th International Conference on Ribosome Synthesis, 2012 — Poster presentation
Cross-Campus Biophysics Student Evening Series, 2012 — Invited speaker

Professional Societies

National Association of Science Writers — Student member
RNA Society — Current member
Sigma Xi — Associate member

Science Writing Internship

American Society for Biochemistry and Molecular Biology Feb–May 2015

- Translated cutting-edge scientific discoveries for a diverse audience, balancing detailed explanations with clearly articulated background knowledge and newsworthiness.
- Interviewed and profiled ASBMB members about their science, activities, and achievements.
- Attended a scientific symposium for newsgathering purposes.
- Pitched and wrote original story ideas.

- Edited articles for accuracy, content, clarity, and grammatical correctness.
- Recruited and mentored an undergraduate magazine contributor.
- Proofread magazine and website content.

- Promoted magazine content via social media such as Twitter, Facebook, and Storify. Spearheaded a social media campaign for National Graduate Student appreciation week.
- Contributed to weekly news and social media team meetings.
- Located images appropriate for magazine content and wrote photo captions.
- Directed the marketing team to potential advertisers.

Science Writing Publications

Two drugs are better than one – **ASBMB Today**	March, 2015
The state of science book writing in 2015 – **DCSWA**	March, 2015
Using hamsters to study hemorrhagic fever – **ASBMB Today**	April, 2015
Mitochondrial replacement therapy – **Wild Types blog**	April, 2015
A lab with a view – **ASBMB Today**	May, 2015
A majestic model – **ASBMB Today**	May, 2015
A small STEP toward peace – **ASBMB Today**	May, 2015
Microglia: the sentinels of the central nervous system – **ASBMB Today**	May, 2015
Meet Svetlana Lusenko – **ASBMB Today**	June/July, 2015
Why are some spider bites much worse than others? – **ASBMB Today**	Sept, 2015

Professional Recognition

DCSWA Professional Development Day Scholarship Recipient	2015
Cross-Campus Biophysics Student Evening Series Invited Speaker	2012
Mills-Wylie Physical Chemistry Student of the Year	2008
Outstanding Teaching Assistant for General Chemistry	2006